SESSION 5A

Chairman: Dr. J. KLOOSTERMAN (Netherlands)

STATUS OF THE PNC HIGH POWER ELECTRON ACCELERATOR

T.Emoto, Y.L.Wang, S.Toyama, M.Nomura, H.Takei, K.Hirano, Y.Yamazaki
Power Reactor and Nuclear Fuel Development Corporation (PNC)
4002 Narita, Oarai-mach, Ibaraki-ken 311-13 Japan

Design and construction of a high power CW(Continuous Wave) electron linac for studying feasibility of nuclear waste transmutation was started in 1989 at PNC. The PNC linac is the 10MeV, 20mA (average current, 20% duty) accelerator with eight normal conducting TWRR(Traveling Wave Resonant Ring) disk loaded accelerating tubes. Various methods have been proposed to transmute long-lived fission products using accelerators. The transmutation by photonuclear reaction using a electron accelerator has advantages of the small production for secondary radioactive waste and broad base of accelerator technology.

The PNC high power CW electron accelerator has been pre-commissioned with the injector and the first accelerating tube. By December 1995, the accelerator was partially built and the injector pre-commissioning began. Then 3.1 MeV beam had coasted though the beam dump. We have been very successful to produce 1 ms pulse width electron beam with 100 mA peak and energy about 3.1 MeV at present.

The whole facility will be completed in March 1997.

INTRODUCTION

Many research efforts have been spent in PNC to establish technologies for safety disposal of radioactive waste. The high level radioactive waste produced from the reprocessing of spent fuel is essential for the completion of nuclear fuel cycle. Current national policy in Japan is to solidify the high level radioactive waste into a stable form and to dispose it in a deep geological repository after 30 to 50 years of storage for decay heat reduction. However, the Japanese Atomic Energy Commission approved the long-term program for research and development on nuclide partitioning and transmutation in October 1988 beside solidification disposal mentioned above. The objective of the program (called OMEGA) is to explore a possibility to utilize the high level radioactive waste as useful resources and make the geological disposal more efficient.

The program is composed of two major area. One is the nuclear partitioning from the high level radioactive waste based on its potential value for utilization. The other is the transmutation of minor actinides and long-lived fission products into short-lived or stable nuclide. It is usually difficult to transmute long-lived fission products in reactors because of small neutron capture cross section. Various methods have been proposed to transmute long-lived fission products using accelerators. The transmutation by photonuclear reaction using a electron accelerator has advantages of the small production for secondary radioactive waste and broad base of accelerator technology. A high power electron accelerator will be required in future transmutation system.

Upon this projection, design and construction of a high power CW electron linac to study feasibility of nuclear waste transmutation was started in 1989 at PNC. Until now, a high power L-band klystron and a prototype high power TWRR accelerating tube were built and successfully validated many of design concepts until end of 1992. By December 1995, the accelerator was partially built and the injector pre-commissioning began. Then 3.1 MeV beam had coasted though the beam dump. The whole facility will be completed in March 1997.

THE LINAC DESIGN

The parameters of the beam produced by the linac are summarized in Table 1. These are very unique specifications for among the existing electron linear accelerators. The long pulse, 4 msec, is used for the beam stability studies of CW linac. The RF source parameters are summarized in Table 2.

Table 1 Beam parameters for the linac

Energy	10 MeV
Max. Beam Current	100 mA
Average Beam Current	20 mA
Pulse Length	0.1 ~ 4 ms
Pulse Repetition	0.1Hz ~ 50 Hz
Duty Factor	0.001 ~ 20 %
Norm. Emittance	50 π mm mrad*
Energy spread	0.5 %*

* estimated value by simulation

Table 2 Parameters of the RF source.

Accelerating Frequency	1249.135 MHz
Accelerating Mode	$2\pi/3$ mode
Number of Klystron	2
Klystron Power	1.2 MW

Injector

The injector consists of a 200kV DC gun, magnetic lens, a RF chopper, chopper slits, a prebuncher, and a buncher. Solenoid coils cover these elements from the exit of the gun to the first accelerating tube except

between the RF chopper and chopper slits. Fig. 1 shows these injector components and schematic with the solenoid magnetic fields.

Electron Gun

The pulse characteristics of the accelerator beam are initially determined by the electron gun system. The accelerator requires a range of pulse widths from 100 μsec to 20 msec, rise and fall times of ~1 μsec.

As average beam current is very high (20 mA), a grid (intercepting wire mesh) cannot be used for current control because of exceeding electron beam energy deposit to the grid wire. A non-intercepting aperture grid is only capable of high beam current control. The two aperture grids configuration is necessary to control a greater range of beam current according to numerical simulation. The gun electrode configuration was designed using a computer code EGUN [2] calculated the electron trajectories through the gun in the presence of space charge.

RF Chopper

The RF chopper [4] consists of a RF chopping cavity and a slit. The RF chopping cavity is a rectangular cavity driven at f_0 (fundamental frequency: 1.249135MHz) with TM_{210} mode and $2f_0$ with TM_{410} mode. There are three field mixed together in the chopper cavity. First one is a fundamental (f_0) magnetic field, second one is second harmonic ($2f_0$) magnetic field, and third one is a DC magnetic field bias. Adjusting RF field amplitude and phase, a superposed magnetic field can be equal to zero on the beam center line in 120 degree phase length. The wave form from the chopper cavity is shown in Fig.2. This chopper provide small transverse emmitance and bigger acceptance for phase angle.

Buncher

The buncher is a TM_{010} room-temperature cavity at same frequency (1.249135 GHz) as the fundamental of the accelerating tubes. Bunching in the PNC injector occurs in two components: the prebuncher and the 1.2 m long, traveling-wave resonant ring buncher.

The beam current from the DC gun is 300 mA and one third of RF periodic (120 degree) beam passes through the chopper slits. In the buncher the wave phase velocity varies linearly from 0.695 to 1.0 of light velocity. The bunch width becomes about 10 degree at prebuncher exit and 5 degree at buncher exit. The injector has been modeled with the code PARMELA [5], which simulates the beam trajectory from the exit of the electron gun to the accelerating tube.

Accelerator Section

The accelerator proper is a traveling-wave accelerator with TWRR excited with microwave power at a frequency of 1249.135 MHz. The accelerating tube has a cylindrical, disk-loaded shape made by OFHC (Oxygen Free High-purity Copper). The structure is designed to produce a constant axial electric field over the length of each independently fed. The number of the accelerating sections is seven and one injector section. Each of the accelerating section whose length is 1.2 meters contains 13 of $2/3\pi$ mode cavities and two coupling cavities.

All accelerating sections are designed to have constant gradient structure under the condition of 100mA beam loading. The regenerative type and the cumulative type of BBU (Beam Break Up) will be suppressed partially in the constant accelerator structure because the one accelerator sections of each cavity are designed with the same frequencies of TM_{01} mode and with very different frequencies of TM_{11}-like mode. According to the progressive stop-band technique, the iris diameters in the initial region of the accelerator section are smaller than those in any preceding ones but larger than those in subsequently located ones. The choice of short accelerating section and low attenuation constant structures made possible increase the threshold BBU current and liberate the tolerance of the TWRR resonate frequency, temperature stability, and fabrication. A detail TWRR with accelerating section is described else where [6].

Beam Dump and Vacuum System

The conceptual design of the beam dump is based on the following design criteria: (1) to disperse the beam by magnet in front of the beam entry, (2) to stop the beam part by part in spatially separated

blocks, (3) to minimize the induction of radioactivity.

The first criteria is for making the power density smaller by defocusing/spreading the beam. It is also assuring to avoid mishaps of the pin point beam hitting the component. The second criteria makes also a reduction of power deposition in a small region of the beam dump. The third criteria eliminates the use of water to stop the beam. Liquid target does increase the total inventory of the activated materials.

The concept of the present design is, as shown in Fig. 3, Ring and Disk (RD) system. The part where energy is deposited consists of 17 rings and 5 disks (thickness of 5 cm). Each plate is made from OFHC (Oxygen Free High-purity Copper). All the rings have different inside diameters (the beam runs inside this ring.). The frontmost ring has the inside diameter of 19.6 cm and other rings have smaller diameter with increment of 1.2 cm from upstream to downstream. In a module a cooling water flows in series from ring to ring. In order to reduce radiolysis of cooling water and to eliminate the vacuum window between the beam dump (target) and the accelerating tube, cooling water is not exposed to direct incident electron beam. These modules form a total target block and it also electrically insulated from the main body of the beam dump. The problem of connecting between the beam dump and the accelerator (the pressure difference between 1×10^{-5} torr and 1×10^{-7} torr in the accelerating tube) was solved by using a differential pumping stations and a low conductance beam transport tube.

RF modulator and Klystron

The klystron is able to operate complete CW (1.2MW CW). But the facility power station could not supply such large power(~5MW), which made the klystron operate 20% duty. Modulation of the klystron pulse voltage is accomplished by controlling the anode voltage for 90kV operation. For 147kV, the beam voltage modulation is employed, using pulse transformers and solid-state switch.

The klystrons used on the PNC accelerator were developed specifically to operate in CW and pulse with good efficiency(> 65%). Extensive window development was necessary to achieve continuous power of 1.2MW at L-band. The output window was designed and tested for pill-box type windows with using TWRR unit replaced the accelerating tube. The test results agree the characteristic of field decrease and reduction of VSWR in the pill-box by the design and suggests that the klystron will be able to produce more than 1.2MW RF with this new window [9].

Control and Data Acquisition Systems

A control system consists of two major parts: (1) computer control and monitor system, (2) an interlock system for use of the machine protection that shuts off the accelerator equipment and to protect personnel.

The computer control and monitor system is consisted of three network layers, which are Ethernet layer, VME-bus layer (SCRAM-net), and high speed communication layer. The beam control contains controls and status displays for each individual linac equipment . These systems are connected Ethernet layer (Ethernet with TCP/IP protocol). The communication network is supervised by the system control work stations which also manage the whole linac operation. These processors are not responsible for crucial operations such as interlock system.

The VME-bus layer (served as the beam control and some of them contained PIOP (Parallel Input/Output Processor) system) is interfaced with the linac equipment and each VME-bus systems connected with Ethernet and SCRAM-net(15MB/sec). Each PIOP node is connected with high speed communication lines as horizontally(or hypercube shape connection), which makes each node communicate with another node a short time as compared with shared bus system. A combination with high speed communication layer and DSP (Digital Signal Processor as node processor) makes fast data processing for large number input events simultaneously. This concept of data processing could not be achieved in conventional system.

The interlock system employs hard wire programmable sequencer system connected crucial equipments, which is completely independent from computer assist system because of more redundancy for safety aspect.

COMMISSIONING

Pre-Commissioning

The commissioning was carried out with partially build accelerator. The injector, the first accelerator section, the beam dump, and RF source was completed in December 1995. The RF conditioning was made in site using

own RF source. Within a few days after the RF conditioning, the buncher and accelerating section was able to store about 1 MW RF peak power in the resonant ring. The unique aspect of this power RF conditioning is burst-pulse operation, which is nine short pulse(100μsec) within 4 msec period. The 4 msec pulse power and the CW klystron allow to this kind operation.

Beam-Commissioning

Beam commissioning began and 3.1MeV beam had coasted though the linac to the beam dump. By March 22, 50mA of 1 msec beam was achieved. The resonant ring of the buncher and first accelerating section were tuned to the maximum resonated RF power. The RF chopper and the chopper slits were adjusted by the RF power to apply the cavity with a fundamental (f_0) RF power, then DC magnetic baias, finally second harmonic ($2f_0$) RF power. Fig. 4 shows the beam current in each beam current monitor. The beam current after the chopper shows one third current from the electron gun exit. The energy spectrum measured by bending magnet are shown in Fig. 5. After using the RF chopper, the energy resolution ($\Delta E/E$) is about 5%. This is rough adjustment because the bunch monitors have not been prepared and all phase and bunch length have not be tuned yet. Until now ~100 mA beam with pulse width 1 msec repetition 0.5 Hz has been accelerated. Studies continued at design goal of 100 mA beam with 4 msec and repetition 50Hz, including the resonant rings control with high power operation. The temperature control of resonant rings and accelerating tubes is getting critical with high duty operations.

CONCLUSION

The PNC high power CW linac injector and first accelerating section was installed and pre-commissioned during the beginning of 1996. This pre-commissioning shows important results that the accelerator with the traveling wave resonant ring under 100 mA beam loading is easily handled and verified the acceleration of long pulse beam such as 1 msec. Studies continued at design goal of 100 mA beam with 4 msec repetition 50Hz. The rest of accelerating section will be installed by March 1997, then 10MeV high power CW(average 20mA 20%duty) electron linac commissioning will be ready.

ACKNOWLEDGMENTS

We would like to strongly our deep appreciation to the professors at National Laboratory for High Energy Physics (KEK) for their incalculably guidance and helpful contributions from beginning of this project Professors are : I. Sato, H. Kobayashi, and A. Enomoto. Our appreciation goes to Dr. Y. Takeda at Paul Scherrer Institut (PSI) especially for the beam bump design.

REFERENCES

[1] S.Toyama et. al., "Transmutation of long-lived Fission Product (^{137}Cs, ^{90}Sr) by a Reactor-Accelerator System" , Proceeding of the 2nd International Symposium on Advanced Nuclear Energy Research (1990)
[2] W.B. Herrmannsfeldt, "EGUN an electron optics and gun design program", SLAC-Report-331, (October 1988).
[3] Y. Yamazaki et. al.,"The Electron Gun for the PNC High Power Linac", in this proceedings.
[4] Y.L.Wang et.al., "A Novel Chopper System for High Power CW Linac", in this proceedings.
[5] "Phase and Radial Motion in Electron Linear Accelerator" code modified by many contributors.
[6] Y.L.Wang et.al.,"Design of High Power Electron Linac at PNC", Journal of Nuclear Science and Technology, 30 [12] 1261 (1993).
[7] W.R.Nelson, H.Hirayama, and D.W.O.Rogers,"The EGS4 Code System", SLAC-Report-265, (1985).
[8] ALGOR ®, Heat Transfer Analysis Processor,ALGOR,INC., 150 Beta Drive, Pittsburgh, PA 15238-2932.
[9] S. Toyama et. al., "High Power CW Linac in PNC", Proceeding of the Particle Accelerator Conference, (1) 546 (1993)

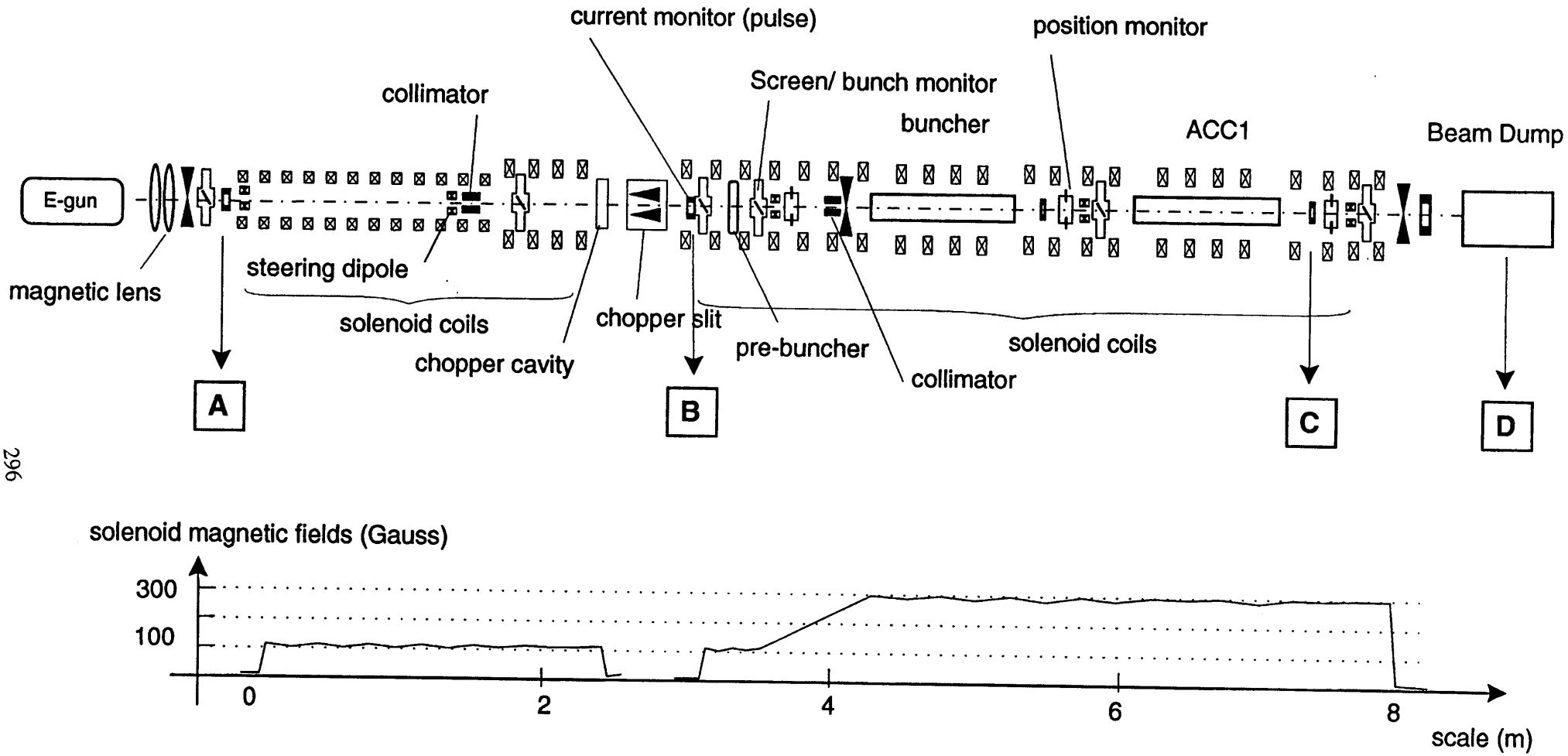

Fig. 1 Injector components and schematic.

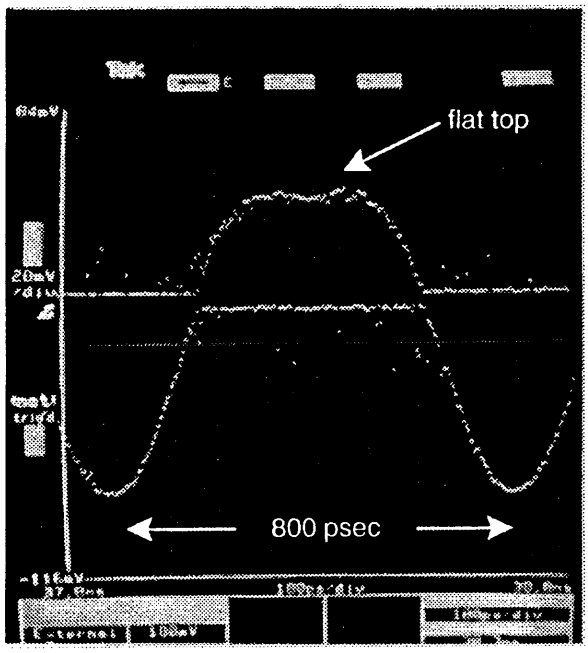

Fig. 2 Waveform in chopper cavity.

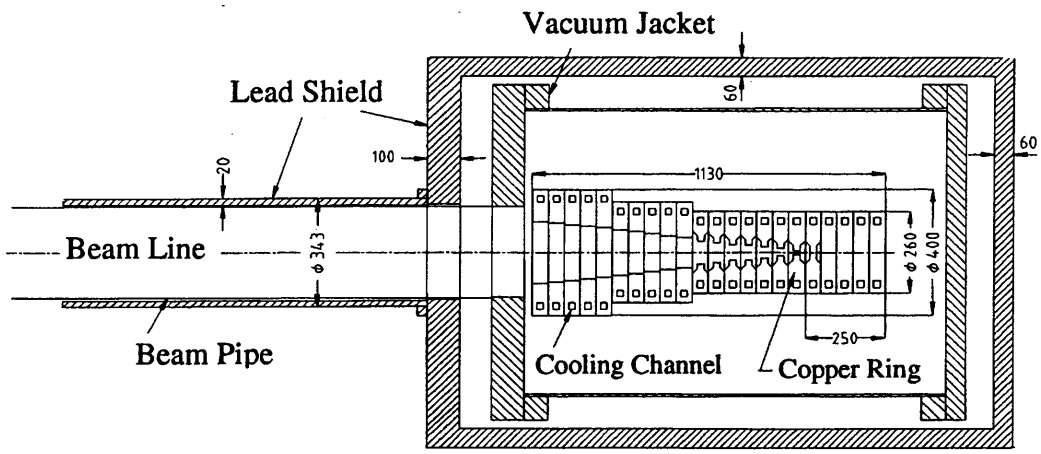

Fig. 3. A cross section view of the beamdump.

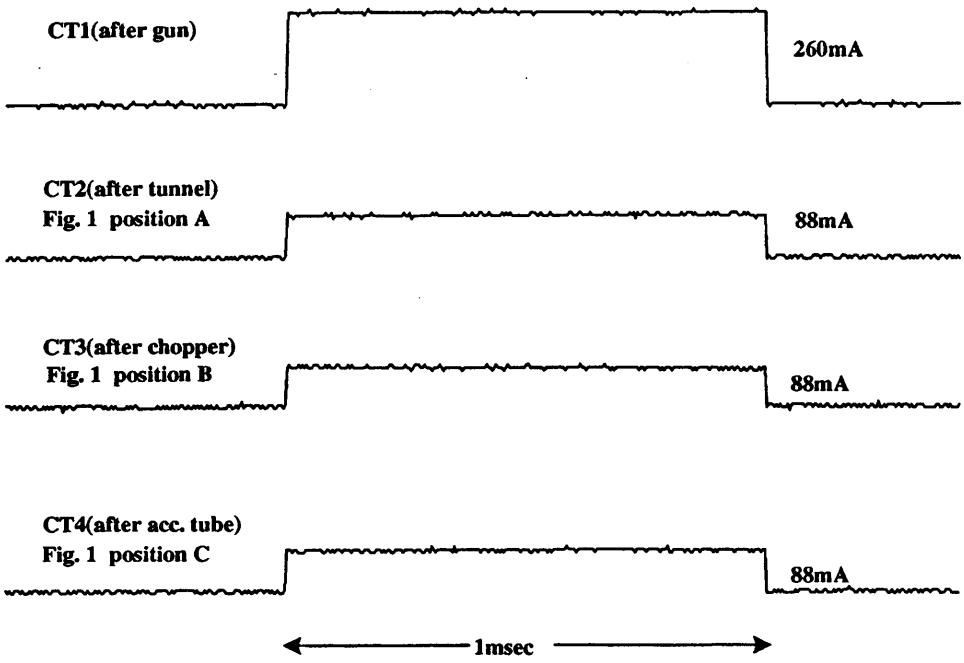

Fig. 4 The beam current in each current monitor.

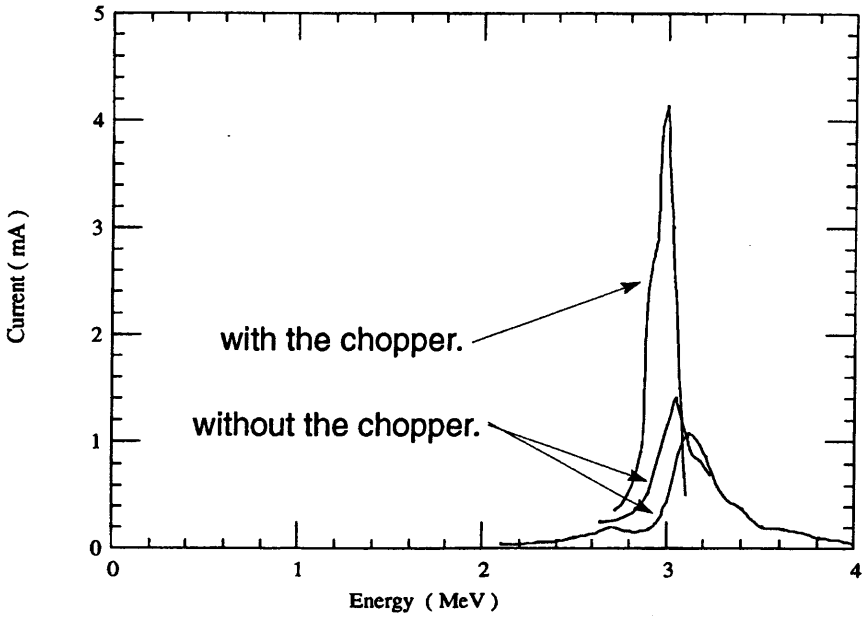

Fig. 5 Energy spectrum.

STATUS OF THE HIGH INTENSITY PROTON LINEAR ACCELERATOR DEVELOPMENT IN JAERI

J. Kusano, M. Mizumoto, K. Hasegawa, N. Ito, H. Oguri,
K. Mukugi, Y. Touchi and H. Ino

Proton Accelerator Laboratory
Japan Atomic Energy Research Institute (JAERI)
2-4 Shirakata, Tokai-mura, Naka-gun, Ibaraki-ken, 319-11 Japan

Abstract

JAERI has been proposed a high intensity proton linear accelerator to be utilized in future accelerator-driven Partitioning and Transmutation (P&T) system. The R&D of the high intensity proton accelerator was started in 1991 as one of the approaches for the OMEGA program in Japan. The first phase of the R&D has been made successfully on the components of the front-end part of the accelerator i.e., an ion source and RFQ, resulting in the peak current of 70 mA with duty factor of 7~10 % operation was obtained at the energy of 2MeV after the RFQ acceleration.

In these years, JAERI has been planned the Neutron Science Research Program (NSRP) for exploring basic researches and nuclear waste transmutation technology based on a next generation spallation neutron source driven by the high intensity proton linac. The conceptual design of the high intensity proton accelerator is rearranged slightly to achieve various operation modes in the NSRP. The second phase R&D has been started for the study of whole accelerator system with 1.5GeV and 10mA, beam power of about 15 MW. This report describes the summary of the first phase R&D and the present status of the second phase development of the high intensity proton linear accelerator.

Introduction

A progress of the technology in the field of charged particle accelerator gave a possibility of high intensity neutron source by nuclear spallation reaction. In 1980's research activities have been made for high intensity proton linacs to be applied to the nuclear fuel breeding and high-level long-lived radioactive waste transmutation. One of the approaches for the OMEGA program in Japan, JAERI has been carrying out the design study of an accelerator-driven nuclear transmutation system of minor actinides. The required beam current to drive a subcritical nuclear reactor for Partitioning and Transmutation (P&T) system is more than 40mA by preliminary evaluation. The initial concept of the high intensity proton accelerator to be used for the OMEGA program is a pulsed linear accelerator with an energy of 1.5GeV and an average current of 10mA (peak current of 100mA with 10% duty factor).

The average proton beam current of 10mA with the energy of above 600MeV is much higher than those for the present operating machines in the world. Most important issue in the proton accelerator is the handling of an intense beam with lower beam loss rate. The velocity of the accelerated proton is changed along with the beam energy. When the energy reaches at 1.5GeV, the velocity still does not get to the light speed. Acceleration method and accelerator structure must be changes to match an effective acceleration and in particular to keep low beam loss rate. In addition, the beam current and the beam quality of the high intensity accelerator are mainly determined by the low energy part of the accelerator because of the space charge effect. The stepwize development for the high intensity proton accelerator has been planned in JAERI. The first phase development was assigned to develop a low energy part components such as a high current and a low emittance ion source, a high peak current RFQ, a DTL hot test model and a high power RF source with a frequency of 200MHz.

To make the best use of the high intensity proton accelerator, JAERI has been proposing the Neutron Science Research Program (NSRP) in these years aiming at the exploring basic researches and nuclear waste transmutation technology by means of the proton accelerator application. The second phase R&D of the high intensity proton accelerator has been started to associate the accelerator design and the NSRP issues[1]. The various proton beam conditions are required such as high peak current, variable intensity, short pulse (less than μs), long pulse (2~3 ms) or continuous wave (CW) beam to realize the experiments in the NSRP. Figure 1 shows a conceptual layout of the accelerator for the NSRP.

The conceptual profiles of the accelerator are; 1) energy and current of the accelerator are 1.5GeV and about 10mA respectively, 2) positive and negative ion beam are simultaneous accelerated with a peak currents of 30 mA,

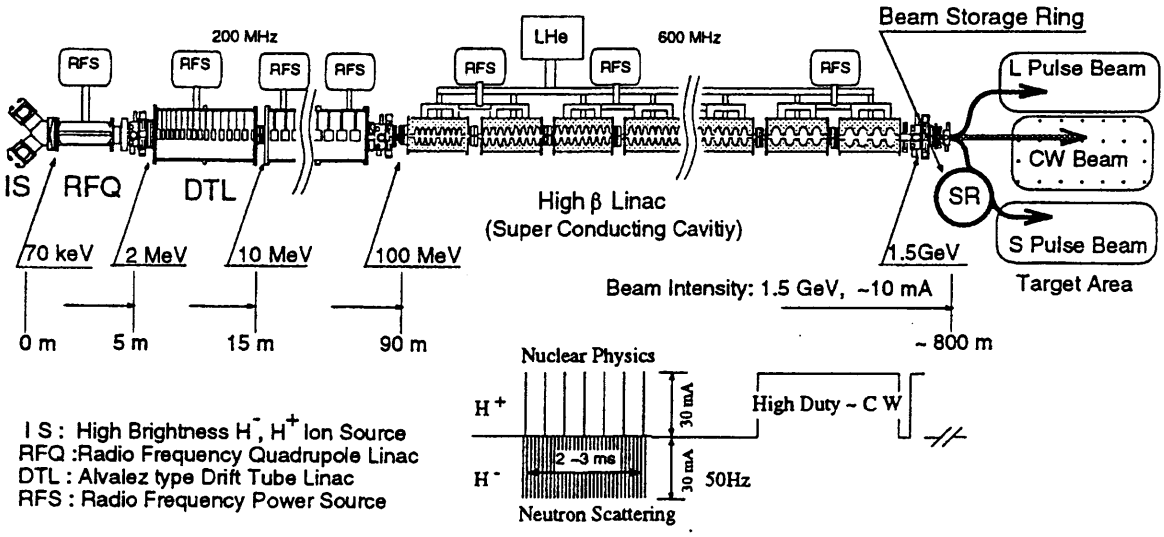

Fig. 1 A Condeptual layout of the Accelerator for the JAERI NSRP

3) main option of the high energy accelerating structure above 100MeV region is a superconducting cavity system, 4) a beam storage ring is used to make an intense short pulse neutron and 5) the development for CW proton accelerator is kept in mind to apply a driver of future transmutation system. Preliminary parameters for the NSRP accelerator are given in Table 1.

Table 1 A preliminary specification for the JAERI NSRP accelerator

Energy	1.5 GeV
Accelerated particle	Negative and positive hydrogen ion
Average current	1st stage: 1 mA 2nd stage: 10 mA maximum
Peak current	Nominal 30 mA
Low energy part	Normalconducting linac / 200 MHz
High energy part	Superconducting linac / 600 MHz
Beam operation mode	1st stage: Pulse mode operation 2nd stage: CW / Pulse mode operation
Repetition rate	50Hz maximum
Macro-pulse width	2 ms (at 1mA operation) to CW maximum
Intermediate pulse width	400 ns (interval 270 ns)
Chopping factor	60 %

The development of the technologies for the nuclear waste transmutation system is one of the major subjects of the NSRP. In the scale of the NSRP, the R&D experiment for a P&T target system, cross section measurement of minor actinide (MA) nucleus and basic reactor physics experiments with MA fuel subcritical reactor will be made by using the high intensity proton accelerator.

General Aspects of the R&D

The low energy accelerator components have been developed since 1991 for the R&D to study the front end of the accelerator. An ion source, an RFQ, and an RF source for 10 % duty factor operation were fabricated and 2MeV beam tests have been performed[2]. The characteristics of the RFQ such as beam current, energy spectra and emittance have been studied. The layout of the RFQ beam test is illustrated in Fig 2. To demonstrate the RF characteristics and the cooling capability at the high duty factor operation, a DTL hot test model with 9 cells was fabricated and high power tests were carried out.

The present activity of the second phase R&D attempts a high current negative hydrogen ion source development, high duty factor (up to CW mode) component development in the low energy portion (for RFQ and DTL), superconducting accelerating cavity development and evaluation of high current proton beam dynamics for the conceptual accelerator design.

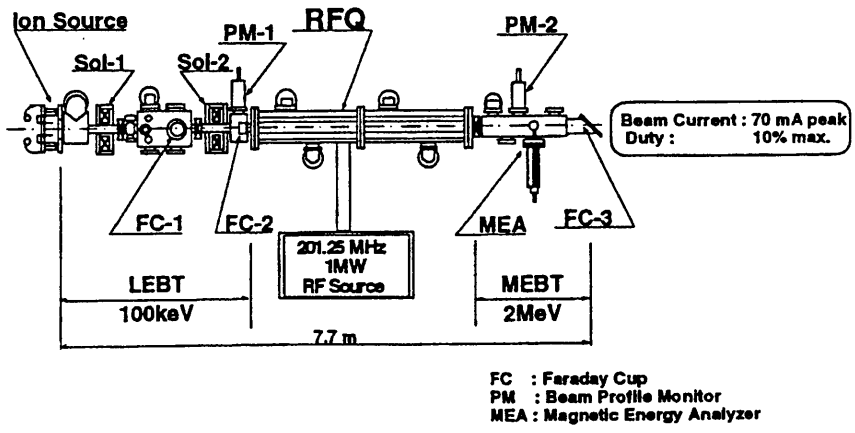

Fig. 2 A Schematic Layout of 2 MeV RFQ Beam Test Line

Ion Source

A multicusp type hydrogen ion source with two-stage extractor has been developed to obtain a high brightness proton beam. The ion source has been operated successfully with more than the designed current of 140 mA at 100 keV[3]. Normally, the ion source is operated by pulsed mode with a duty factor of 10 % to inject into the R&D 2MeV RFQ. Fundamental capability of the ion source allows an operation with a CW mode. This work was carried out in collaboration with the JT-60 NBI group of JAERI. A typical beam extraction characteristic of the ion source is shown in Fig. 3

To inject the beam into a beam storage ring at a beam energy of 1.5 GeV for applications of the basic researches, a high brightness negative hydrogen ion source is required. The development of the negative ion source has been started[4]. The structure of the negative ion source is based upon the multicusp type hydrogen ion source and the first beam test of the negative ion source coupled with the R&D RFQ is scheduled at the beginning of 1997.

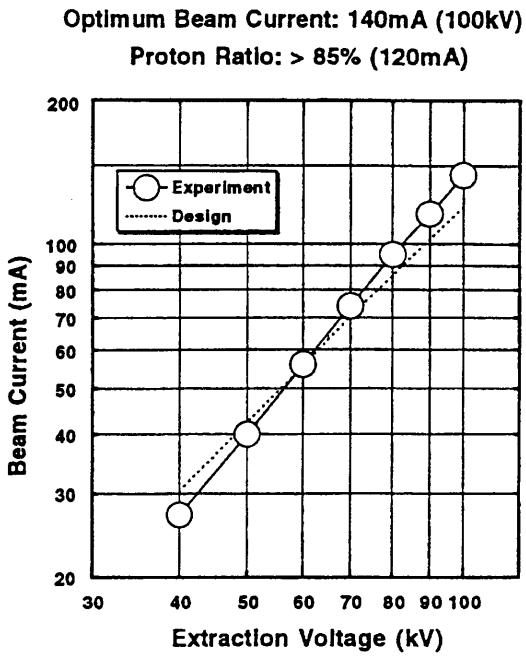

Fig. 3 A Proton Beam Extraction Characteristics of the Multi-cusp Ion Source

RFQ

The R&D RFQ is a four-vane type and its frequency is 201.25 MHz. It is designed to accelerate 100 mA (peak) of protons to 2 MeV with a duty factor of 10 %. After the low power tuning and the high power conditioning, the beam tests have been made at JAERI since November 1994. The maximum RFQ output current was 80 mA at the ion source extraction current of 155 mA. The energy of the proton beam from the RFQ was measured by a compact magnetic energy analyzer installed in the Medium Energy Beam Transport (MEBT). The energy resolution is assumed to be 5 % for 2 MeV proton beam. The RFQ beam emittance has been measured by the conventional double-slit type monitor. Typical value of the normalized rms emittance for the RFQ beam were X-X' = 0.62 πmm-mrad and Y-Y' = 0.76 πmm-mrad at 80 cm downstream of the RFQ.

At the beginning of the beam test in JAERI, the maximum duty factor was limited to less than 2 % due to the partial burn out of the RF contact at the RFQ. A silver plated spiral type RF contact, which is made of beryllium copper alloy, was used between the tank and the vane. The diameter of the contact was 3.2 mm and the thicknesses of the base beryllium copper alloy and the silver plate were 100μm and 30 μm, respectively. To improve the heat transfer properties, the RF contact was replaced by a 100μm thickness silver-plated type. In addition to the contact replacement, copper blocks were installed to cover the open space between the vane and the tank to reduce the heat dissipation at the vane end region. As a result of these modifications, steady operations with 7 % duty factor, and short-duration operation at 10 % duty factor can be achieved at the beam current of 70 mA.

A high power test model of CW-RFQ of 50cm in length is fabricated and tested in 1996 to demonstrate the manufacturing technique and the RF characteristics.

RF Power Source System

A 201.25 MHz RF system was designed and manufactured for the RFQ beam tests and the DTL high power tests. A tetrode, 4CM2500KG (EIMAC), is used in a final-stage amplifier[5]. Dummy load tests were completed resulting in a peak RF power output of 1 MW was achieved at a duty factor of 0.6 % and high duty operation of 12 % with an RF power of 830 kW was generated, which satisfied the requirement for the tests in the R&D. The power efficiency was 60 %, which is in good agreement with the designed value of 62 %.

The voltage and the phase stability during the beam acceleration should be controlled within ± 0.5 % and ±1 degree, respectively. To satisfy these specifications, the RF control system has a feedforward-circuit combined with a feedback-circuit. The performance of the feedback-circuit was examined in the RFQ beam tests. The amplitude and the phase errors were on the order of 0.5 % and 5 degree, respectively, during 100μs period after the beam injection when the beam loading was 110 kW.

DTL

A high power test model of DTL with 9 cells, which is a mock-up of the low energy portion of the DTL, has been fabricated to study the RF characteristics and the cooling requirements. A DC excited electromagnetic quadrupole using a hollow conductor (5 mm x 5 mm) was developed successfully for the focusing magnet, of which field gradient is 80 T/m with 5.5 turns at 780 amperes. The high power tests were carried out with the RF power source[6]. Fig. 4 shows the schematic layout of the test. At first, the duty factor had been limited to less than several percent due to the RF contact problem at the end plate. After an improvement of the RF contact structure, RF power of 128 kW with a duty factor of 20 % was fed to the model without any troubles, this power corresponds to the average axial field of 2 MeV/m. The gap voltage was estimated to be 195 kV at an RF power of 128 kW by a spectrum measurement of Bremsstrahlung X-ray from the model, which was in good agreement with the calculated value of 197 kV by the SUPERFISH code. The measured RF power dissipation in the each drift tube and the end plates was in good agreement with the calculation. The calculations were performed with the combination of the thermal deformation from the ABAQUS FEM code and the frequency shift from the SUPERFISH code. These high power test results have confirmed the heat dissipation calculation and the cooling design of the DTL.

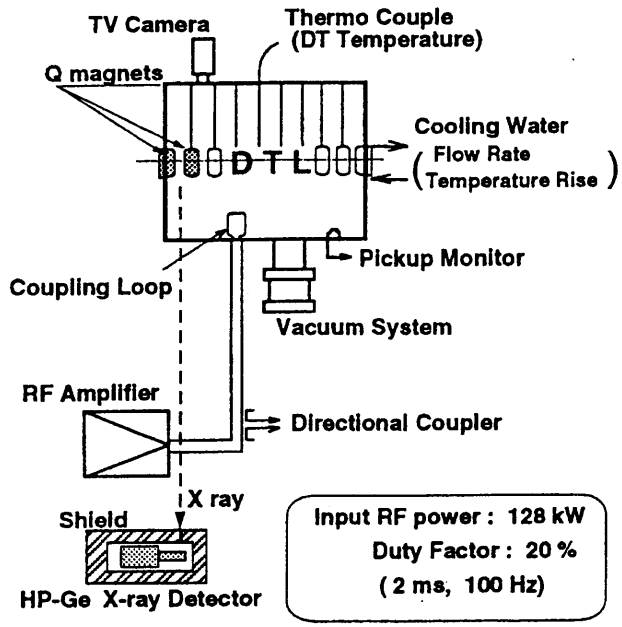

Fig. 4 Schematic Layout of the DTL High Power Test

To extend the capability of CW operation based upon the previous DTL design parameters, a cold model of CW-DTL will be fabricated in 1996 to examine RF characteristics. Accelerating gradient of the CW-DTL may be lowered to be 1.5 MeV/m in order to reduce the RF consumption and the RF heating. The end point energy for the DTL is 100 MeV which will be determined from the beam dynamics and mechanical consideration of the high energy structure.

Superconducting Cavity

Superconducting (SC) cavity is a main option for high energy portion of the accelerator. Resulting with basic studies for the structure of high energy part of the accelerator, several favorable characteristics were pointed out with SC option in comparison with normal conducting cavity option. There are a high electrical field gradient for beam acceleration of 10 to 25 MeV/m, high quality factor of ~10^9 and acceptable wide beam tube aperture of 100 to 180 mm.

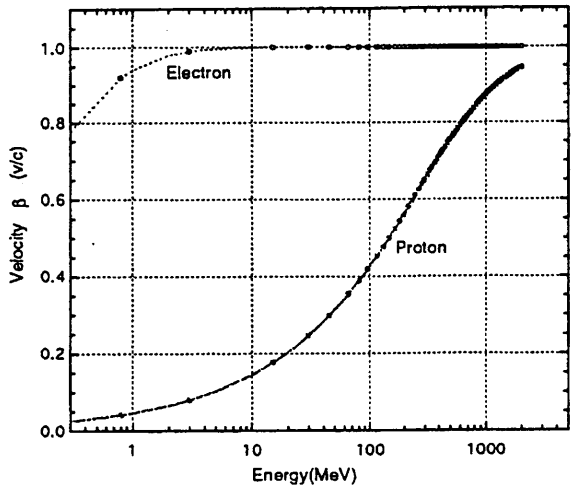

Fig. 5 Accelerating Particle Velocity

In the CW electron accelerator, technologies of SC accelerators are established. The experiences of design, manufacturing and operation for the electron SC accelerator are accumulated for years such as KEK-TRISTAN and other many laboratories[7], [8]. The high energy part of these electron SC accelerator operates single velocity of light speed. This condition leads uniform cavity shape and uniform cryomodule design for all accelerating cavity structure. In the proton accelerator, however, velocity varies sequentially from 100MeV to 1.5GeV. Fig. 5 illustrates the velocity changes in accelerating electron and proton. Accordingly, the length of the cavity also changes. Main concern is the mechanical strength of the cavity under the vacuum load for the energy range of 100 to 200MeV because of the more flatter shape than electron accelerator's one.

The R&D work for SC accelerator has been started since 1995 in collaboration with KEK SC group[9]. The mechanical structure calculations with the ABAQUS code have been done to determine the cavity shape parameters as well as electromagnetic ones with the SUPERFISH code. The schematic drawing of the JAERI SC accelerator cryomodule is shown in Fig. 6. Niobium superconducting test cavity for the 150MeV region will be fabricated and

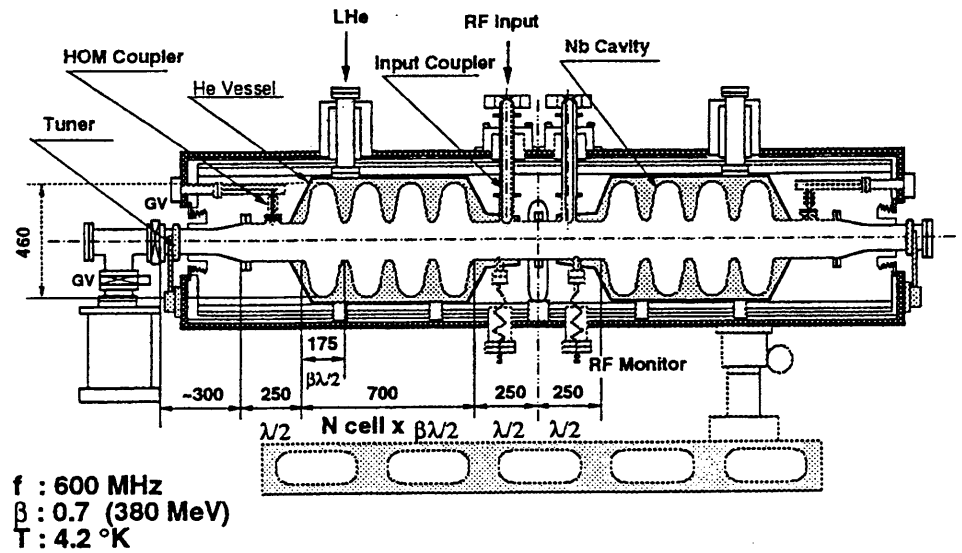

Fig. 6 A Conceptual Drawing of the Proton Accelerator Superconducting Cavity and Cryomodule

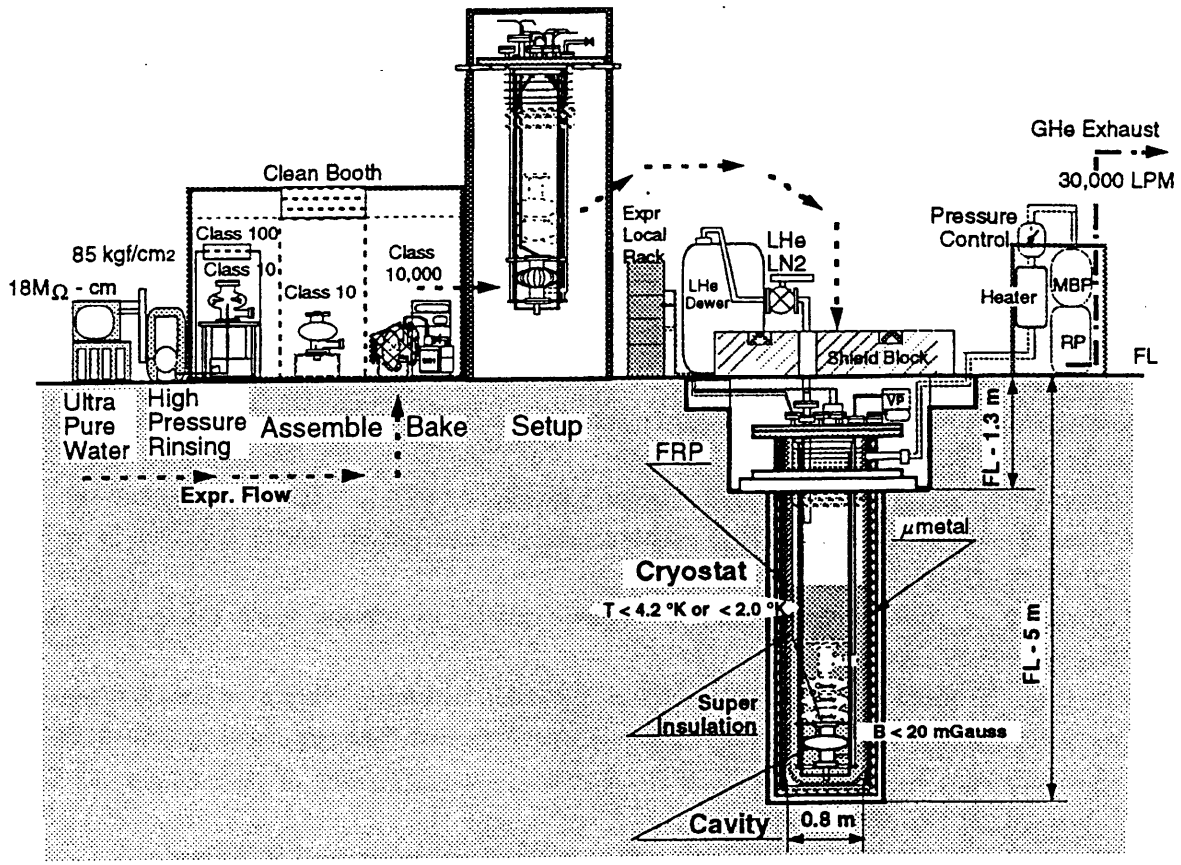

Fig. 7 An Image view of a Superconducting Cavity Vertical Test

examined in 1996 according to the preliminary design. A test stand for the vertical tests of 600MHz cavities has been installed at JAERI with a cryostat of 80 cm in diameter and 350 cm in depth.

The temperature of the vertical test for SC cavity experiments can be adjusted at 2 °K or 4 °K by evacuating the liquid helium vessel. A clean room of class 10 to prepare the clean surface of a test SC cavity with an ultra pure water of 18 MΩ-cm generating system, a high pressure of 8.5 MPa water rinsing system and an oil-free ultra high vacuum of 10^{-9} Pa pumping system was installed. An image view of the SC cavity preparation work and the vertical test set-up are shown in Fig. 7.

Summary

The first phase R&D with the design and the fabrication of the prototype accelerator structures (ion source, RFQ, RF source and DTL) have been carried out. The good performance of the components has been confirmed. In the RFQ beam tests, acceleration current of 70 mA with a duty factor of 7 to 10 % has been achieved.

Since 1995, the basic specification for the accelerator has been changed to match the NSRP in JAERI such as negative and positive ion simultaneous acceleration, variable beam intensity, SC cavity option and storage ring. The second phase R&D work has been started. For the injector of the SC cavities, much longer duty factor or CW beam operation will be required. Design work on the RFQ and DTL for the CW operation is being performed. Negative hydrogen ion source beam acceleration test coupled with 2MeV RFQ beam line is planned in 1997. SC cavity development has been started to establish mechanical property and electromagnetic performance for energy range of 100 MeV to 1.5 GeV with a frequency of 600MHz.

Acknowledgment

The authors would like to thank Drs. S. Noguchi, K. Saito, E. Kako and M. Ono of KEK for discussion and help on the SC cavity development. They also thank Drs. T. Kato, Y. Yamazaki of KEK and Dr. R. A. Jameson of LANL for valuable suggestion about the beam dynamics calculations and accelerator system optimization.

References

[1] M. Mizumoto et al., "A High Intensity Proton Linac Development for Neutron Science Research Center", 2nd Int. ADTT Conf. 2-7 June 1996, Kalmar, Sweden.

[2] K. Hasegawa et al., "First Beam Test of the JAERI 2 MeV RFQ for the BTA", 1994 International Linac Conference, Tsukuba, Japan, pp.113-115 (1994)

[3] H. Oguri et al., "A High Brightness Hydrogen Ion Source for the BTA at JAERI", ibid., pp.381-383

[4] H. Oguri et al., "Development of a High Brightness negative Hydrogen Ion Source" Rev. Sci. Instrum. 67(3), p1051 (1996)

[5] Y. Touchi et al., "An RF system for the BTA", Fourth European Particle Accelerator Conference, London, 1994, pp.1900-1902 (1994)

[6] N. Ito et al., "Fabrication and Tests of the DTL Hot Model in the R&D Works for the Basic Technology Accelerator (BTA) in JAERI", 1994 International Linac Conference, Tsukuba, Japan, pp.119-121 (1994)

[7] Kojima. Y, et al. : "Upgrading of TRISTAN by Superconducting RF System", Particle Accelerator Conf. Chicago, p1789-1791 (1989)

[8] Dylla. H. F., et al. : " Operating Experience with High Beta Superconducting RF Cavities" Particle Accelerator Conf. Washington DC, p748-752 (1993)

[9] N. Ito et al., "Development of a Superconducting Cavity for the High Intensity Proton Linac in JAERI", Proc. of 1996 International Linac Conference, Geneva, Switzerland

Code Development and Design Study on Accelerator-driven Transmutation Resaerch at JAERI

T. Nishida, T. Sasa, T. Takizuka, H. Takada, K. Tsujimoto

Japan Atomic Energy Research Institute
Tokai-mura, Naka-gun, Ibaraki-ken 319-11, Japan

Abstract

The calculation models in the cascade code NMTC/JAERI have been improved on bases of the new nuclear theory and new measured data. The intranuclear nucleon-nucleon scattering process calculation has been modified taking into accounts the effects of reflection and refraction of nucleon in nucleus and nucleon-nucleus scattering cross section. The preequilibrium process model was adopted to improve the prediction about nucleon back scattering. Adjustment was made for parameters in the high energy fission model and the adoption of total reaction cross section estimated systematically. Some benchmark calculations were carried out to verify the peidiction capability of the modified cascade code. The ACCEL code system for designing an accelerator-driven system has recently been upgraded as the ATRAS system. The Sn transport code TWOTRAN2 and Monte Carlo transport code MORSE have been replaced by new codes TWODANT with faster computation time and MCNP4A with the continuous Monte Carlo method repectively. The 73 groupwised cross sections upto 20 MeV have newly been produced to be used with the TWODANT code. The burnup code BURNER linked with TWODANT was also prepared well.

The conceptual design study on proton accelerator-driven transmutation systems with nitride fuel and new molten salt of minor actinides were carried out as another promising options. The solid fuel system consists of a sodium-cooled subcritical core with pin-bundle type assemblies of actinide nitride fuel and a multi-layer type spallation target of tungsten. It is expected to have the better thermal charachertistics than metal fuel system. When the system is driven by several tens mA proton beam with an energy of 1 GeV, amounts of minor actinides transmuted per year and the power generation were given respectively. The burnup calculations upto 300 days and the preliminary dynamics analysis were performed to examine the transmutation capability and tne nuclear safety in this system. The nuclear characteristics of the system with MA-$PbCl_3$ type chrolide molten salt fuel was examined and compared with MA-NaCl type one researched already.

1. Introduction

According to the national research and development program OMEGA on partitioning and transmutation [1], the research activities on the accelerator-based transmutation technologies are being promoted at JAERI in the following items,

(1) Development of simulation code system including the spallation cascade code,
(2) Design study on accelerator-based transmutation system,
(3) Spallation experiment with high energy proton beams [2-3],
(4) Development of an intense proton linac (1.5 GeV, 10 mA). [4]

In the present paper the recent works on the conceptual design study of the transmutation system and the development of the design code system are reported. Descriptions on the items (3) to (4) are given at other sessions in this meeting.

As well known, the calculation for designing the accelerator-driven transmutation system must treat the nuclear proocess in the wide range from ~eV to a few GeV. Unfortunitely there is not yet the single code that covers all reaction and transport in the energy range because of few available nuclear data in the high energy range. For the sake the hadron cascade code simulates the nuclear reaction and particle transpoet in the energy range higher than 20 MeV. Its prediction accuracy affects heavily on estimation of ability of accelerator-based transmutation system. So the cascade code NMTC/JAERI [5, 6] has been recently upgraded, taking into accounts new experiment data and calculational model, and the new version code named NMTC/JAERI94. In order to calculate the nuclear process in the accelerator-based system, the code system ACCEL [7] had been originally developed at JAERI before~ 1985 and includes the NMTC/JAERI and the neutron transport codes corresponding to ENDF-B4. To calculate more accurately and efficiently the nuclear reaction and particle transport process in the accelerator transmutation system over the energy range, the "ATRAS"(code system) has been recently developed at JAERI by adopting more powerful codes and the nuclear data library urgraded for higher actinides.

The radioactive nuclides to be transmuted in the JAERI transmutation research program are MAs such as ^{237}Np, ^{241}Am, ^{243}Am, ^{243}Cm, ^{244}Cm, ^{245}Cm and Long-Lived Fission Product (LLFP) such as ^{99}Tc, ^{129}I wtih half lives between a few hundred years and several million years. MA should be transmuted through fission reactions because the transmutation of MA by neutron capture has the possibility of increasing higher actinides. For designing the accelerator transmutation system at JAERI, we adopted the design guide lines as

(I) application of spallation neutrons to transmutation system,
(II) exclusive system for MA and long-lived FP burning,
(III) self-supporting system in energy ,
(IV) transmutation rate of MA (260 kg/y) from ten units of 1 GWe LWRs.

Fissioning of MA, which is a non-fissile material for thermal neutrons, occures dominantly to neutron capture above the threshold energy of about 500 keV. So JAERI selected the transmutation method of MA by fast fission reactions controlled by spallation neutron source although it requires the large initial MA inventory. LLFP can be transmuted only through thermal neutron capture to stable nuclides because of small capture cross sections for fast neutron. From the reason the thermalized neutron region may be set up around fast subcritical target/core to transmute MA and LLFP simultaneously in one system.

The design studies for two different types of accelerator-driven transmutation system, that is, solid fuel type and liquid fuel type, are being carried out at JAERI. The solid MA (alloy, nitride) fuelled system is composed of tungusten target and solid fuel subassemblies like fast reactor for MA burning. Its R&D works are considered to be the relatively short term project, except an intense proton accelerator, since most of technologies and know-hows already obtained in the fast reactor development can be effectively apllied to perform the design study of this type system. The system with the liquid fuels will be developed in the long term project. The molten salt system is expected to be the more promising transmutation system with possibility of on-line fuel reprocessing but of containing more problems to be resolved than the solid fuel one. The liquid alloy fuel system has a graphite moderator blanket to transmute LLFP by using thermalized neutrons. Both liqud fuel systems have the active, subcritical core region with the hard neutron energy spectra.

For the proton beam-controlled core operated in the subcritical mode, some advantages are considered in the following,

(a) No control rod, no safety rod, simple core configuration,
(b) Large flexibility in the core design due to less severe requirement to reactivity coefficient,
(c) Operation stop by shutting down the proton baem,
(d) Less limitation to the burnup time of fuel and
(e) Mild requirement to the fine adjustment of fuel composition.

2. Development of code system for desiging the accelerator-driven tranamtor [8)-10)]

In the intranuclear cascade calculation in the NMTC/JAERI code, the nuclear medium effect for nucleon (N) scattering in a nucleus was sutdied and the accuracy of perdictions of reactions induced by lower energy protons was improved. For the the OECD/NEA code intercomparison task force, the benchmark calculations on the proton-induced nuclide production cross sections in some targets at the energy of 20 MeV to 5 GeV were carried out using the HETC/3STEP code. The calculated cross sections for heavier resultants had good agreements with experimental one except the accuracy of producing lighter nuclides. Neutronic calculations below 20 MeV in the transmutation system are carried out using the well-prepared transport code connected with the cascade code. Here informations about spallation neutrons with energies below 20 MeV is transfered from the cascade code to the neutron tanasport code as source neutron terms. For the calculation in the entire energy region, more excellent new code sytem ATRAS, including the new version cascade code and the 73 groupwised cross sections below 20 MeV extending the JAERI-fast set corresponding to the JENDL3.2, has been newly developed.

2.1 Improvement of cascade codes

For the energy region above 20 MeV, the spallation reaction with many reaction channels occurs dominantly as shown in Fig.1. However there is few nuclear reaction data in this range for various nuclides. At present the best way to analyze these high energy processes is to use the cascade simulation codes. JAERI is using the NMTC/JAERI (High Energy Nuclear Rreaction and Nucleon-Meson Transport Code)and NUCLEUS (only intranuclear cascade). The Bertini model in the cascade code [11)] successfully had treated the intranuclear cascade(INC) above 200 MeVof incident particles, using " two-bodies collision approximation between nucleons in a nucleus. Since the nucleons with the energy of 20 MeV to 200 MeV in a nucleus have gradually more wave-like nature, the disagreement between experimental data and predictions calculated by the INC model becomes larger. Some of calculation models and collision cross sections in the simulation code were installed before ~1975.

They have been improved and upgraded by the newly developed nuclear theory and the data measured on the recent high enegry experiments in the following items,

a) adoption of the in-medium nucleon-nucleon scattering cross section ,
b) the effects of reflection and refraction of nucleon in nucleus,
c) addition of preequilibrium process based on the exiton model,
d) modification of high energy fission model (Nakahara model),
e) replacement of original total cross section by Parlstein's systematics one,
f) adoption of level density parameter a_0 by Baba and new mass formulas.

In the original INC calculation the mean free path (mfp) for nucleon collision in a nucleus was approximated by the nucleon(N)-nucleon(N) scattering cross section in free space. The influence of nuclear matter mean field (nucleon-nucleus collision) becomes larger for an incident nucleon with less than ~200 MeV. So the parameterized in-medium N-N cross sections dependent on nucleon energy [12) - 15)] have been installed through the subcode ISOBAR into NUCLEUS to compare more accurate calculation data with recent experimental ones. Figure 2 shows the in-medium total neutron-proton cross sections in the energy range of 50 to 300 MeVcalculated by taking into accounts the nucleon-nucleon pairing effect. The use of upgraded cross sections result in prolongation of mfp of nucleon in a nucleus. In Fig.3 the calculated angular distributions of emitted protons with 60 MeV are compared with experiment one in the Au thin foil bombarded by 100 MeV protons[16)]. The lines except solid line represent the contribution from each step in multiple scattering. As seen in these figures the distribution calculated by ISOBAR code with free space N-N cross section gives about a half experimental one, whereas the calculated distribution with in-medium N-N cross section agrees well with experimental one, in particular, in the backward direction. Figure 4 compared the calculated neutron production differential cross sections (DDX) with the experimental data by Amian et al.[17)] for the reaction Al(p,xn) induced by 800 MeV proton irradiations. There are some differences between both data in the energy range of a few MeV and a few tens MeV when the free space NN cross sections are used, while the result calculated with the in-medium cross section shows good agreement in each direction.

For the cross section of (p,n) and (n,p) reactions the threshold value has been adopted to treat the quasi-elastic colloision properly as many researchers suggested. The refraction and reflection effect [18)] has been also taken into acounts at boundaries assumed in a nucleus according nuclear matter density. Then a moving nucleon with a lower energy changes its direction even when crossing the boundaries. The exiton model [19) - 21)] was inserted in the Bertini INC model to consider the nucleon emission at the preequilibrium state. The calculated data using this improved version code were compared with ones measured in thin and thick (stopping

lengh) targets. Figure 5 shows e xperimental and calculated production yields of 56Co in thenatNi reaction with threshold energy of 20 MeV in the tungsten target-installed lead assembly for 500 MeV proton bombardment.22), 23) Here the letter r denotes the radius distance from the axis of cylidrical target/assembly. New version code (NMTC/JAERI94; solid line) with total cross section estimated by Parlstein's systematics reproduces experiment data better than the original version code (NMTC/JAERI ; dotted liine) with geometric total cross section. In Fig.6 experimental and calculated neutron yields are shown in the stopping length Au target bombarded by 68 MeV protons.24) The Bertini model with preequilibrium process overestimates by a factor of three to ten the experiment neutron yields at the forward angle of 15° and 30° above 30 MeV but reproduces well at the angle of 60° and 120° due to the preequilibrium contribution. The ISOBAR code with free space NN cross section reduces the neutron emission at all angles and underestimates the experimental data relatively low. The ISOBAR code with the in medium N-N cross section parameterized by Cugnon reproduces the experimental data quite well. Especially at angles over 30° the calculation is in excellent agreement with the experiment and even at the angle of 15° still gives the lower neutron yield by 30 % than experiment. The applicability of The INC model foe both thin and thick target calculations was extended down to the incident energy of 68 MeV by the inclusion of the medium effects in terms of the relection and refraction and the in-medium NN cross sections.

The cascade code calculates also the high energy fission (HEF) reaction as competing process for particle evaporation reaction in an excited nucleus at equilibrium state after intranuclear cascade ceased. We have done the modification of HEF (Nakahara) model by adjusting the parameter in the the model and adopting of total reaction cross section revised by the systematically estimation. Experimental data of fission cross sections for ^{238}U(p, fission) in the high energy from 10 MeV to 10 GeV were surveyed and compared wtith predictions by both cascade codes of NUCLEUS and HETC/KFA2 as seen in Fig.7. Although experimental data are relatively distributed among authors, both code's predictions agreed within 50 % to them. It was often pointed out that the original Nakahara HEF model gives flatter mass distribution of residual nuclides than other model such as Atchison's one in HETC/KFA2[25]. In this model the mass distribution in actinide fisson reaction is calculated by superposing three Gaussian ones with different central values and a half width$<W_{1/2}>$(= E - E_f+ 7, E; excitation energy, E_f; fission barrier height). The adjustable parameter $< W_{1/2} >$ has been searched by changing E to be fitted to experimental data for ^{238}U(p, fission) reaction with a 300 MeV proton [26] as shown in Fig 8 and fixed to be $< W_{\mathbb{E}} >$(E_{max}=15 MeV) for E>E_{max}. The mass distribution for ^{238}U(p, fission) reaction with proton energy of 2.9 GeV was calculated by this adjusted model in NUCLEUS to compare the adjusted result with experimental data [27] as seen in Fig.9 and both distributions showed farely the good agreement. This fact suggests that the excitation energy stored in an actinde has the maximum value, at least for high energy fission process. In calculating the Fission probability from the statistical theory, the level density parameter a_0 makes an important role. The a_0 dependent on mass number A was replaced from the value proportioal to A to Baba's estimated data. [27]. Figure 10 shows experimental fission cross sections from 1 MeV to 10 GeV for ^{235}U(n, fission) and ones predicted with Baba's data.

2.2 Benchmark calculations of cascade codes

For the OECD/NEA code intercomparison task force[28], proton-induced nuclide production cross sections in the targets made of mono nuclide such as ^{16}O, ^{27}Al, ^{nat}Fe, ^{59}Co, ^{nat}Zr and ^{197}Au were calculated at incident encrgies of 20 MeV to 5 GeV with the HETC-3STEP code[29]. This code was improved at JAERI to include the preequilibrium process in the original HETC code and newly to employ the level density parameter introduced by Ignatyuk[30], the atomic mass table of Audi and Wapstra[31] and the mass forrmula given by Tachibana et al.[32]. The HETC-3STEP code cannot estimate the production of isomar because the level structure of a nucleus is not considered in the evaporation model. Consequently the isomar production was not calculated.

The cross sections were calculated at 39 incident energies. The number of incident protons was chosen as 250,000 for ^{16}O, ^{27}Al and ^{nat}Fe, 200,000 for ^{nat}Zr and ^{197}Au, and 50,000 for ^{59}Co, respectively. In Figs 11 to 13 the cross sections calculated with HETC-3STEP are compared with the experimental results for the productions of ^{7}Be, ^{89}Zr, ^{190}Ir and ^{197}Hg in the ^{197}Au target. As seen in Fig. 11, this code cannot estimate the ^{7}Be production because of lack of the fragmentation process model. The similar discrepancies are observed for all the other tragets. For the ^{89}Zr production, the HETC-3STEP reproduces the experimental result quite well in Fig 12. Aithough the high energy fission of sub-actinide nuclides is taken into account in HETC-3STEP, the calculated result indicates that the present fission model is applicable to the estimation of the medium-mass nuclide production by the spallation reaction of a heavy nuclide. It is observed in Fig. 13 that HETC-3STEP's results also agree well with the experimental ones of the ^{190}Ir production. Even for the other nuclides in the mass range

of 177 to 197, a fairly good agreement with a factor of two to three is obtained between the calculated and experimental results. For the other target, however, ligher the mass of produced nuclides become, worse the agreement between the calculated and experimental results becomes. Therefore the accuracy in the HETC-3STEP calculation for the other targets is poorer than that of ^{197}Au even in the production of a nuclide with mass number close to the target one.

As the present intranuclear cascade/evaporation model calculates the nuclear reaction in a very classical manner, the accuracy of a factor of two to three for resultant production seems to be acceptable. In order to improve the accuracy of the nuclide production cross section in the framework of the intranuclear cascade/evaporation model, the following physical aspects should be taken into account: (i) the accurate treatment of the threshold energy of the nuclear reaction, (ii) the inclusion of the fragmentation reaction, (iii) more accurate estimation of the charged particle emission in both the INC and preequilibrium processes, (iv) more precise simulation of the statistical decay process by the use of the Hauser Feshbach model.

There are many light nuclei such as Cl in active fluid tagrets in the JAERI-type liquid transmutation system as described later. In the target region the spallation reaction of MA and light nuclei occur simultaneously in addition of fast fission transmutation of MA. So cascade calculations for the high energy hadron nuclear rection in a light nucleuus and the transport process in the dilute fluid target/core should be analyzed with the higher precision.

2.3 Development of the entire code system ATRAS

The design code system ATRAS (Accelerator-based Transmutation Reacotr Analysis System) has been developed to carry out the accelerator transmutation calculation more accurately and effectively. This system consists of the cascade code NMTC/JAERI94, Sn transport code TWODANT, Monte Carlo one MCNP4A, and the burnup code BURNER linked with TWODANT as seen in Fig. 14 . The 73 groupwised cross section set below 20 MeV was newly developed on base of the JFS-3-J2 set from the cross section library JENDL-3.2, where the connecting energy between cascade and transport codes was changed from 15 MeV to 20 MeV corresponding to the available energy in the JENDL 3.2.

The ACCEL has been revised and named the ATRAS, which is the integrated code system which can perform following calculations

1) spallation, evaporation and high energy fission processes above 20 MeV,
2) neutron transport process below 20 MeV and
3) core burnup process below 20 MeV.

The first process was calculated with the NMTC/JAERI4 code in which many modifications were applied as described above. For the calculation of the neutron transport below 20 MeV, the two-dimensional Sn transport code TWODANT[33] and the three-dimensional Monte Carlo transport code MCNP-4A[34] were selected. Both codes were modified to apply the non-isotropic volume source of spallation neutrons emitted from the target for the fixed source calculation. The effective microscopic and macroscopic cross sections needed for the transport calculation can be generated by the CSASI module from the SCAL-4 code system[35]. For the third burnup process the ATRAS code is capable for the burnup analysis of the accelerator-based transmutation systems. The BURNER code, burnup calculation module in the VENTURE[36] code system, was used for this purpose. The code was used, linking with TWODANT code to include the effect of the changes of core-averaged neutron spectrum corresponding to each burnup step.

The new file of groupwised cross sections was also prepared for the ATRAS code from the latest JENDL-3.2 library. Structure of this groupwised cross section file is almost the same as the fast reactor group constants set JFS-3-J2. Three groups were added to the energy range from 10 MeV to 20 MeV to connect smoothly the transport code with the NMTC/JAERI code. About 30 nuclides, which are necessary to calculate the JAERI-proposed accelerator-based transmutation systems, were selected from the JENDL-3.2 library. Higher actinides such as Bk and Cf and long-lived fission products (Tc-99, I-129) were also selected for this groupwised cross section file.

By using these codes we could calculate the nuclear characteristics about the accelerator driven transmutation systems in the whole energy range more efficiently and accurately. The ATRAS will be opened for outside use in the near future.

3. Design Studies on accelerator-driven transmutation system

The design studies for two different types of accelerator-driven transmutation system, that is, solid fuel type and liquid fuel type, are being carried out at JAERI.[37),38)] In the present paper the MA nitride fuelled core and the Pb-type chrolide molten salt core were researched respectively as the another promising option.

3.1 Nitride fuel system

The JAERI system concept with TRU-nitride fuel is now under study to take full advantage of the excellent thermal performance of nitride fuel. Neutronics analysis of the accelerator-based transmutation system with solid disk tungsten target and TRU-nitride fuel was performed using the ATRAS codes. This core is a cylinder in dimensions of 80 cm height and 40 cm radius, surrounded by the stainless steel reflector with thickness of 50 cm. The fuels with composition of TRU (90{Np, Am, Cm}:10Pu) -^{15}N are arranged as pin-bundle type assemblies around tungsten target in the core and cooled by sodium flow. Specifications of the core are listed in the Table 1. The target was divided into the thin-disk part and thick-part to flatten the released neutron distribution from the side surface of the target. Results of neutronics calculation are summarized in Table 2. The calculation results showed that this system with k_{eff} of 0.927 and average neutron fluxes of 2.67 x 10^{14} n/cm^2/mA can transmute about 5.18 kg/mA of TRU per year and generate a thermal power of 15.7 MW/mA in operation with the 1 GeV proton beam. TRU inventory in the core is about three times lower than the metallic fuel system because of higher density of heavy metal in the nitride fuel. Much higher power density, enough trasmutation ratio and neutron spectrum as hard as in the metallic fuel system have been gotten also. The specification of the system was proposed for a benchmark problem in the " OECD/NEA/NSC Benchmark on Physics Aspects of Different Transmutation Concepts".

3.2 Molten salt system [39)]

The system with the liquid fuel such as the molten salt is being developed as the long term project in the OMEGA plan. In the liquid target/core transmutation system using MA molten salts, there are no limitations for preventing the melt down accident of fuel and target due to local power peaking. The minor actinides (MA) concentration in molten salt fuel is lower than one in solid fuel. The power peaking around the beam-irradiated zone is not a critical factor because of the relaxed heat condition due to liquid fuel. So the high energy proton beam can be injected directly on the center of the MA fuelled zone where there is no target region with the definite boundary. The concept of an advanced MA molten-salt system has been studied to apply the advantages of a simple fluid target/core to the transmutation system. The flowing MA molten salt forms the subcritical core and itself acts also as spallation target and primary coolant circulating between target/core and heat exchanger in the calculational model in Fig. 15. This system has the reaction vessel with 170 cm in height and 105 cm in radius and the stainless steel reflector with thickness of 20~40 cm. The compact heat exchanger and molten salt pump are installed inside the vessel to reduce TRU molten salt inventory. Nuclear characteristics in the subcritical core filled by the promising chloride molten salt 70PbCl_2-30TRUCl_3, with hard neutron spectrum, has been examined for the same configuration in reaction vessel to one with 64NaCl-36TRUCl_3 which was already studied as the previous case. The flouride molten salt $NaBF_3$-NaF was selected as the secondary coolant. The plotting curves in Fig. 16 (a) and (b) represent the neutron hard energy spectra in both molten salt target/core irradiated by 1.5 GeV protons and the outer torus region where the primary cooling system (heat exchangers and pumps) is installed. These regions are separated by an inner cylidrical reflector to protect the heat exchangers and pumps against high neutron flux. The neutron flux in the outer region is kept to be lower by about two orders of magnitude than one in target/core. The power density distribution in the target/core region irradiated with 1.5 GeVprotons is shown in Fig.17, where the maximum power density is about 70 MW/m^3 at proton current of 1 mA. This system with k_{eff} of 0.93 and 1.5 GeV-20 mA proton beam can transmute 238 kg of MA per year and produce the electricity of 228 MW sufficeint to power up the accelerator. The operating condition is compared with one in the case of 64NaCl-36TRUCl_3 fuel salt in Table 3.

As reported already, the molten salt transmutation system is expected to have the possibility of removing reaction products from the system through He purge method, Cd metal extraction method, cold trapping method and oxidation method respectively.

3.3 Burnup calculations of the JAERI accelerator-driven transmter

To examine the transmutation capability and the nuclear safety the burnup calculations were carried out in the energy region below 20 MeV for the accelerator-driven MA transmutation systems composed of tungsten target and solid nitride-fuelled core, using the BURNER-TWODANT code in the ATRAS. The one group cross sections were made by averaging the microscopic cross sections produced from JENDL 3..2 with the neutron spectrum calculated by the TWODANT and with the decay data library. From the burnup calculation, it revealed that the transmuted amount is about 300 kg of TRU annually at the constant thermal output of 800 MW through the burning period by adjusting the proton beam current. The evolution of actinide compositions with burnup

time was calculated up to 300 days. Figure 18 represents the dependences of the minor actinide compositions. It is apparent that main minor actinide ^{237}Np is reducd to about three fifth of initial inventory at 300 burningdays. The fact implies the transmutation ability of about 200 kg per year. The BURNER code in the latest version has been improved to include the fission product effects, based on the lamped FP method. Figure 19 shows the comparison of dependences of k_{eff} on the burnup time calculated by the BURNER without and with the fission product effects. The k_{eff} was recalculated by the code TWODANT for the renewed compositions of actindes on each step. It has been recognized that the system for both cases always keeps the subcritical state with sufficient margin ($k_{eff} < 0.96$) although k_{eff} swings to the positive side over this stage. It seems that the FPs produced in core due to actinide burning makes the good role to supress thereactivity swing for this short burning period.

3.4 Dynamics calculations of the JAERI accelerator-driven transmter

The dynamic analysis on the proton beam-driven subcritical transmutation system is very improtant from a point of view of nuclear safty at normal operation and accidental stiuation. The prelimary dynamic calculations were done for the metal fuelled fast reactor at subcritical stste simulating the proton beam-driven subcritical core, using the EXKARS code. The transient process of the fast reactor with the effective neutron multiplication factor k_{eff} of 0.96～0.99 and neutron source was calculated by solving the standard dynamic equation including only Doppler and coolant's temperature reactivity coefficients for some reactivity insertions.

4. Summary

The ACCEL code system calculating the nuclear process in the accelerator-driven transmutation system in the wide energy range of eV to GeV has recently been upgraded as ATRAS. For the energy region above 20 MeV the cascade codes NMTC/JAERI and NUCLEUS have been upgraded by taking into accounts the in-medium nucleon-nucleon cross sections, the effects of reflection and refraction of nucleon in nucleus, the preequilibrium process, modification of high energy fission model and Baba's level density parameter. These improvements have increased the accuracy of prediction of main parameters estimating the transmutation ability. For Neutronic calculations below 20 MeV in the transmutation system more excellent transport code such as Sn code TWODANT and Monte Carlo code MCNP 4A have newly been prepared respectively. The 73 groupwised cross sections below 20 MeV were produced for the TWODANT calculation from the JENDL3.2 library to calculate effectively the nuclear process of system with spallation neutron spectrum harder than fission neutron one. To examine the transmutation capability and the nuclear safety the burnup code BURNER linked with the TWODANT code was prepared well. By using these excellent and powerful codes we could calculate more efficiently the nuclear characteristics about the accelerator-driven transmutation system in the whole energy range.

The conceptual design studies were also carried out on two promising transmutation systems, MA nitride fuelled and MA Pb-type chrolide molten salt cores, using the ATRAS codes. The proposed prototype nitride fuel accelerator transmutation system with k_{eff} = 0.927 can transmute 5.18 kg/mA of MA per one year and generates the thermal power of 16 MW/mA when operated by the proton beam with the energy of 1 GeV. From the burnup calculation, it was shown that the TRU amount transmuted in the nitride fuel system is about 300 kg annually at the constant thermal output of 800 MW. The evolution of actinide compositions with burnup time was calculated up to 300 days. It was also recognized, from the calculation considering the FP production in the core, that the system always keeps the subcritical state with sufficient margin ($k_{eff} < 0.96$) upto 300 days. The Pb-type chloride molten salt has been chosen due to better nuclear characteristics for studying the new MA molten salt transmutation system. This system with k_{eff} = 0.93 can transmute about 238 kg/y of actinides and generates the electric power of 228 MW in operation with a 20 mA proton beam with an energy of 1.5 GeV. The prelimary dynamic calculations was started for the subcritical fast reactor simulating the proton beam-driven subcritical core.

Aknowledgement

Authors express the great appreciation for helpful discussions with for Dr.s M. Mizumoto, T. Mukaiyama, Y. Nakahara, H. Katsuta, Y. Kato, O. Sato and Mrs. S. Meigo, N. Yoshizawa.

References

1) Yoshida, H., et al., " A Strategic Study of the Partitioning and Transmutation System being Developed at JAERI," OECD/NEA/P&T REPORT No.7, pp.79 (1992) .

2) Takada, H., Kanno, I., Hasegawa, K., and Sasa, T., "Production of Radioactive Nuclides in a Lead Assembly wirh 500 MeV Protons," PSI Proc. 92-02, ISSN 1019-6447, pp.568 (1992).

3) Takada, H. et al., JAERI-M 93-181, pp. 210 (1993).
4) Mizumoto, M., et al. : "High Intensity Proton Accelerator for Nuclear Waste Transmutation," Proc. 16th Int. Linear Accelerator Conf. LINAC-92, (1992) (Ottawa).
5) Nakahara, Y. and Tsutsui, T. , " NMTC/JAERI : A Simulation code system fot High Energy Nuclear Reactions and Nucleon-Meson Transport Processes", JAERI-M 82-198, (1982)(in Japanese).
6) Nishida, T. ,Nakahara, Y. and Tsutsui, T. , "Development of a nuclear spallation simulation code and calculation of primary spallation products", JAERI-M 86-116, (1986)(in Japanese).
7) Nakahara Y., et al. : " ACCEL : Code System for Analizing the Nuclear Characteristics on Acclerator-Target/Blanket System," (1981) (Private communication in Japanese).
8) Atchison, F., 1980, Jul-Conf-34.
9) Nishida T., Takada H., Nakahara Y., Takizuka T., Yoshizawa N. and Iwai S. : "Benchmark Study On the Computational Model in Accelerator-Based Transmutation Simulation Code," PSI Proc. 92-02, ISSN 1019-6447, pp.535 (1992).
10) Prael, R.E., Lichtenstein, H. : " USERS GUIDE TO THE LAHET CODE SYSTEM," LA-UR-89-3014.
11) Bertini, H,W.,, Phys. Rev. 188, pp.1711 (1969).
12) Nakahara, Y., J. Nucl. Sci. Technol., 20, pp.511 (1983).
13) Suetomi, E., Kishida, N. and Kadotani, H., Phys. Lett., B333, pp.22 (1994).
14) Li, G.Q. and Machleidt, R., Phys. Rev. C49, pp.556 (1994).
15) Takada, H., J. Nucl. Sci. Technol., 33, pp.275-282 (1996).
16) Cowley, A.A., et al., Z. Phys..A336, p.p. 189 (1990).
17) Amian , W.B. et al , Nucl. Sci. Eng. 112, pp.78 (1992).
18) Cugnon, J., Lemaare, M.-C., Nucl. Phys. .A489, (1988) and Private Communication.
19) Tuma, J.J., " Handbook of Physical Calculation," McGraw-Hill Book, p.p. 251 (1976).
20) Yoshizawa, N., Ishibashi, K. and Takada, H., J. Nucl. Sci. Technol., 32, pp.601(1995).
21) Feshbach, H., Kerman, A. and Koonin, S., Ann. Phys. 125, , p.p. 429 (1980).
22) Takada H., et al. : "Production of Radioactive Nuclides in a Lead Assembly wirh 500 MeV Protons," PSI Proc. 92-02, ISSN 1019-6447, pp.568-583 (1992).
23) Takada H., et al. : J. Nucl. Sci. Technol. 31(1), p. p. 80-82 (1994).
24) Meigo, S., Private communication (1995).
25) Nishida T., Takada H., Nakahara Y., Takizuka T., Yoshizawa N. and Iwai S. : PSI Proc. 92-02, ISSN 1019-6447, p.p. 535-553 (1992) .
26) Friedlander, G., et al., Phys. Rev.,129, p.p.1809 (1963).
27) Baba H. : Nucl. Phys. A159, p.p. 625 (1970).
28) Michel R. and Nagel P. : NEA/NSC/DOC995) 8, "Specification for an International Codes and Model Intercomparison for Intermediate Energy Activation Yields," (1995).
29) Yoshizawa N., Ishibashi K. and Takada H. : J. Nucl. Sci. Technol., 32, p.p. 601 (1995).
30) Ignatyuk A. V., Smirenkin G. N. and Tishin A. S. : Sov. J. Nucl. Phys., 21, p.p. 256 (1975).
31) Audi G. and Wapstra A. M.: Nucl. Phys. A, 565, p.p. 1(1993).
32) Tachibana T., et al.: At.Data Nucl. Data Tables, 39, p.p. 251 (1988).
33) Alcouffe R.E. et al. :" Usersguide for TWODANT : A Code Package for Two-Dimensionnal, Diffusion-Accelerated, Neutral-Particle Transport," LA-10049-M, (1990).
34) Briesmeister J.F. (Ed.) : " MCNP-A General Monte Carlo N-Particle Transport Code, Version 4A," LA-12625, (1993).
35) " SCALE-4 A Modular Code System for Performing Standarised Computer Analysis for Licensing Evaluation," CCC-545, (1990).
36) " BOLD VENTURE IV, A Reactor Analysis Code System, Version IV," CCC-459, (1980).
37) Takizuka, T., Nishida, T., Takada, H., Meigo, S. and Mizumoto, M., :" Conceptual Design Study of an Accelerator-based Actinide Transmutation Plant with Sodium-cooled Solid Target/Core," OECD/NEA/P&T REPORT No.7, pp.397 (1992).
38) Takizuka, T., Nishida ,T., Mizumoto, M. and Yoshida, H., : " Present Status of Accelerator Based Transmutation Research," Proc. 8th Journees SATURNE, LNS/Ph/94-12, pp.109-113 (1994) (Saclay).
39) Kato, Y., et al., PSI Proc. 92-02, ISSN 1019-6447, p.p. 133 (1992).

Table 1 Design specifications for the nitride fuel transmutation system

Proton beam	1.0 GeV
Proton beam radius	15 cm
Proton beam profile	uniform
Beam duct radius	15 cm
Target/Core	concentric cylinders with a height of 1 m
Radii	15 cm / 40 cm
Target	tungsten (disk layer type)
Upper target	height 26 cm, disk thickness 1.5 cm
Lower target	height 54 cm, disk thickness 13 cm
Fuel	
(90MA-10Pu)N (MA:Np, Am, Cm)	
Fuel pin outside diam.	7.3 mm
Pin pitch	9.9 mm
Effective fuel height	80 cm
Fuel pellet diam.	6 mm
Sodium bond	thickness 0.35 mm
Cladding	thickness 0.3 mm (HT-9 SS)
Reflector	stainless steel
Sodium Volume Fraction	
Upper target	86 %
Lower target	37 %
Core	62 %
Reflector	41 %
TRU initial inventory	1150 kg

Table 2 Neutronics charateristics in the nitride fuel transmutation system

k-effective	0.927
Thermal output	15.7 MW/mA
TRU disappearance	
Np	1.93 kg/mA/year
Pu	1.00 kg/mA/year
Am	1.96 kg/mA/year
Cm	0.29 kg/mA/year
Average neutron energy	840 keV
Neutron fraction above 1 MeV	24.6 %
Average neutron flux	2.67×10^{14} (n/cm^2/mA)
Maximum reactivity swing	+ 6.7 % delta-k/k at 210 days

Table 3 Comparison of operating conditions for both molten salt system

	$PbCl_2$ type	NaCl type
Target/Fuel/Primary coolant	Chroride molten salt	
(composition)	$70PbCl_2$-30(Pu+MA)Cl_3	64NaCl-36(Pu+MA)Cl_3
Secondary coolant	Fluroride molten salt	
(composition)	$92NaBF_3$-8NaF	
Actinide inventry	4932 kg	5435 kg
k_{eff}	0.92	0.91
Proton beam	1.5 GeV-28 mA	1.5 GeV-25 mA
Thermal power	800 MW	800 MW
Transmutation	250 kg/y (5.1 %/y)	250 kg/y (4.6 %/y)

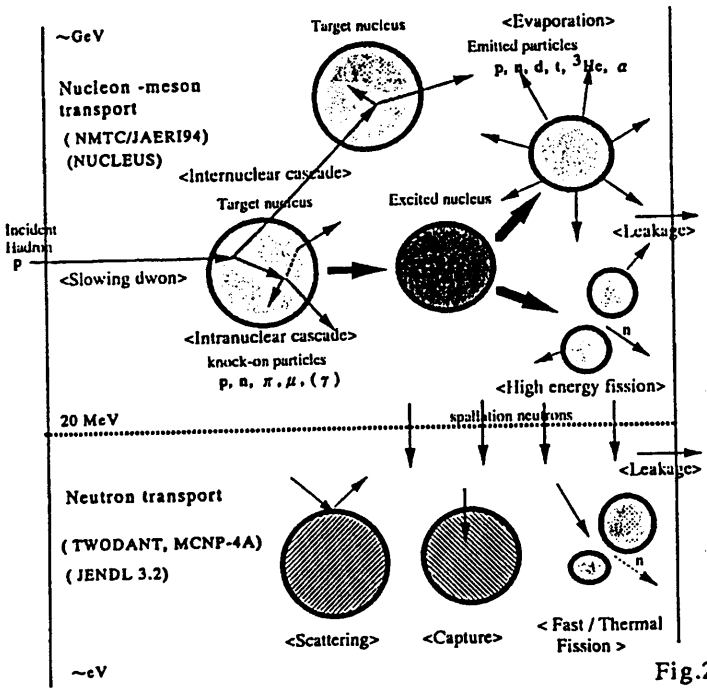

Fig.1 Schematic illustration of spallation & cascade and neutron transport

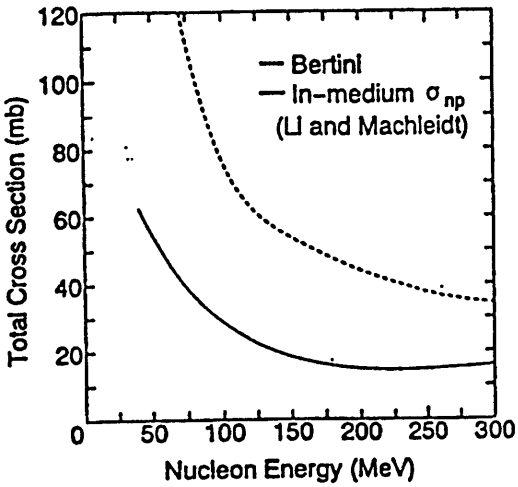

Fig.2 Comparison betweem the free nucleon-nucleon cross section and in-medium ones parameterized by Li, Machleidt and Zhuo

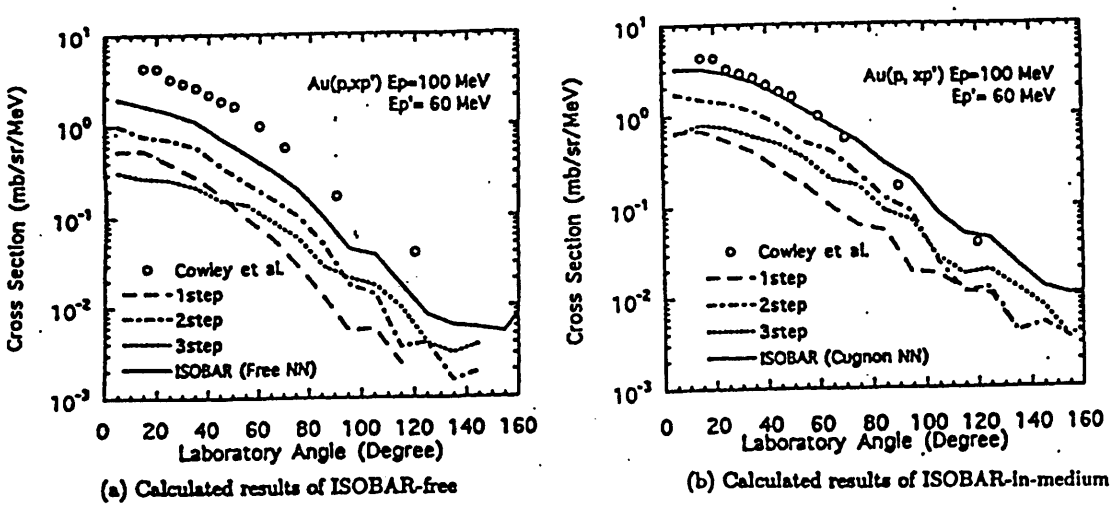

Fig.3 Angular distributions of protons emitted with 60 MeV in the Au (p,xp') reaction for 100 MeV ptoton incidence

The open circle indicates the experimental data. The solid, dashed, dot-dashed and dotted lines represent the total, 1st step, 2nd step and 3rd step contributions of multi scatering in the calculation with ISOBAR respectively.

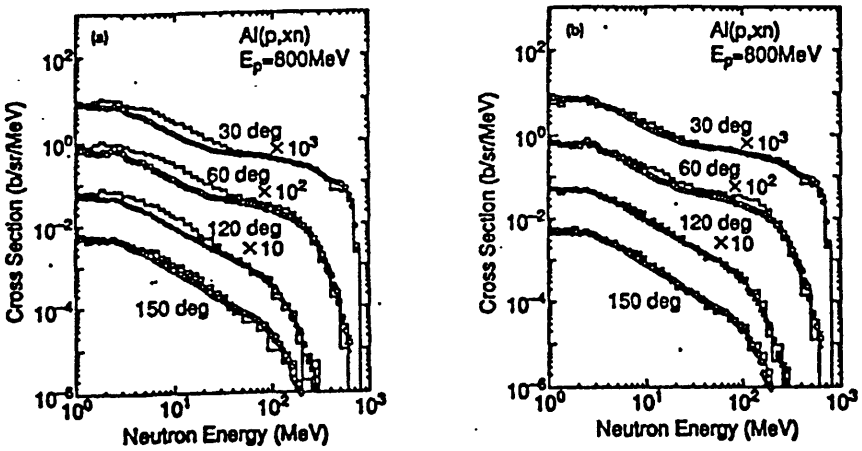

Fig.4 Calculated neutron production DDX in thin Al target bombarded by 800MeV protons are compared with the experimental data The solid linees stand for the calculated values with statistical error $\pm\sigma$ (a) free space NN cross sections and (b) in-medium cross section. The open symbols show the experimental data by Amian.

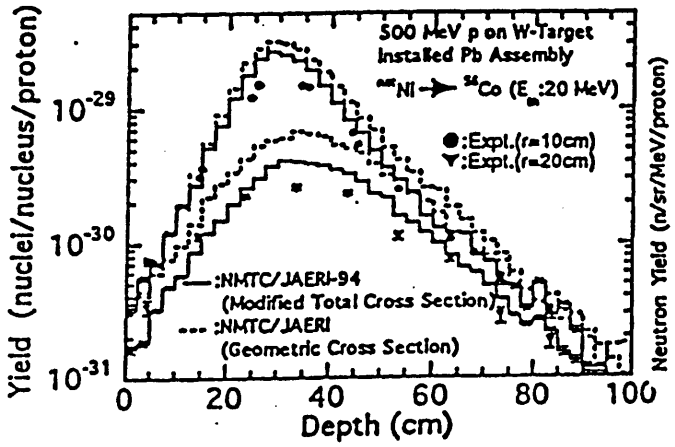

Fig.5 Experimental and calculated yields of ^{56}Co in ^{nat}Ni samples in the tungsten target-installed lead assembly for 500 MeV proton bombardment.

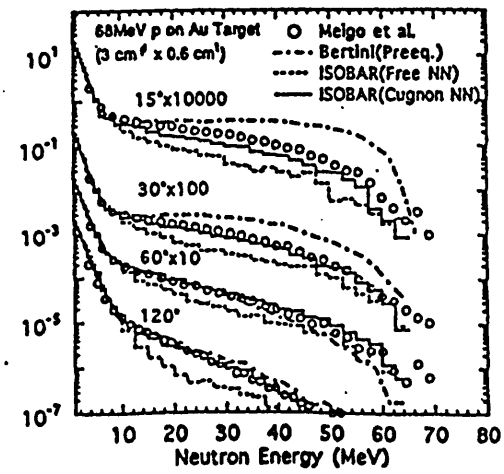

Fig.6 Experimental and calculated neutron yield from the stopping length Au target bombarded by 68 MeV protons

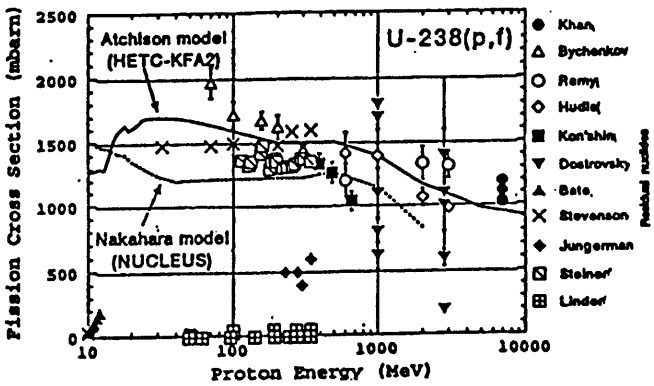

Fig.7 Experimental fission cross sections for ^{238}U(p, fission) from 10 MeV to 10 GeV and ones predicted by both cascade codes of NUCLEUS and HETC/KFA2

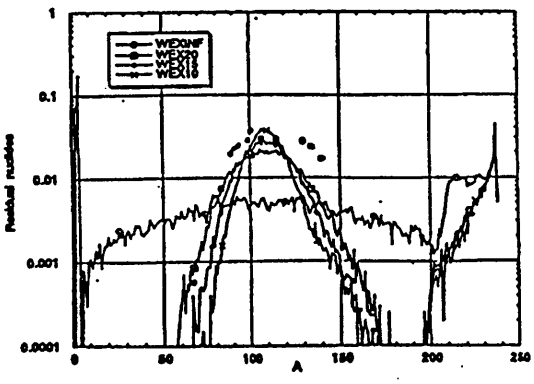

Fig.8 Adjustment of width in the FP yield curve in Nakahara's HEF model to be fitted to experimental data for ^{238}U(p, fission) reaction with proton energy of 300 MeV

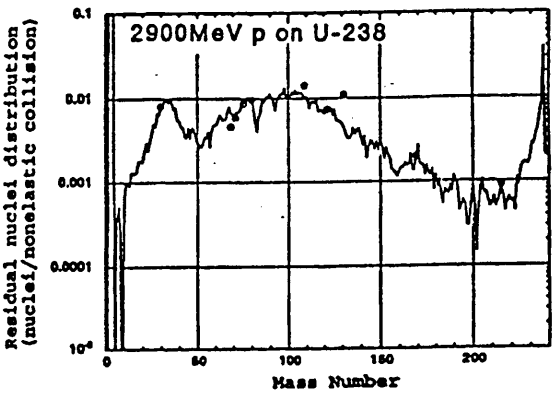

Fig.9 Comparison of the mass distribution of products of calculated by the modified Nakahara model with experimental data for $^{238}U(p, fission)$ reaction with proton energy of 2.9 GeV

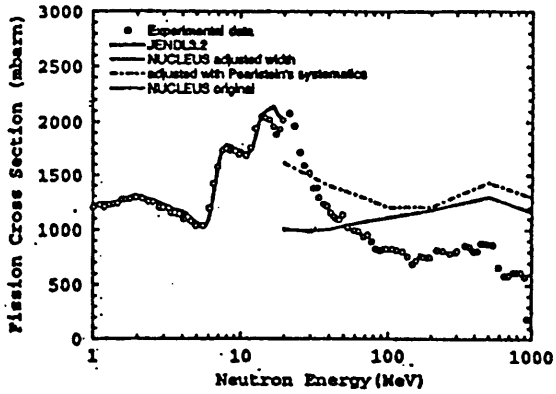

Fig.10 Experimental fission cross sections from 1 MeV to 10 GeV for $^{235}U(n, fission)$ and ones predicted by the NUCLEUS with Baba's data and Ignatyuk formula

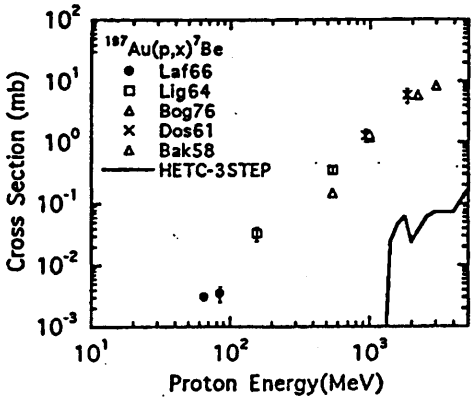

Fig.11 Cross sections of the $^{197}Au(p,x)^{7}Be$ reaction The marks indicate the experimental results. The solid line stands for the calculated resuls of HETC/3STEP.

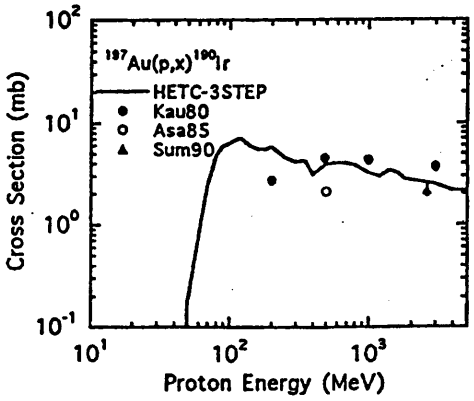

Fig.13 Cross sections of the $^{197}Au(p,x)^{190}Ir$ reaction

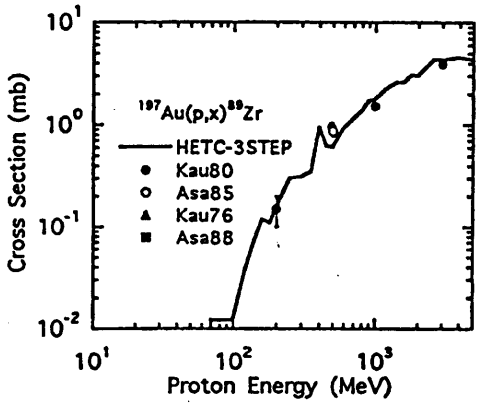

Fig.12 Cross sections of the $^{197}Au(p,x)^{89}Zr$ reaction

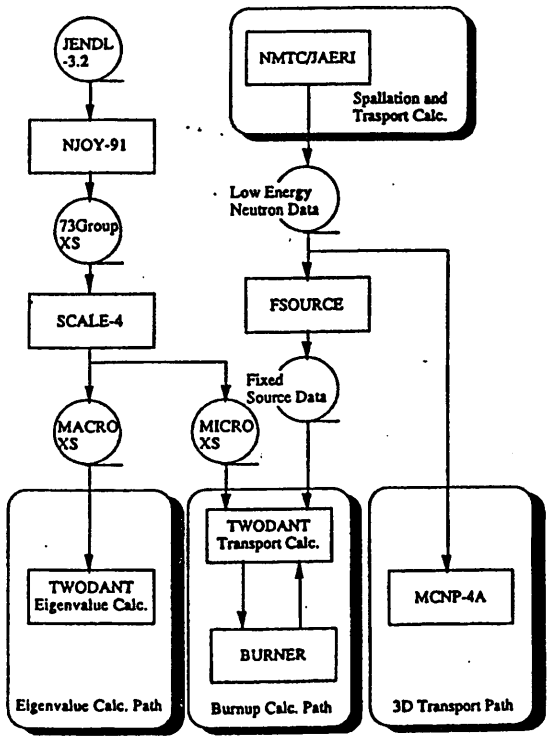

Fig.14 Flow chart of the ATRAS code system

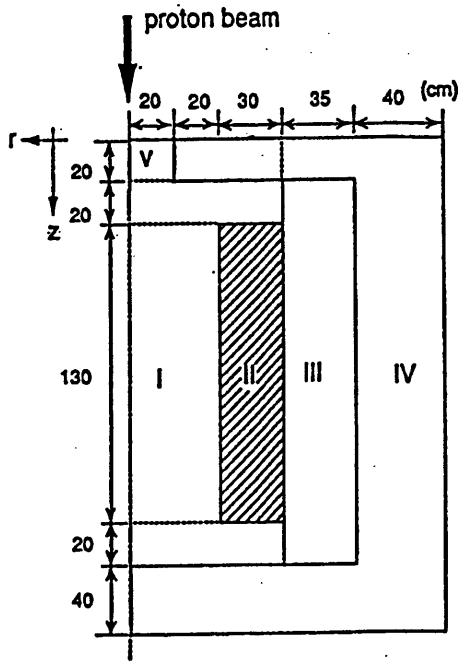

Fig.15 Calculational model of MA molten salt target/core transmutation system

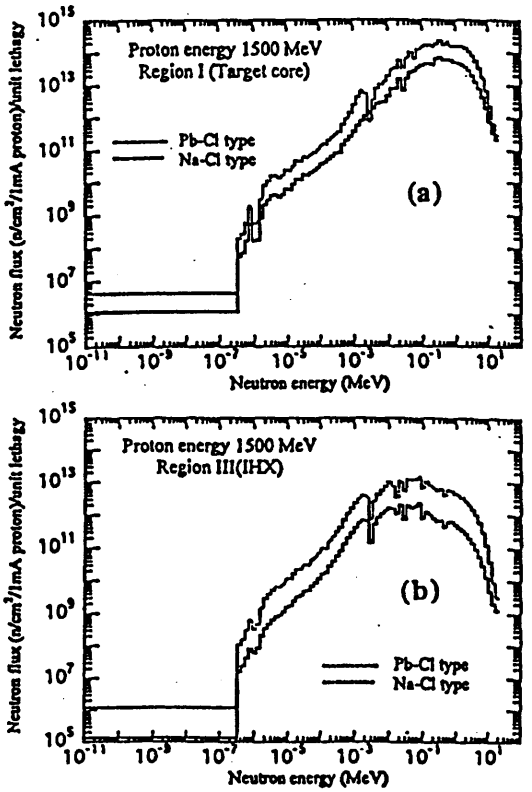

Fig.16 Calculated neutron energy spectra in the target/core filled with TRU chloride molten salt and the outer porus region for heat removal

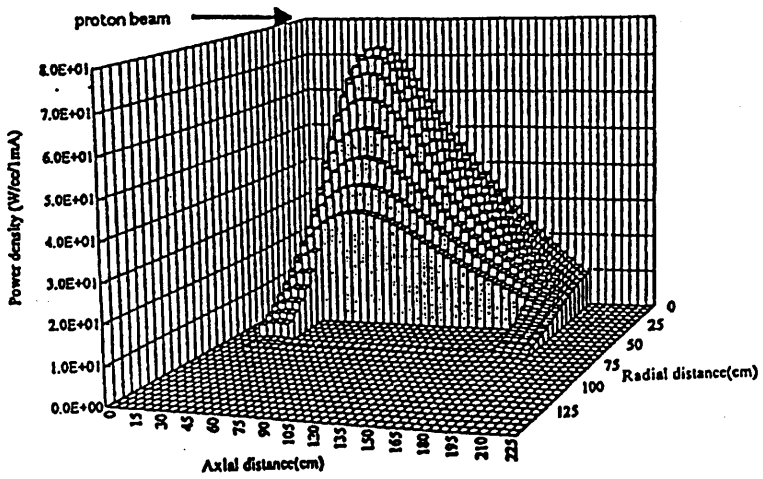

Fig.17 Power density distribution in the target/core region

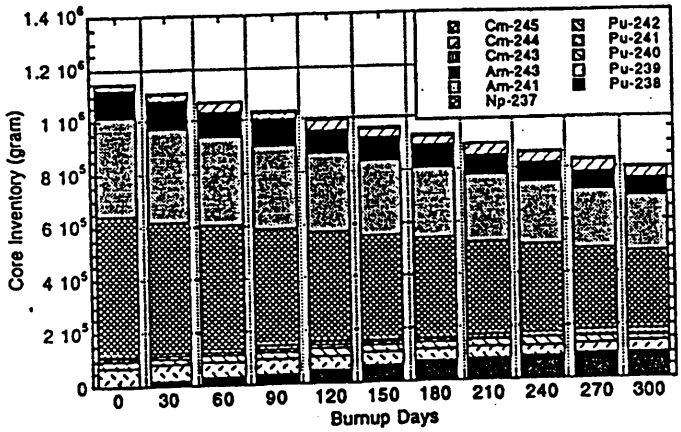

Fig.18 Variation of minor actinides in the nitride fuel core upon burnup

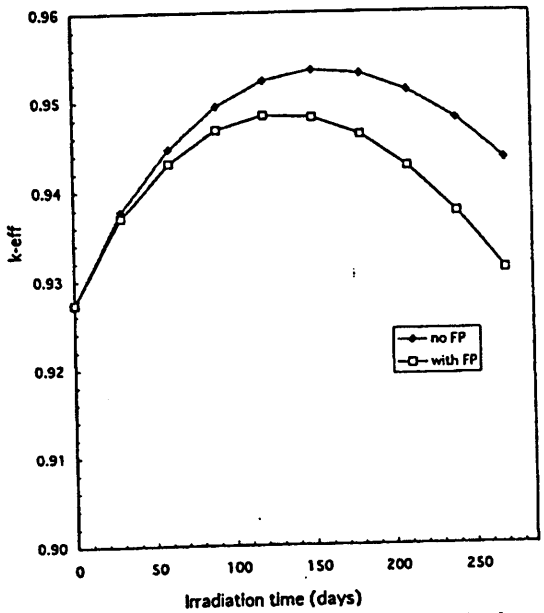

Fig.19 Comparison of dependences of k_{eff} on the burnup time without and with the fission product effects.

ANALYSIS OF REACTION RATE DISTRIBUTIONS ON A THICK TUNGSTEN TARGET BOMBARDED WITH PROTONS OF 0.8 TO 1.2 GEV

H. Takada, S. Meigo, T. Sasa, T. Fukahori
Japan Atomic Energy Research Institute
Tokai-mura, Naka-gun, Ibaraki-ken, JAPAN

V. I. Belyakov-Bodin, G. I. Krupny
Institute of Theoretical and Experimental Physics,
B.Cheremushkinskaya, 25, Moscow, RUSSIA

Yu. E. Titarenko
Institute of High Energy Physics,
Protvino, Moscow Region, RUSSIA

Abstract

In order to estimate the accuracy of the NMTC/JAERI-MCNP-4A code system, an analytical study is performed for the distributions of reaction rates of various activation samples on the surface of a cylindrical thick tungsten target bombarded with 0.8 and 1.2 GeV protons. It is found through the comparison between the experiment and calculation that the NMTC/JAERI-MCNP-4A code system can represent the reaction rates of the activation detectors which are sensitive to the sub-10 MeV neutrons with an accuracy of 10 to 15%. As the threshold energy of the activation detector increases, however, the agreement becomes worse. The calculated results are 50 to 75% in the C/E ratios for the activation detectors sensitive to the neutrons with tens of MeV. The disagreement suggests that the NMTC/JAERI estimates too low the production of neutrons with energies of several tens of MeV in the thick target.

1. Introduction

An accelerator-driven subcritical system is proposed as one of options for the transmutation of long-lived transuranic (TRU) nuclides. Various concepts[1-5] have been proposed for the accelerator-driven transmutation systems. Many of them adopt the design concept that the subcritical core consists of a spallation neutron target surrounded with a blanket including TRU fuels. The target is bombarded with intermediate energy protons of 0.8 to 1.6 GeV with a current of several tens of mA. A heavy metal such as tungsten and lead has been generally selected as target material in design studies because it has high neutron yield of a couple of tens of neutrons per incident proton and can suppress the power density distribution within an acceptable level.

The neutron yield and source neutron energy spectra are important factors to characterize not only the neutronic performance of the subcritical core but for the shielding design. The neutronic calculation of accelerator-based transmutation systems has been carried out with a Monte Carlo simulation code system combining the nucleon-meson transport code such as LAHET[6], HETC-KFA[7] and NMTC/JAERI[8] with the neutron transport code of MORSE[9] and MCNP[10]. Since there are few available nuclear data covering the energy region up to a few GeV yet, it is necessary to enhance the accuracy of the nucleon-meson transport code for detailed neutronic design studies.

It is known that the nucleon-meson transport codes can describe the spallation reaction qualitatively well. However, there still remains some points to be improved in the code. Those aspects were recently confirmed through a code intercomparison conducted by OECD/NEA[11-13]. In JAERI, we have also been estimating the accuracy of the NMTC/JAERI code in comparison with our own experimental data[14-18] in the intermediate energy region of 40 MeV to 3.0 GeV.

As an extension of the study, a reaction rate distribution measurement on a thick tungsten target was carried out using protons of 0.8, 1.0 and 1.2 GeV as a cooperative work between JAERI and Institute of Theoretical and Experimental Physics under the contract of International Science and Technology Center project #157. Analytical study has just started using the NMTC/JAERI-MCNP-4A code system. This paper presents the comparison of the calculated results with experimental ones for the reaction rates of some activation detectors for 0.8 and 1.2 GeV proton incidence.

2. Experimentals

The experiment was carried out at the booster beam line of Institute of High Energy Physics in Russia. In the experiment, 0.8, 1.0 and 1.2 GeV protons were injected into a cylindrical tungsten target having the size of 20 cm in diameter and 60 cm in length. The purity and density of the tungsten target was 19.1 g/cc and 99.95%, respectively. Reaction rate distributions on the cylindrical side surface of the target were measured using various kinds of activation detectors. For the 0.8 and 1.2 GeV proton incidence, the high purity foils of ^{27}Al, ^{12}C, ^{31}P, ^{32}S, ^{103}Rh, ^{115}In, ^{197}Au and ^{209}Bi were put on the side surface at the distances of 2, 8, 12, 17, 30 and 55 cm from the beam incident surface. In this study, the reaction rates of the ^{27}Al, ^{31}P, ^{32}S and ^{209}Bi samples were analyzed. The physical and nuclear characteristics of the activation detectors are summarized in Tables 1 and 2, respectively.

During the irradiation period, proton beam intensity was monitored using an induction current sensor with an accuracy of about 3 %. The profile of the beam was the Gaussian distribution with a FWHM of 2.4 cm. The number of protons injected in the target was 1.3×10^{14} to 4.3×10^{15}. The γ and β rays from the activation detectors were measured using Ge-detectors and polystyrene scintillation counters, respectively. The error in determining the activities of the activation samples were less than 3% at 0.95 confidence level for the γ-ray measurement, while less than 22% at 0.95 confidence level for the β-ray measurement.

3. Calculation

The calculation was carried out using the nucleon meson transport code NMTC/JAERI and the continuous energy Monte Carlo code MCNP-4A. The flow of the calculational procedure is shown in Fig. 1. NMTC/JAERI calculated the nuclear reactions on the basis of the intranuclear cascade[19] evaporation[20] model including the high energy fission process[21] and also simulated the particle transport in a thick medium. The parametrized in-medium nucleon-nucleon (NN) cross sections[22] similar to those of Cugnon[23] were employed instead of the free NN ones in the intranuclear cascade calculation. The level density parameter derived by Ignatyuk[24] with the parameters proposed by Mengoni et al.[25] was selected in the evaporation calculation. In

the particle transport calculation, the cutoff energy was set to be 5 MeV for charged particles and 20 MeV for neutron. The nucleon-nucleus collision cross sections based on the systematics derived by Pearlstein[26] were employed in the energy region below 1 GeV, while the geometric cross sections were used in the energy region above 1 GeV. The transport of neutrons in the energy region below 20 MeV was calculated with MCNP-4A using a continuous energy cross section library, FSXLIB-J3R2[27], which was processed from the nuclear data file JENDL-3.2[28]. Here, the neutron induced nuclear reactions below 20 MeV are taken into account as the cross section data in FSXLIB-J3R2.

Reaction rate of the activation detector, j, on the cylindrical surface of the tungsten target is obtained as

$$R_j = \int_{Eth}^{Emax} \sigma_j(E)\phi(E)dE \quad , \tag{1}$$

where $\sigma_j(E)$ represents the nuclide production cross section and $\phi(E)$ stands for the neutron or proton flux. In this calculation, the energy group structure defined in the HILO-86R library[29] was employed up to 400 MeV. In order to cover the higher energy region, supplemental energy groups of 50 MeV interval were added up to 800 MeV and then those of 100 MeV one were given between 800 and 1200 MeV.

As for the nuclide production cross section, the data of JENDL Dosimetry file[30] were used in the MCNP-4A code in the energy region below 20 MeV. In the energy region above 20 MeV, on the other hand, the nuclide production cross sections were calculated with the ALICE-F code[31] at the energy boundary of the energy group structure. The cross section in each energy group was obtained by the weighted average of the calculated values with 1/E spectrum.

The neutron or proton flux was calculated with the NMTC-JAERI-MCNP-4A code system for the incident protons of 400,000 with the revised data and parameters described above. The profile of proton beam was selected as the gaussian distribution of 2.4 cm in FWHM. In the error estimation, the statistical error of the neutrons counted in each energy group was only taken into account. The ambiguity of the nuclide production cross section was not included. For the C/E ratios, the error was obtained from the experimental error and the statistical error in the calculation based on the propagation theory.

The contribution of leakage protons to the reaction rates was estimated with the nuclide production cross sections calculated with ALICE-F. It was found that the contribution of the proton induced reactions was so small as a few percent of the total reaction rate even in the most sensitive case. In consequence, the calculated results of the neutron induced reaction are compared with the experimental ones in the following discussion.

4. Results and Discussion

The calculated reaction rates are compared with the experimental ones in Figs. 2 to 5. The C/E rations of the reactions are shown in Fig. 6. The sensitivity of the reaction rates to the neutron energy are shown in Fig. 7 for the activation detectors whose threshold energies are lower than 20 MeV. It is observed in Fig. 2 that the calculated reaction rate distributions agree well with those of experimental ones for all the reactions at incident energy of 0.8 GeV. Judging from the results of C/E ratios, good agreement is obtained between the calculated and experimental reaction rates of $^{32}S(n,p)^{32}P$ and $^{27}Al(n,p)^{27}Mg$. A large difference appears between the calculated and experimental results of the $^{31}P(n,p)^{31}Si$ reaction in the region from 2 to 12 cm. For the $^{27}Al(n,p)^{24}Na$ reaction, the calculated reaction rates are constantly lower than the experimental ones about 25 to 30% at all the positions. The most sensitive neutron energy is between 8 and 25 MeV for this reaction as seen in Fig. 7. Since the ambiguity of the cross section data of the $^{27}Al(n,p)^{24}Na$ reaction is not so large as 30% in that energy region, the disagreement indicates that the NMTC/JAERI-MCNP-4A code system estimates the leakage neutron in that energy region as low as about 25 to 30%.

As shown in Fig. 3, the agreement between the calculated and experimental reaction rates is poor for the activation detectors with higher threshold energy. It is observed in Fig. 6 that the calculated results are about 25 to 30% lower than the experimental ones for $^{209}Bi(n,4n)^{206}Bi$, $^{209}Bi(n,5n)^{205}Bi$, and $^{209}Bi(n,7n)^{203}Bi$. As far as the $^{209}Bi(n,6n)^{204}Bi$ reaction is concerned, a significant disagreement of a factor of 2 or more is observed between the calculated and experimental results. The sensitivity of the reaction rates to the neutron energy are shown in Fig. 8 for the $^{209}Bi(n,xn)$ reactions. The $^{209}Bi(n,6n)^{204}Bi$ reaction is dominant in the energy range of 45 to 90 MeV. Figures 9 to 12 compare the calculated nuclide production cross sections of the $^{209}Bi(n, xn)$ reactions with

recent experimental results[32]. It is observed that the calculated nuclide cross sections are in fairly good agreement with the experiment ones and never deviate from those more than a factor of 2 in the sensitive energy region of 45 to 90 MeV. Therefore, the disagreement in the ^{209}Bi(n, xn) reactions seems to mainly come from the underestimation of the amount of leakage neutron by the NMTC/JAERI calculation.

For the 1.2 GeV proton incidence, it is observed in Figs. 4 and 6 that the calculated results are in good agreement with the experimental ones for the ^{32}S(n,p)^{32}P reaction except at the distance of 55 cm. The fairly good agreement is obtained in the results of the ^{31}P(n,p)^{31}Si reaction although the calculated results are slightly higher than the experimental ones. The calculated reaction rates of the ^{27}Al(n,p)^{27}Mg reaction are lower than the experimental results by 15 to 20% near the front surface, while they agree well with the experimental results between 12 and 30 cm. A significant underestimation of 21 to 34% is observed in the results of the ^{27}Al(n,p)^{24}Na reaction except for the position of 55 cm. This is the same tendency as for the analysis of the 0.8 GeV proton incidence.

In Fig. 4, it should be noted that the experimental reaction rates decrease rapidly from 30 cm to 55 cm. Such phenomena, on the other hand, do not appear in the calculated results. This leads to the significantly large C/E ratios at 55 cm for those reactions although they are not shown in Fig. 6. The neutron production at the deep position seems to be estimated too large by the reason that the mean free path of high energy neutron or proton is overestimated by NMTC/JAERI. This problem is, however, not resolved for the time being.

As far as the ^{209}Bi(n,xn) reactions are concerned, the NMTC/JAERI calculation again gives lower reaction rates than the experimental ones as seen in Fig. 5. Judging from the C/E rations shown in Fig. 6, the degree of agreement is almost the same as for the case of the 0.8 GeV proton incidence. The C/E ratios of the ^{209}Bi(n,4n)^{206}Bi reaction are poorer than that for the 0.8 GeV proton incidence. These results indicate that the present NMTC/JAERI code estimates the production of neutrons with energies of several tens of MeV too low even for the 1.2 GeV proton incidence. At the position of 55 cm, the phenomena mentioned above does not appear for the ^{209}Bi(n,xn) reactions.

The present NMTC/JAERI code has already been employed in the analysis[16] of the neutron spectra of a thick lead target bombarded with the 0.5 and 1.5 GeV protons. It was pointed out in Ref. 16 that the code gave lower neutron yield than the experimental results especially in the energy region between 20 and 80 MeV. The present analysis points out the same feature of NMTC/JAERI as for the previous one. Since various microscopic factors are mixed in the results of integral experiment, the cause of the problem is not attributed only to the treatment of the nuclear reaction process. It is also necessary to investigate the accuracy of the nucleon-nucleus cross sections employed in the energy region above 20 MeV.

At last, a large fluctuation is observed in the C/E ratios of a part of the reaction rates, e.g. ^{209}Bi(n,4n)^{206}Bi and ^{209}Bi(n,7n)^{203}Bi at the distance of 30 cm for the 0.8 GeV proton incidence. Some additional error may be included in those experimental results.

5. Concluding Remarks

The reaction rate distributions of various activation detectors on the cylindrical surface of a tungsten target bombarded with 0.8 and 1.2 GeV protons were analyzed with the NMTC/JAERI-MCNP-4A code system. It was found through the comparison with the experimental results that the code system predicted the reaction rates induced by the sub-10 MeV neutrons with an accuracy of 10 to 15%. Considering that some approximations are included in both the nuclear reaction and particle transport calculation parts of NMTC/JAERI, the accuracy of the code is reasonable.

For the activation detectors sensitive to the neutrons with tens of MeV, however, the agreement between the calculated and experimental results reduced and the C/E ratio was in the level of 50 to 75%. These results suggested that NMTC/JAERI estimated the neutrons in tens of MeV region too low. This feature of NMTC/JAERI was consistent with the conclusion obtained from the other work on neutron spectra measurement and should be improved by further studies from both the microscopic and macroscopic point of view.

References

[1] Venneri F., Bowman C. D., Wender S. A.: "The Physics Design of Accelerator-Driven Transmutation Systems", Proc. of Int. Conf. on Evaluation of Emerging Nuclear Fuel Cycle Systems, GLOBAL '95,

Sep. 11-14, 1995, Versailles, France, pp. 474-481 (1995).
[2] Takizuka T., Nishida T., Sasa T., Takada H., Meigo S., Mizumoto M., Hasegawa K.: Research and Development on Proton Accelerator Based Trans,mutation of Nuclear Waste", *ibid.*, pp. 489-496.
[3] Takahashi, H., Rief, H.: "Concept of Accelerator Based Transmutation Systems", Proc. of the Specialists' Mtg. on Accelerator-Based Transmutation, PSI, Villigen, Switzerland, Mar. 24-26, 1992, pp. 2-26 (1992).
[4] Chuvilo I. V., Kiselev G. V., Bergelson B. R., Kochurov B. P.: "Nuclear Fuel Cycle Using Nuclear Power Facilities Based on Subcritical Blankets Driven by the Proton Accelerator", Proc. of Int. Conf. and Technol. Exposition on Future Nucl. Systems: Emerging Fuel Cycles and Waste Disposal Options, GLOBAL '93, Sep. 12-17, 1993, Seattle, Washington, pp. 924-933 (1995).
[5] Rubbia C., Rubio J. A., Buono S., Carminati F., Fiétier N., Galvez J., Gelès C., Kadi Y., Klapisch R., Mandrillon P., Revol J. P., Roche Ch.:"Conceptual Design of A Fast Neutron operated high Power Energy Amplifier", CERN/AT/95-44 (ET), (1995).
[6] Prael R. E., Lichtenstein H.: LA-UR-89-3014, "Users Guide to LCS: The LAHET Code System", (1989).
[7] Cloth P., Filges D., Neef R. D., Sterzenbach G., Reul Ch., Armstrong T. W., Colborn B. L., Anders B., Brückmann H.: "HERMES A Monte Carlo Program System for Beam Materials Interaction Studies", Jül-2203, (1988).
[8] Nakahara Y., Tsutsui T.: "NMTC/JAERI A Code System for High Energy Nuclear Reactions and Nucleon-Meson Transport Code", JAERI-M 82-198, (1982), [in Japanese].
[9] Emmett M. B.: "The MORSE Monte Carlo Radiation Transport Code System", ORNL-4972, (1975).
[10] Briesmeister J.F. (Ed.) : MCNP A General Monte Carlo N-Particle Transport Code, Version 4A, LA-12625, (1993).
[11] OECD/NEA: "Proc. of Specialists' Mtg. on Intermediate Energy Nucl. Data: Models and Codes", May 31 - June 1, Issy-les-Moulineaux, OECD Publications, Paris, (1994).
[12] Filges D., Nagel P., Neef R. D. (Eds.): "International Code Comparison for Intermediate Energy Nucl. Data: The Thick Target Benchmark", NEA/NSC/DOC(95)-2, (1995).;Sobolevsky N. : "Conclusions of International Code Comparison for Intermediate Energy Nucl. Data, Thick Target Benchmark for Lead and Tungsten", NEA/NSC/DOC(96)-15, (1996).
[13] Michel R., Nagel P.:"Specifications for An International Codes and Model Intercomparison for Intermediate Energy Activation Yields", NEA/NSC/DOC(95)-8, (1995).
[14] Takada H., Hasegawa K., Sasa T., Meigo S., Kanno I.: "Integral Spallation Experiment with a Thick Lead Assembly Irradiated with 500 MeV Protons", Proc. of the 1992 Symp. on Nucl. Data, Nov. 26-27, JAERI, Tokai, Japan, JAERI-M 93-046, pp. 72-81 (1993).
[15] Nakamoto T., Ishibashi K., Matsufuji N., Maehata K., Shigyo N., Meigo S., Takada H., Chiba S., Numajiri M., Wakuta, Y., Watanabe Y.: J. Nucl. Sci. Technol., 32, 827 (1995).
[16] Meigo S. Takada H., Chiba S., Nakamoto T., Ishibashi K., Matsufuji N., Maehata K., Shigyo N., Wakuta, Y., Watanabe Y., Numajiri M.: "Measurements of Spallation Neutrons from a Thick Lead Target Bombarded with 0.5 and 1.5 GeV Protons", Joint Proc. of the 13th Mtg. of the Int. Collaboration on Advanced Neutron Sources held at Paul Scherrer Institute, Oct. 11-14, 1995 and 4th Plenary Mtg. of the European Spallation Source Project, ESS, held at Weinfelden, Oct. 16-19, 1995, PSI-Proceedings 95-02, pp. 442-453 (1995).
[17] Nakao N., Nakashima H., Nakamura T., Tanaka Sh., Tanaka Su., Shin K., Baba M., Sakamoto Y., Nakane Y.: Nucl. Sci. Eng. 124, (1996), (to be published).
[18] Nakashima H., Nakao N., Nakamura T., Tanaka Sh., Shin K., Tanaka Su., Takada H., Meigo S., Nakane Y., Sakamoto Y., Baba M.: *ibid.*, (to be published).
[19] Bertini H. W.: Phys. Rev., 188, 1711 (1969).
[20] Dresner L. W.: ORNL-TM-196, "EVAP - A Fortran Program for Calculating the Evaporation of Various Particles from Excited Compound Nuclei", (1962).
[21] Nakahara Y.: J. Nucl. Sci. Technol., 20, 511 (1983).
[22] Niita K., Chiba S., Maruyama T., Takada, H., Fukahori T., Nakahara, Y., Iwamoto A.: Phys. Rev. C 52, 2620 (1995).[23] Cugnon, J., Mizutani, T., Vandenmuren, J.: Nucl. Phys. A352, 505 (1981); Cugnon, J.: Phys. Rev. C 22, 1885 (1980).
[24] Ignatyuk A. V., Smirenkin G. N., Tishin A. S.: Sov. J. Nucl. Phys., 21, 256 (1975).

[25] Mengoni A., Nakajima Y.: J. Nucl. Sci. Technol., 31, 151 (1994).
[26] Pearlstein, S.: Astrophys. J., 346, 1049 (1989).
[27] Kosako, K., Maekawa, F., Oyama, Y., Uno, Y., Maekawa, H.:"FSXLIB-J3R2 : A Continuous Energy Cross Section Library for MCNP Based on JENDL-3.2", JAERI-Data/Code 94-020, (1994).
[28] Shibata K., Nakagawa T., Asami T., Fukahori T., Narita T., Chiba S., Mizumoto M., Hasegawa A., Kikuchi Y., Nakajima Y., Igarasi S. : "Japanese Evaluated Nuclear Data Library, Version-3 -JENDL-3-", JAERI-1319, (1990); Nakagawa T., Shibata K., Chiba S., Fukahori T., Nakajima Y., Kikuchi Y., Kawano T., Kanda Y., Ohsawa T., Matsunobu H., Kawai M., Zukeran A., Watanabe T., Igarasi S., Kosako K., Asami T.: J. Nucl. Sci. Technol., 32, 1259 (1995).
[29] Kotegawa H., Nakane Y., Hasegawa A., Tanaka Sh.:"Neutron-photon Multigroup Cross Sections for Neutron Energies up to 400 MeV; HILO86R", JAERI-M 93-020, (1993).
[30] Nakazawa M., Kobayashi K., Iwasaki S., Iguchi T., Sakurai K., Ikeda Y., Nakagawa T.: "JENDL Dosimetry File", JAERI-1325, (1992).
[31] Fukahori T.:"ALICE-F Calculation of Nuclear Data up to 1 GeV", Proc. of the Specialists' Mtg. on High Energy Nucl. Data, Oct. 3-4, 1991, JAERI, Tokai, JAERI-M 92-039, pp. 114-122 (1992).
[32] Kim E., Nakamura T., Konno A., Imamura M., Nakao N., Shibata T., Uwamino Y., Nakanishi N., Tanaka Su., Nakashima H., Tanaka Sh.: "Measurement of Neutron Spallation Cross Sections", Proc. of the 1995 Symp. on Nucl. Data, Nov. 16-17, 1995, JAERI, Tokai, Japan, JAERI-Conf 96-008, pp. 236-241 (1996), and private communication.

Table 1. Physical characteristics of activation detectors.

Sample	Size (mm)	Density (g/cc)	Purity (%)
P	20ϕ x 3	2.20	100
S	20ϕ x 3	2.07	95.02
Al	25 x25x1.6	2.699	100
Bi	20ϕ x 1	9.747	99.99

Table. 2. Nuclear characteristics of activation detectors.

Reaction	Half-Life	γ-/β-ray Energy	Emission Rate	Threshold Energy
$^{32}S(n,p)^{32}P$	14.3 days	694.7 keV (β)	1.0	0.96 MeV
$^{31}P(n,p)^{31}Si$	157.3 min	595.7 keV (β)	0.999	0.73 MeV
$^{27}Al(n,p)^{27}Mg$	9.45 min	843 keV (γ)	0.7	1.9 MeV
$^{27}Al(n,\alpha)^{24}Na$	15.0 hours	1369 keV (γ)	1.0	3.27 MeV
$^{209}Bi(n,4n)^{206}Bi$	6.243 days	803.1 keV (γ)	0.989	22.56 MeV
$^{209}Bi(n,5n)^{205}Bi$	15.31 days	703.4 keV (γ)	0.311	29.63 MeV
$^{209}Bi(n,6n)^{204}Bi$	11.22 hours	374.7 keV (γ)	0.737	37.99 MeV
$^{209}Bi(n,7n)^{203}Bi$	11.76 hours	820.2 keV (γ)	0.296	45.31 MeV

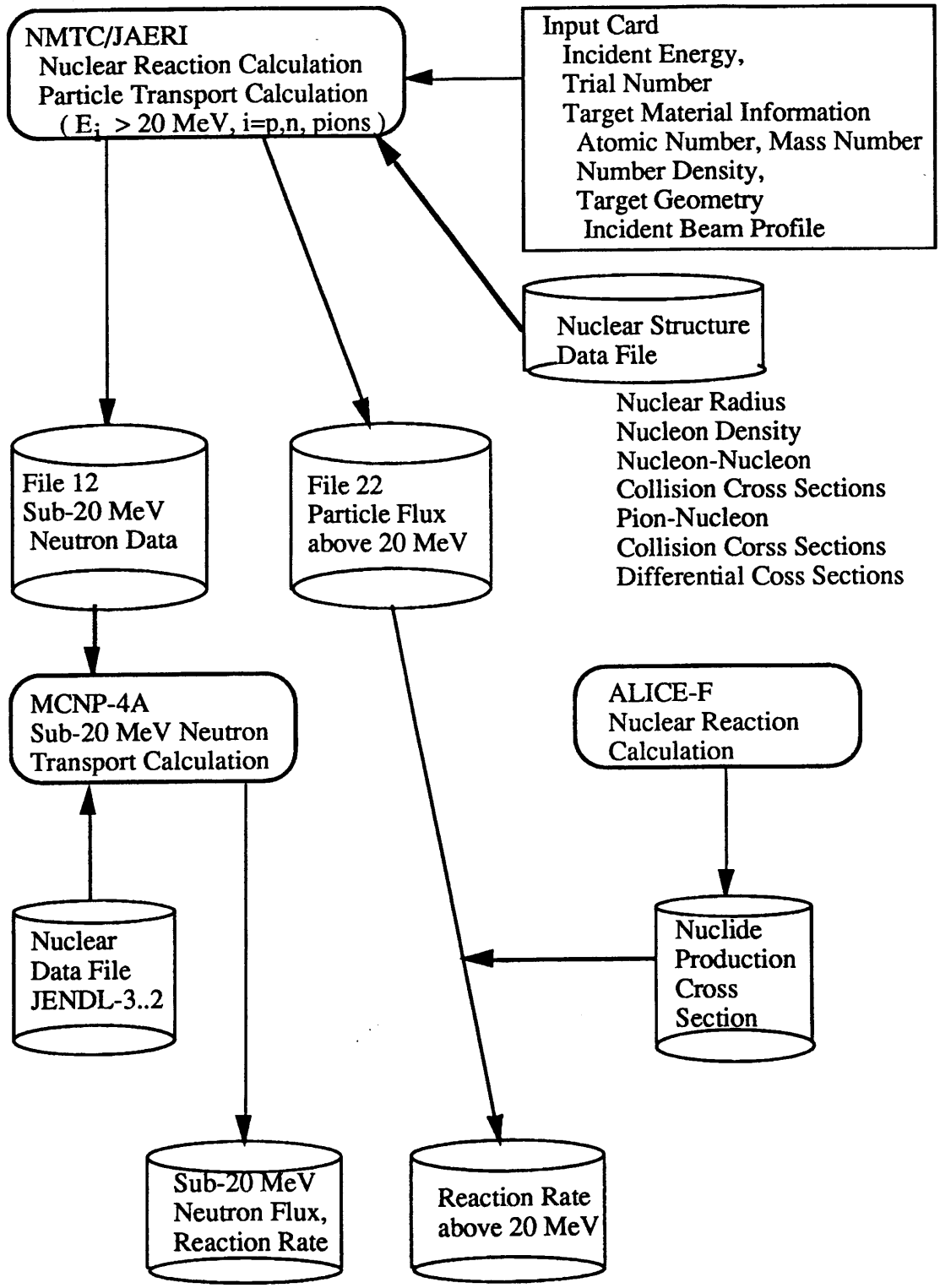

Fig. 1. Calculation flow of the NMTC/JAERI-MCNP-4A code system.

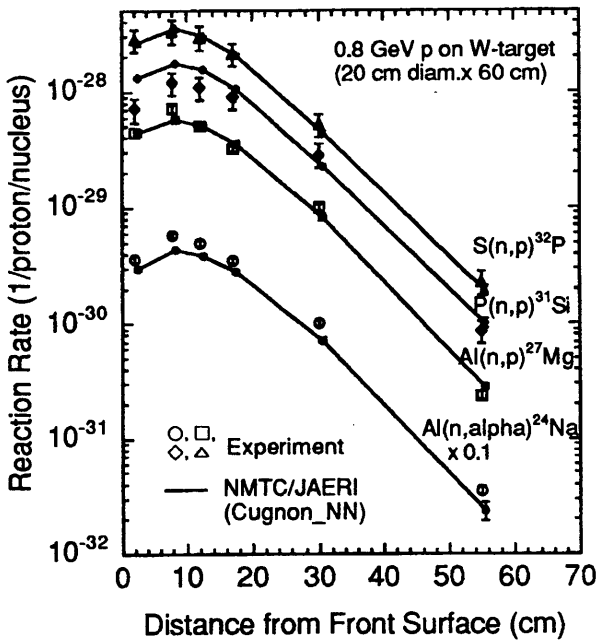

Fig. 2 Experimental and calculated reaction rates of $S(n,p)^{32}P$, $P(n,p)^{31}Si$, $Al(n,p)^{27}Mg$ and $Al(n,\alpha)^{24}Na$ for the 0.8 GeV proton incidence on the thick tungsten target. The open and solid marks indicate the experimental and calculated results of NMTC/JAERI-MCNP-4A, respectively. The lines are for eye-guide.

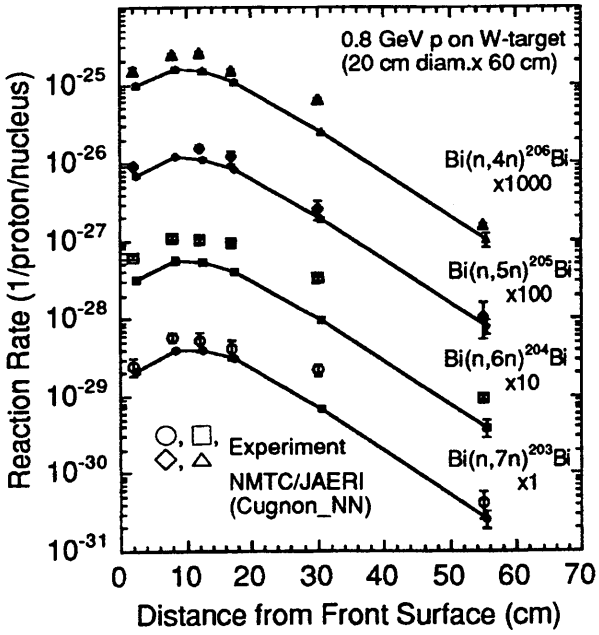

Fig. 3. Experimental and calculated reaction rates of $Bi(n,4n)^{206}Bi$, $Bi(n,5n)^{205}Bi$, $Bi(n,6n)^{204}Bi$ and $Bi(n,6n)^{203}Bi$ for the 0.8 GeV proton incidence on the thick tungsten target. The notes to the marks and lines are the same as for Fig. 2.

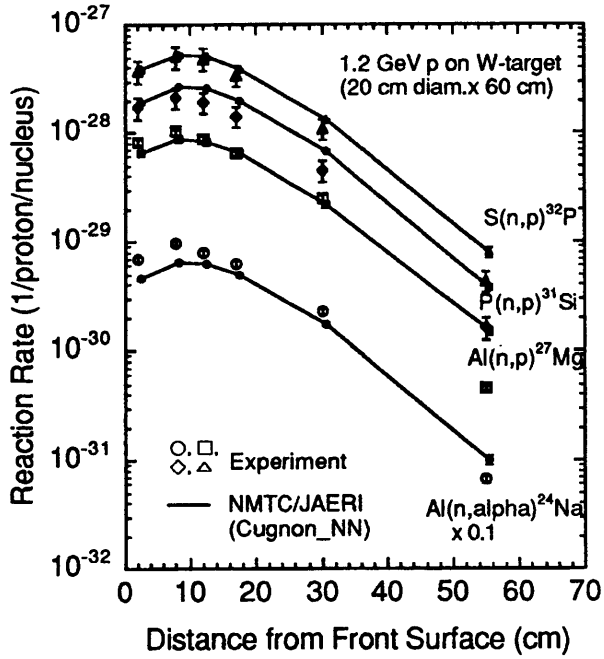

Fig. 4. Experimental and calculated reaction rates of $S(n,p)^{32}P$, $P(n,p)^{31}Si$, $Al(n,p)^{27}Mg$ and $Al(n,\alpha)^{24}Na$ for the 1.2 GeV proton incidence on the thick tungsten target. The notes to the marks and lines are the same as for Fig. 2.

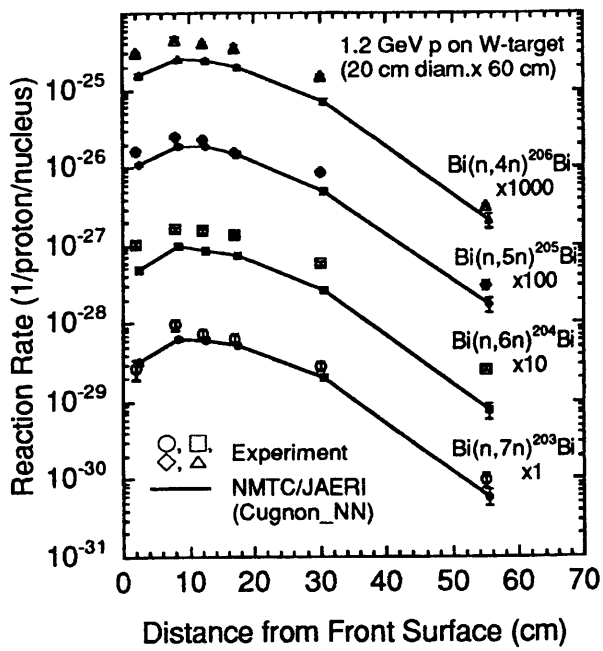

Fig. 5. Experimental and calculated reaction rates of $Bi(n,4n)^{206}Bi$, $Bi(n,5n)^{205}Bi$, $Bi(n,6n)^{204}Bi$ and $Bi(n,6n)^{203}Bi$ for the 1.2 GeV proton incidence on the thick tungsten target. The notes to the marks and lines are the same as for Fig. 2.

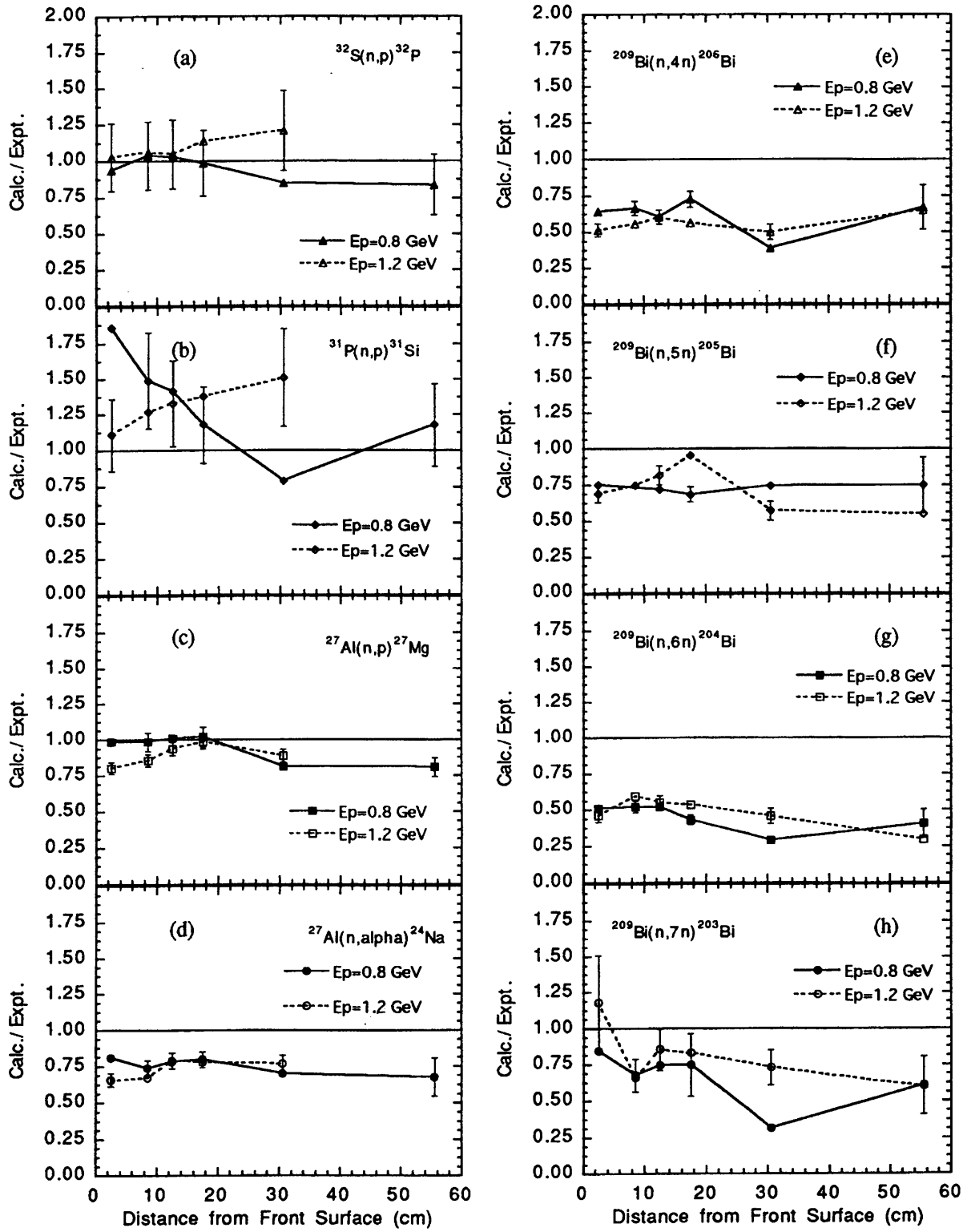

Fig. 6. C/E ratios between the calculated and experimental reaction rates of the activation detectors : (a) $^{32}S(n, p)^{32}P$ reaction, (b) $^{31}P(n, p)^{31}Si$ reaction, (c) $^{27}Al(n, p)^{27}Mg$ reaction, (d) $^{27}Al(n, \alpha)^{24}Na$ reaction, (e) $^{209}Bi(n, 4n)^{206}Bi$ reaction, (f) $^{209}Bi(n, 5n)^{205}Bi$ reaction, (g) $^{209}Bi(n, 6n)^{204}Bi$ reaction, (h) $^{209}Bi(n, 7n)^{203}Bi$ reaction. The solid and open marks indicate the results of the 0.8 and 1.2 GeV proton incidence, respectively. The lines are for eyeguide.

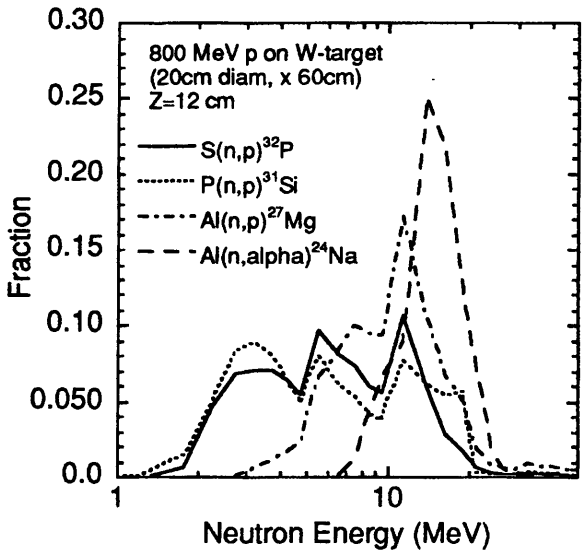

Fig. 7. Sensitivity of the reaction rates to the neutron energy for $S(n,p)^{32}P$, $P(n,p)^{31}Si$, $Al(n,p)^{27}Mg$ and $Al(n,\alpha)^{24}Na$ at the distance of 12cm from front surface.

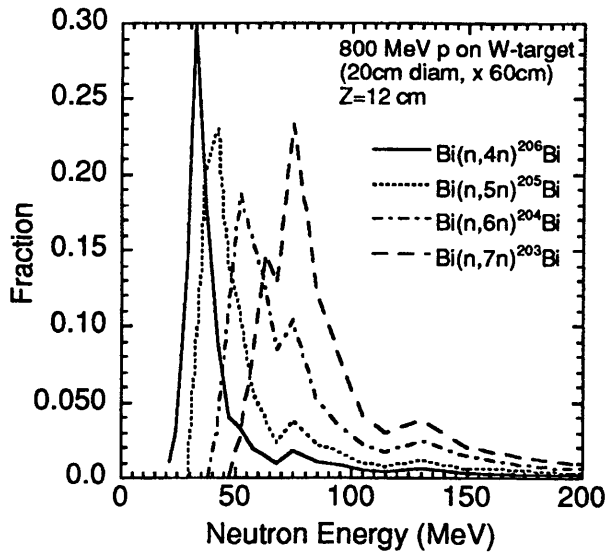

Fig. 8. Sensitivity of the reaction rates to the neutron energy for $Bi(n,4n)^{206}Bi$, $Bi(n,5n)^{205}Bi$, $Bi(n,6n)^{204}Bi$ and $Bi(n,7n)^{203}Bi$ at the distance of 12cm from front surface.

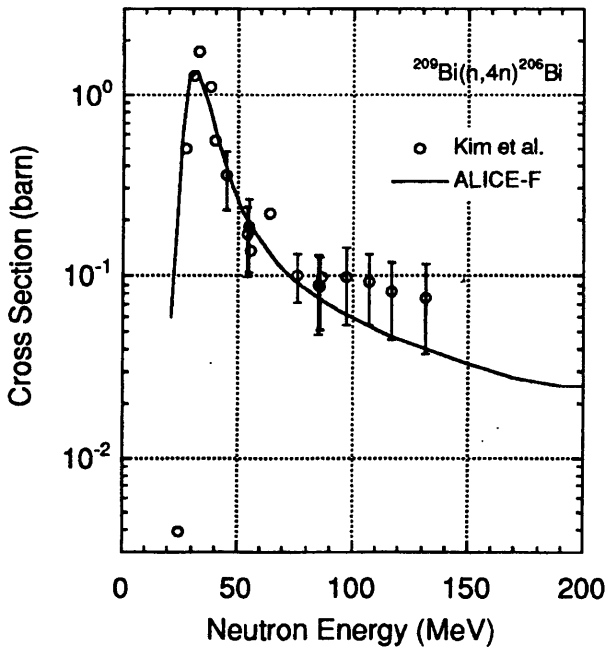

Fig. 9. Experimental and calculated cross section of $^{209}Bi(n,4n)^{204}Bi$. The open marks indicate the experimental data[32]. The solid lined represents the calculated results of ALICE-F.

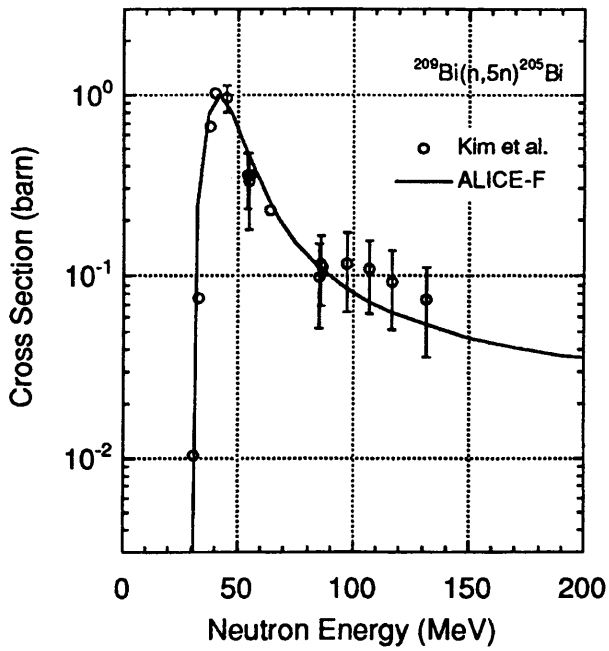

Fig. 10. Experimental and calculated cross section of $^{209}Bi(n,5n)^{205}Bi$. The notes to the marks and lines are the same as for Fig. 9.

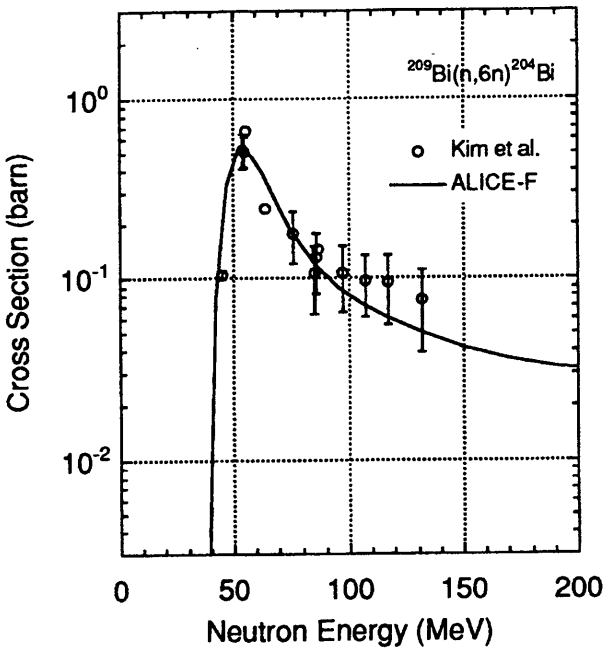

Fig. 11. Experimental and calculated cross section of ^{209}Bi(n,6n)^{204}Bi. The notes to the marks and lines are the same as for Fig. 9.

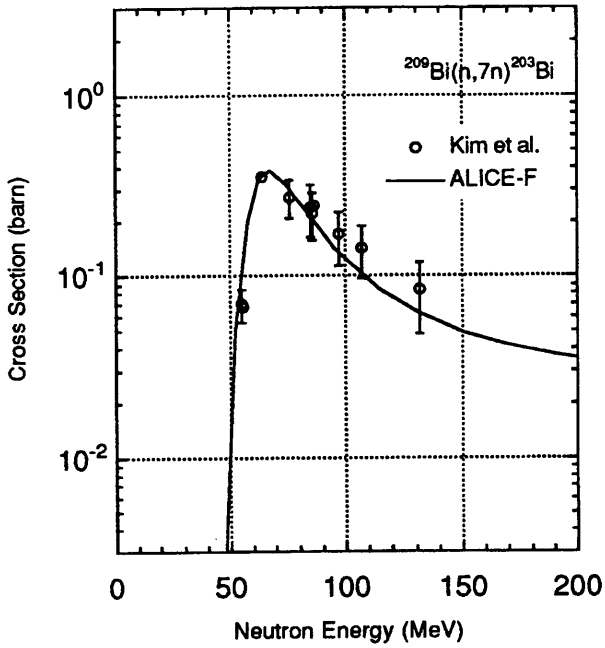

Fig. 12. Experimental and calculated cross section of ^{209}Bi(n,7n)^{203}Bi. The notes to the marks and lines are the same as for Fig. 9.

NUCLEAR MEASUREMENT ACTIVITIES OF PNC FOR TRANSMUTATION OF FISSION PRODUCTS

Hideo Harada, Shoji Nakamura, Yoshiaki Shigetome and Toshio Katoh

Power Reactor and Nuclear Fuel Development Corporation, Tokai works, Tokai-mura, Ibaraki-ken, 319-11 JAPAN

Abstract. This paper reviews the PNC's activity on nuclear data measurements for the study of the transmutation of fission products. Thermal neutron capture cross sections and resonance integrals of ^{137}Cs, ^{90}Sr, ^{99}Tc, and ^{129}I were measured for the study of the transmutation method using thermal neutrons. High resolution measurements of photonuclear reaction cross section are also in progress for the study of the transmutation method using monocromatic photons.

INTRODUCTION

To investigate the system transmuting fission products(FP), accurate nuclear reaction cross sections are required for FP. What kind of nuclear reactions should be used for FP transmutation depends on how large is the cross section utilized. For the study of the transmutation methods using a high flux fission reactor, a high intensity proton accelerator, and also a high flux fusion reactor, thermal neutron cross sections(σ_0) and resonance integrals (I_0) are especially important. However, these data are old and sometimes reported values differ each other. Therefore, we have measured these cross sections first for ^{137}Cs, ^{90}Sr, ^{99}Tc, and ^{129}I. As a results, we have found out that the σ_0 and I_0 of ^{90}Sr and ^{137}Cs are too small to be transmuted by using thermal neutrons.

As an alternative method transmuting ^{90}Sr and ^{137}Cs, we started the study of a monochromatic photon method; a high energy photon can transmute a nucleus via photonuclear reaction. If there is a sharp and intense resonance peak in the photonuclear reaction cross section, the monochromatic photon of the same energy with the resonance can effectively transmute a nucleus. However, very little is known about the precise photon energy dependence of the photonuclear reaction cross section. To obtain the intrinsic resonance peak width and intensity, we proposed a new experimental method.

The results of the experiments and the simulations are briefly described below.

THERMAL NEUTRON CAPTURE CROSS SECTIONS AND RESONANCE INTEGRALS

Accurate data of neutron cross sections are required for the research of the transmutation method of nuclear waste. Data reported, however, show discrepancies between them. Therefore, we designed experiments to obtain more accurate data of neutron cross sections of important long-lived fission products, ^{137}Cs[1,2], ^{90}Sr[3], ^{99}Tc[4] and ^{129}I[5]. Standardized solution of each radioactive nuclide was irradiated at a thermal neutron reactor of Japan Atomic Energy Research Institute(JAERI) or Rikkyo University. Samples were irradiated with or without a Cd shield. The number of nuclei in the target to be irradiated was determined by an isotope ratio method(IRM) or an efficiency tracing technique(ETT) which meets the nuclear property of each nuclide. The amount of reaction products, ^{138}Cs, ^{91}Sr, ^{100}Tc and ^{130}I, by neutron capture were obtained by measuring gamma-ray intensities from these nuclei. The reaction rates obtained were analyzed, and thermal neutron cross sections and resonance integrals were deduced. The results were compared with the data reported by others[6-13]. Some data of cross sections were revised from the data by others and some data of resonance integrals were newly obtained[1-5]. Measurements of neutron capture cross section of ^{135}Cs are in progress.

The targets of ^{137}Cs and ^{90}Sr were irradiated at the swimming pool type reactor JRR-4 of JAERI with or without a Cd shield by using a pneumatic tube system. The reactor has a 1/E neutron spectrum in the resonance neutron region. The irradiation position was characterized as having a thermal neutron spectrum of 4×10^{13} n/(cm^2 • s) and an epithermal index in the Westcott's convention[14] of 0.03. After the irradiation, a chemical procedure for purification of the irradiated target was carried out[2,3]. The impurity activities such as ^{24}Na and ^{38}Cl were removed from the target. The targets of ^{99}Tc and ^{129}I were irradiated in the rotary specimen rack(RSR) of the TRIGA MARK II reactor of Rikkyo University. The

thermal neutron flux of this irradiation position was 5 x 10^{11} n/(cm^2 · s) and the epithermal index 0.03. The chemical procedure was not applied to the targets of ^{99}Tc and ^{129}I since half-lives of these are short.

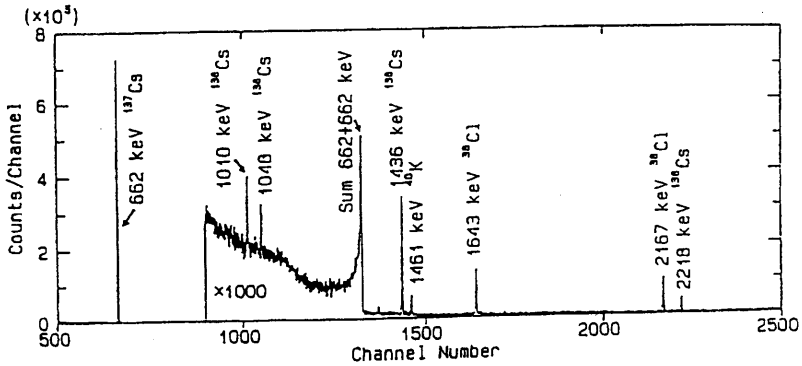

Fig.1 Gamma-ray spectrum obtained from neutron-irradiated and chemically purified ^{137}Cs sample in 10-min measurement

Table I. Results of the neutron capture cross section and resonance integrals

Nuclides	present results(b)	previous data(b)	Authors
^{137}Cs	$\sigma_0 = 0.25 \pm 0.02$[2] $I_0 = 0.36 \pm 0.07$[2]	$\sigma_0 = 0.110 \pm 0.033$	Stupegia[6]
^{90}Sr	$\sigma_0 = 0.0153$ $^{+0.0013}_{-0.0042}$[3] $I_0 \leqq 0.16$[3]	$\sigma_0 =$ 0.0140 ± 0.0024 0.8 ± 0.5	McVey et al.[7] Zeisel[8]
^{99}Tc	$\sigma_0 = 22.9 \pm 1.3$[2] $I_0 = 398 \pm 38$[2]	$\sigma_0 = 20 \pm 2$ $I'_0 = 186 \pm 16$	Lucas[9] Lucas[9]
^{129}I	$\sigma_0^{2+} = 17.4 \pm 1.7$[2] $I_0^{2+} = 17.8 \pm 2.0$[2] $\sigma_0^{5+} = 12.6 \pm 2.2$[2] $I_0^{5+} = 15.5 \pm 2.9$[2] σ_0 (total)= 30.0 ± 1.4 I_0(total) = 33.2 ± 1.5	$\sigma_0 = 26.7 \pm 2.0$ 31 ± 4 $I_0 = 36.0 \pm 4.0$	Roy[10] Block[12] Roy[10]

The radioactivity of the irradiated targets were measured by using a high purity Ge-detector system of 90% relative efficiency combined with a fast data acquisition system. For example, weak gamma-rays from ^{138}Cs were measured together with strong gamma-

rays from ^{137}Cs simultaneously(see Fig. 1). Details of the experiments and the analysis were published in ref. [1-5]. Results obtained are summarized in Table I.

The results show that the cross section of ^{137}Cs obtained is about twice of the previous one[6] and an experimental data of the resonance integral was newly obtained. Our results for ^{137}Cs are more reliable than that by Stupegia[6], since our method(IRM) could remove various sources of uncertainty as mentioned in ref. [1-3]. The cross section obtained for ^{90}Sr is in agreement with the value by McVey et al.[7] but not with that by Zeisel[8]. The resonance integral of ^{90}Sr was also obtained. The cross section of ^{99}Tc is almost equal to the previous data[9], and an experimental resonance integral is about twice of the value reported previously. The cross sections of ^{129}I were obtained for formation of the ground state and the isomeric state of ^{130}I separately. Previous data[10-13] show only a cross section of formation of the ground states. The resonance integrals were also obtained for formation of two states ^{130}I separately.

FINE STRUCTURE OF PHOTONUCLEAR REACTION CROSS SECTION

Fine structure of photonuclear reaction cross section in the giant resonance(GR) region can provide important information about the excitation mechanism of the GR and also for the study of the nuclear transmutation process using monochromatic photons[15]. In particular, the intrinsic width of fine peak in the GR is important because it determines the peak value of the cross section. However, very little is known about the width at present. The energy resolution for the cross section measurement using tagged photons[16,17] or monochromatic photons[18] was typically 100-500keV. Therefore, peak widths observed for some nuclei were almost determined by the experimental resolution. To obtain the intrinsic peak width, we proposed an experimental method that measures transmitted photons using a high resolution and high energy photon spectrometer(HHS)[19].

Figure 2 shows the conceptual setup of the experiment. The incident white photons should cover the energy range of interest. The photons are obtained by electron induced bremsstrahlung or more effectively by laser Compton scattering[20,21]. The transmitted photons from a thick target is measured by the HHS composed of two large germanium(Ge) detectors surrounded by a $Bi_4Ge_3O_{16}$(BGO) anti-coincidence spectrometer. The energy resolution of the experiment in the GR region should be improved to 10-20keV because the Ge detector has an energy resolution of about 0.1%[22] for high energy photons. The design of the HHS is shown in Fig.3. To obtain the large photopeak efficiency for high energy photons, two large N-type Ge detectors (relative efficiency of each crystal was 90% at 1.33MeV) were arranged like twins along a beam axis. To improve their peak/background (=total-peak) ratio, the twins were surrounded by thick BGO crystals that were used as an anti-coincidence spectrometer. Figure 4 shows the response function of the HHS for a collimated 15MeV photon beam of 2cmϕ. This was the result simulated by a Monte Carlo electron-gamma-shower code EGS4[23]. The response functions of the single Ge detector and the twin Ge detectors are also shown in the figure. The photopeak counts in the three spectra were normalized to be the same number, and the spectra were broaden with the energy resolution($\Delta E\gamma/E\gamma$)10^{-3} of the Ge detector.

To simulate the photonuclear cross section measurement with the HHS, the flux distribution of transmitted photons from a thick water target was calculated as an example. The size of the target was 5cm in diameter and 60cm in length. The density of the water

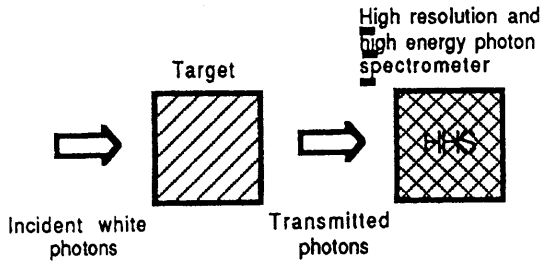

Fig.2 Schematic setup of high resolution measurement of photonuclear cross section using HHS

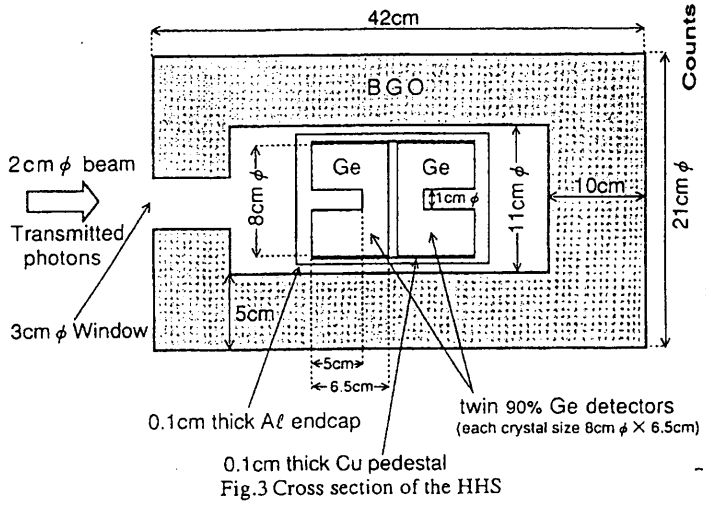

Fig.3 Cross section of the HHS

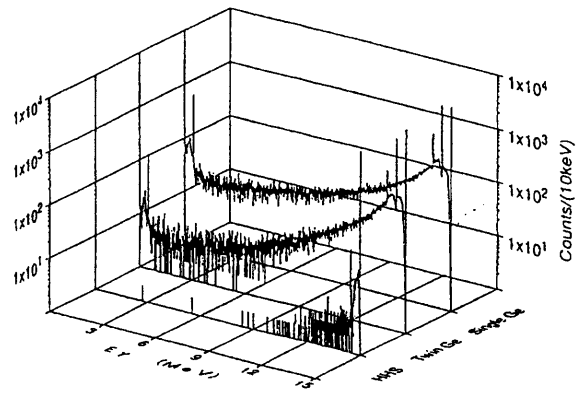

Fig.4 Response functions of three type spectrometer for 15 MeV photon

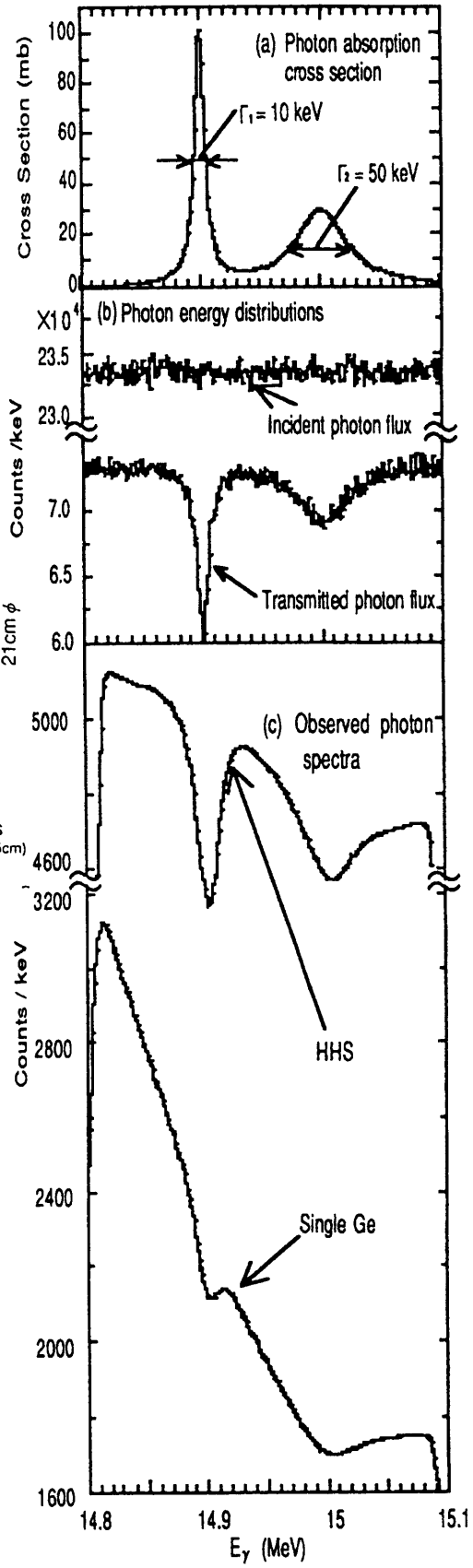

Fig.5 (a) Assumed photonuclear absorption cross section of ^{16}O,
(b) Incident white photon flux (upper) and transmitted photon flux (lower), and
(c) Transmission photon spectrum observed by
a single germanium detector(lower) and the HHS (upper)

target was assumed to be 1.0g/cm^3. The simulation code EGS4 was modified[24] to include the photonuclear cross section of ^{16}O as a part of photon-material interaction. Two narrow photon absorption cross section peaks of ^{16}O were artificially included in the code to simulate narrow dips in the transmission spectrum. The artificial cross section of the Breit-Wigner shape is shown in Fig.5(a). The width and height of the peak at 14.9MeV are 10keV and 100mb, and those at 15.0MeV were 50keV and 30mb, respectively. An incident photon flux was assumed to be white with an energy range of 14.8 to 15.1MeV. Figure 5(b) shows the incident white photon flux and the transmitted photon flux. Two dips can be clearly seen in the transmitted photon flux.

Figure 5(c) shows the transmission spectra observed by the single Ge detector(lower spectrum) and the HHS (upper spectrum). These were obtained by folding the transmitted photon flux(Fig.5(b)) using the response function of each detector. The dips are not clear in the spectrum observed by the single Ge detector because of its low peak/background ratio. On the other hand, the dips are clearly shown in the spectrum observed by the HHS. The FWHM of the dip observed at 14.9MeV is about 20keV. Therefore, widths of fine peaks in the GR region can be measured with the energy resolution of 10^{-3} by observing transmitted photons using the HHS, and correcting the detector energy resolution . Details of the simulation were described in ref. [19].

Fine structure of the photonuclear reaction in the GR energy region was shown to be observable using the specially designed high resolution and high energy photon spectrometer, HHS with an energy resolution of 10-20keV. The measurements using the HHS are in progress to supply data for nuclear transmutation studies using monochromatic photons.

Acknowledgements

The authors wish to acknowledge their indebtedness to Prof. I. Satoh of KEK, Prof. J. Kasagi of Tohoku University, Prof. K. Tomura of Rikkyo University, Drs. T. Sekine and Y. Hatsukawa of JAERI, Drs. T. Yamazaki, T. Noguchi, and H. Ohgaki of Electrotechnical Lab., and Mr. K. Imanishi of CSK Corp. for their help and valuable discussions.

References

[1] HARADA, H., WATANABE, H., SEKINE, T., HATSUKAWA, Y., KOBAYASHI, K., KATOH, T.: *J.Nucl. Sci. Technol.*, **27** (1990) pp.577.
[2] SEKINE, T., HATSUKAWA, Y., KOBAYASHI, K., HARADA, H., WATANABE, H., KATOH, T.:*J.Nucl. Sci. Technol.*, **30** (1993) pp.1099.
[3] HARADA, H., SEKINE, T., HATSUKAWA, Y., SHIGETA, N., KOBAYASHI, K., OHTSUKI, T., KATOH, T.: *J. Nucl. Sci. Technol.*, **31** (1994) pp.173.
[4] HARADA, H., NAKAMURA, S., KATOH, T., OGATA, Y.: *J. Nucl. Sci. Technol.*, **32** (1995) pp.395.
[5] NAKAMURA, S., HARADA, H., KATOH, T., OGATA, Y.: *J. Nucl. Sci. Technol.*, **33** (1996) pp.283-289.
[6] STUPEGIA, D.C.: *J. Nucl. Energy.*, **A12** (1960) pp.16.
[7] MCVEY, L.A.,BRODZINSKI, R.L.,TANNER, T.M.: *J. Radio. Chem.*, **76** (1983) pp.131.
[8] ZEISEL, G.: *Acta. Phys. Austr.*, **23** (1966) pp.223.
[9] LUCAS, M., HAGEMANN, R., NAUDET, R., RENSEN, C., CHEVALIER, C.: *IAEA Report*, **IAEA-TC-119/14** (1977) pp.407.

[10] ROY, J.C., WUSCHKE, D.: *Can. J. Chem.*, **36** (1958) pp.1424.
[11] EASTWOOD, T.A. et al.: *Proc. 2nd Int. Conf. On Peaceful Uses of Atomic Energy, 58 GENEVA,* **16** (1958) pp.54.
[12] BLOCK, R.C., SLAUGHTER, G.G., HARVEY, J.A.: *Nucl. Sci. Engin.*, **8** (1960) pp.112.
[13] PATTENDEN, N.J: *Nucl. Sci. Engin.*, **18** (1963) pp.371.
[14] WESTCOTT, C. et al.: *Proc. 2nd Int. Conf. On Peaceful Uses of Atomic Energy, 58 GENEVA,* **16** (1958) pp.70.
[15] SATOH. I: *Private communication,* (1993).
[16] SPRINGHAM, S.V., et al.: *Nucl. Phys.*, **A517** (1990) pp.93.
[17] ANNAND, J.R.M., et al.: *Phys. Rev. Lett.*, **71** (1993) pp.2703.
[18] BERMAN, B.L., FULTZ,S.C.: *Rev. Mod. Phys.*, **47** (1975) pp.713.
[19] HARADA, H. and SHIGETOME, Y.: *J. Nucl. Sci. Technol.*, **32** (1995) pp.1189-1191.
[20] KASAGI, J.: *Private communication,* (1994).
[21] OHGAKI, H., et al.: *Nucl. Instrum. Methods,* **A353** (1994) pp.384.
[22] CECIL, F.E., et al.: *ibid.*, **A234** (1985) pp.479.
[23] NELSON, W.R., et al: *Nucl. Instrum. Methods,* **A356** (1995) pp.362.
[24] KASE, T., et al.: *PNC Rep.* **TN8410 92-350**, pp.70-72 [in Japanese]; KASE, T.,: Dr. Thesis, Tohoku University, (1995), [in Japanese].

RECENT MEASUREMENTS OF FISSION NEUTRON YIELD DATA OF MINOR ACTINIDES

H. Oigawa, N. Shinohara, T. Mukaiyama,
Japan Atomic Energy Research Institute, Tokai-mura, Ibaraki-ken 319-11, Japan

H. H. Saleh, T. A. Parish,
Department of Nuclear Engineering, Texas A&M University, College Station, TX 77843, USA

W. H. Miller,
Nuclear Engineering Program, Missouri University, Columbia, MO 65211, USA,

S. Raman
Oak Ridge National Laboratory,* Oak ridge, TN 37831, USA

ABSTRACT

An experimental study of the fission neutron yield data for Np-237, Am-241, and Am-243 is under way for both prompt and delayed neutrons. Preliminary results of this experimental program are discussed in this paper.

The fission neutron yields, ν, of Np-237 and Am-243, as well as U-235, were measured for 144 keV silicon-filtered neutron beam at University of Missouri Research Reactor. The measured values were as follows:

ν : Np-237 : 3.13 ± 0.12 Am-243 : 4.00 ± 0.35 U-235 : 2.54 ± 0.06.

These values for minor actinides were about 20 % larger than those of ENDF/B-VI and JENDL-3.2, while that for U-235 was 4 % larger than the data files.

The delayed neutron data for Np-237, Am-241, and Am-243 were measured using fast pneumatic transfer system in Texas A&M University TRIGA reactor. The measured delayed neutron yields, ν_d, per 100 fissions in the thermal neutron spectrum were as follows:

ν_d (per 100 fissions) : Np-237 : 1.29 ± 0.04 Am-241 : 0.49 ± 0.02 Am-243 : 0.84 ± 0.04.

The ratios of the present values to those of the evaluated data files were 1.19, 1.14, and 1.05 for ENDF/B-VI, and 1.06, 1.09, and 0.88 for JENDL-3.2.

The 6-group data for the delayed neutron, λ_i and β_i, were also obtained from the experiment and compared with ENDF/B-VI. The measured decay constant, λ_i, agreed well with the data file. Large discrepancies were, however, found in the group fraction, β_i, especially for Am-243.

*ORNL is operated by Lockheed Martin Energy Research Cooporation for the U.S. Department of Energy (Contract No. DE-AC05-96OR22464).

1. INTRODUCTION

Fission neutron yield data of Np-237, Am-241, and Am-243 play important roles in a minor actinide (MA) burning reactor in which MA's are the major part of the nuclear fuel. The reliability of these data, however, seems insufficient for the design and the safety analysis of such a reactor. At present, new measurements[1),2)] are under way for both prompt and delayed neutron yield data of these nuclei. Preliminary results of this experimental program are to be discussed in this paper.

The accuracy of fission neutron yield, ν, greatly influences the criticality of the nuclear reactor. For Am isotopes, however, there was no experimental work on ν, while some experimental values are available for Np-237. In the present work, the neutron yields of Np-237 and Am-243 were measured for 144 keV silicon-filtered neutron beam at University of Missouri Research Reactor. The measurement for Am-241 was also attempted, but the reliable result can not be obtained because of the strong γ -ray emission from the sample.

The accuracy of delayed neutron yield and 6-group data, ν_d, β_i, and λ_i, greatly influences the reactor dynamics. For Np-237 and Am-241, Waldo et al.[3)] and Benedetti et al.[4)] measured these data in thermal and fast neutron spectra, respectively, while there was no experiment for Am-243. Waldo et al. tried to make measurements for Am-243, but the Am-241 impurity of their sample prevented them. In the present work, the delayed neutron data for Np-237, Am-241, and Am-243 were measured by using fast pneumatic transfer system in Texas A&M University TRIGA reactor. Measurement in the fast neutron spectrum is in progress and is to be reported elsewhere.[5)]

In the next section, the experimental methods are described for both the fission neutron yield measurement and the delayed neutron measurement. Then, the measured values are compared with those form the evaluated nuclear data files, ENDF/B-VI and JENDL-3.2.

2. EXPERIMENT

2.1 Fission neutron yield measurements

Experimental technique adopted here was newly developed to overcome the restriction of the amount of actinide samples. Proton recoil counters were used as the neutron detector, which can discriminate high energy fission neutrons from numerous scattered ones of 144 keV. The absolute fission rate was estimated by solid state track detectors. Both the proton recoil detectors and the track detectors were calibrated by Cf-252 fission source. The experimental arrangement is shown in Fig. 1. Details of the measurement were as follows.

Samples

Two kinds of samples were used in the measurement. One is the neutron emission sample for the fission neutron measurement, which had the dimension of 12.7mm$^{\phi}$ × 1.02mm^{t} and 100~300 mg of the oxide of the target actinide covered by titanium metal of 0.05mm^{t}. The other is the fission rate sample, where the actinide was electroplated on platinum backing disk and covered by a gold or nickel layer. The samples contain the actinide of 0.08 ~ 2.3 mg.

The isotopic purity of both samples were 97.7 % for U-235, 99.999 % for Np-237 and 99.997 % for Am-243, respectively.

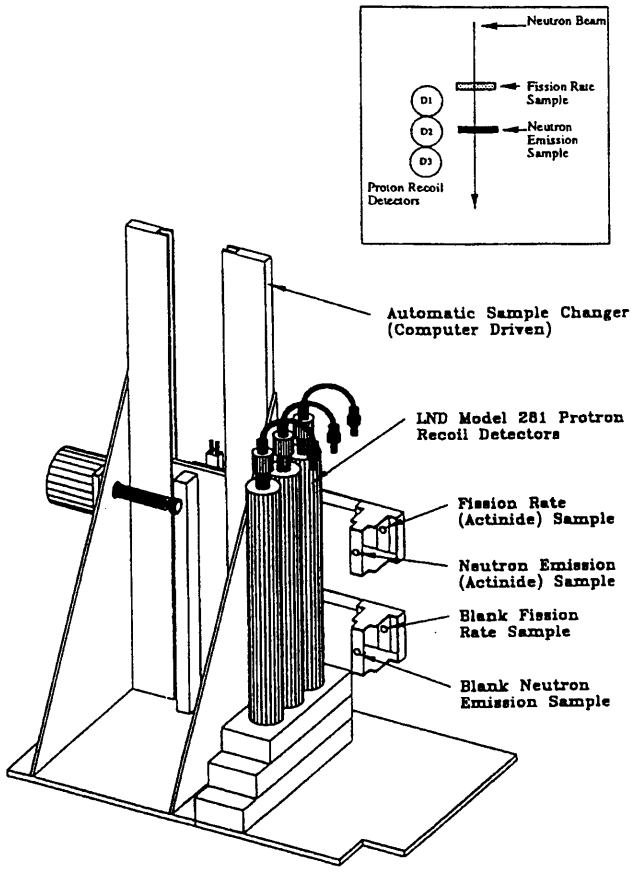

Fig. 1 Samples and detectors for fission neutron yield measurement

In addition to above actinide samples, blank samples and Cf-252 samples were also prepared for the background subtraction and the detection efficiency calibration, respectively.

Fission neutron measurement

A silicon-filtered beam from Missouri University Research Reactor[6] was used as the neutron source. To eliminate the affect of thermal neutrons, a cadmium sheet of 2 mm^{t} was put between the beam outlet and the sample. The neutron beam was collimated to 16 mm^{ϕ}.

Fission neutrons from the neutron emission sample were counted by three proton recoil detectors. To cut the 144 keV neutrons scattered by the sample, the discrimination level of the recoiled proton energy was set to 200 keV for U-235 and Np-237 and to 440 keV for Am-243. The higher discrimination level for Am-243 aimed to prevent signals due to the pile up of the strong γ -ray from the sample affecting the background counts. For the same reason, a lead sheet was placed between the sample and the detectors for the measurement of Am-243.

The detection efficiency was calibrated by using Cf-252 neutron source under the same experimental condition as the measurement of the actinide samples.

To obtain the number of the fission neutrons from the actinide, the background subtraction and the correction for the scattering of the actinide itself were done by using the count rate from the blank sample.

Fission rate measurement

A solid state track detector was attached to the fission rate sample and irradiated in the silicon-filtered beam simultaneously with the fission neutron measurement. The fission reaction was detected by the tracks of the fission fragments which penetrate the gold or nickel cover of the sample and go into the detector.

To obtain clear image of tracks, various detector material and various chemical etching processes were examined, and consequently, polycarbonate was chosen as the material and the optimum process was determined.

The detection efficiency was calibrated by Cf-252 sample covered by gold or nickel which has the same thickness as the fission rate sample.

Determination of ν

The ratio of the neutron emission rate to the fission rate, which were both calibrated to the absolute values, yields the number of the neutron emission per fission, ν.

2.2 Delayed neutron measurement

Experimental technique adopted here was similar to Keepin's.[7] The actinide samples used in the delayed neutron measurements were identical to those for the measurement of ν. The isotopic purity of Am-241 was essentially 100%.

Delayed neutron measurement

A TRIGA-type research reactor at the Texas A&M University Nuclear Science Center was used as the irradiation field. An existing

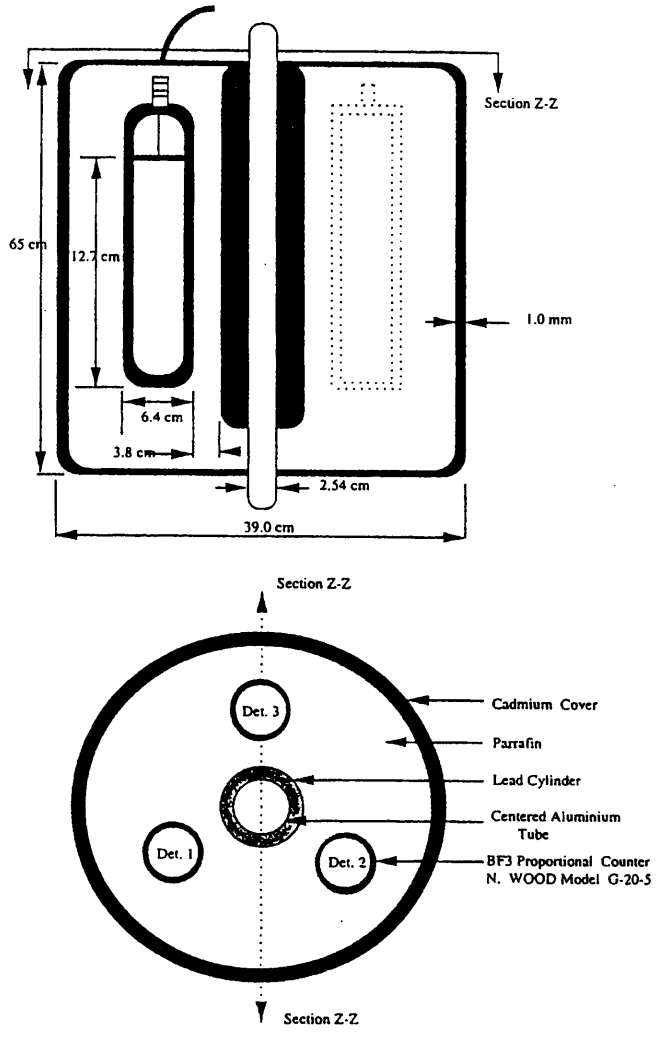

Fig.2 Sample receiver and detectors for delayed neutron measurement

pneumatic transfer system was revised to get enough speed to measure the delayed neutrons belonging to 1 ~ 5th. precursor groups ($T_{1/2}$=0.7 ~ 55sec).

Three BF_3 proportional counters were used for the detection of the delayed neutron emission. The actinide sample contained in a polyethylene vial was irradiated at the core receiver in the reactor and then transmitted to the sample receiver outside the reactor by the pneumatic system. The sample receiver and the BF_3 counters were surrounded by paraffin as shown in Fig. 2 to enhance the neutron detection efficiency. Three irradiation times were chosen to put emphasis on different precursor groups.

The efficiency of the detection system was calibrated by the delayed neutron emission from irradiated U-235 samples whose fission properties were considered to be well known.

Fission rate measurement

After the irradiation of each sample, γ -ray spectroscopy was performed to determine the absolute fission rate. The activities of Ba-140, La-140, Ru-103, I-131, and Mo-99 were measured. The detection efficiency of gamma-rays was calibrated by Eu-152 source depending on the energy of γ -ray. The cumulative fission yields quoted from ENDF/B-VI were used to convert the activities of FP's to absolute fission rates.

Determination of β_i, λ_i, and ν_d

To obtain the relative fraction and the decay constant of each precursor group, a least squares analysis was performed for the measured time attenuation curves of the delayed neutrons. Moreover, by combining the absolute neutron emission rate and the absolute fission rate, the number of delayed neutrons per fission was deduced. Calculated data was used for the 6th. group based upon Tuttle's empirical expression[8] and group-wise parameters given by Benedetti[4].

3. DISCUSSION

3.1 Fission neutron yield

The experimental results of fission neutron yields are shown in Table 1 together with those of the evaluated nuclear data files.

Table 1 Results of fission neutron yields ν (Incident neutron energy : 144 keV)

	Present work	ENDF/B-VI	JENDL-3.2
U-235	2.54 ± 0.06	2.44	2.45
Np-237	3.13 ± 0.12	2.66	2.56
Am-243	4.00 ± 0.35	3.30	3.23

It can be observed that present work gives larger values than both files; 4% for U-235, about 20% for Np-237 and Am-243. The relatively good agreement for U-235 indicates the validity of the present experimental method. For Np-237, however, large discrepancy was observed, though better agreement had been expected since the nuclear data files were evaluated on the basis of previous experimental work. Therefore, some experimental bias may exist in the present measurement.

On the other hand, there has been no experimental data available for Am-243. Hence, if the bias in Np-237 is settled, the present measurement will become invaluable in the evaluation of the minor actinide nuclear data.

3.2 Delayed neutron data

The experimental results of absolute delayed neutron yields are compared with those of the previous measurements and the evaluated nuclear data files in Table 2.

Table 2 Results of delayed neutron yields ν_d (per 100 fission)

	Experimental work			ENDF/B-VI	JENDL-3.2
	Present	Waldo et al.[3]	Benedetti et al.[4]		
Energy range	Thermal	Thermal	Fast	Thermal - 4MeV	Thermal - 6MeV
Np-237	1.29 ± 0.04	1.07 ± 0.10	1.22 ± 0.03	1.08	1.22
Am-241	0.49 ± 0.02	0.51 ± 0.07	0.39 ± 0.02	0.43	0.45
Am-243	0.84 ± 0.04	———	———	0.80	0.95

Since ν_d is considered to be constant below several MeV, the experimental values and those of the data files in Table 2 are comparable in spite of the different energy range.

For Np-237, the present work shows better agreement with JENDL-3.2 and Benedetti than ENDF/B-VI and Waldo. For Am-241, however, the present work agrees with Waldo's measurement very well. On the other hand, for Am-243, there has been no experimental work, and JENDL-3.2 gives 13 % larger value than the present work, while ENDF/B-VI agrees with the present value within the experimental error.

Measured 6-group data are compared with those in ENDF/B-VI in Table 3, 4 and 5 for Np-237, Am-241, and Am-243, respectively.

For decay constants, there is no large discrepancy between the present work and ENDF-B-VI, except for 3rd. and 4th. group of Np-237 and 1st. group of Am-241.

On the other hand, large discrepancies are observed in the relative yields especially for 3rd. and 5th. group of Am-243. Therefore, after the completion of the experiment in the fast neutron spectrum, which is in progress, it is recommended that evaluators of the nuclear data files take this experimental work into consideration.

Table 3 Results of 6-group data for delayed neutron from Np-237

	Decay constant λ_i (s^{-1})		Relative yields β_i	
Group	Present work	ENDF/B-VI	Present work	ENDF/B-VI
1	0.0129 ± 0.0006	0.0133	0.040 ± 0.002	0.040
2	0.0324 ± 0.0010	0.0316	0.233 ± 0.017	0.216
3	0.1048 ± 0.0019	0.1168	0.190 ± 0.010	0.156
4	0.341 ± 0.013	0.301	0.322 ± 0.027	0.363
5	0.85 ± 0.06	0.867	0.193 ± 0.007	0.166
6	———	2.76	0.021[a]	0.059

a) calculated

Table 4 Results of 6-group data for delayed neutron from Am-241

	Decay constant λ_i (s^{-1})		Relative yields β_i	
Group	Present work	ENDF/B-VI	Present work	ENDF/B-VI
1	0.0122 ± 0.0005	0.0133	0.036 ± 0.002	0.036
2	0.0318 ± 0.0016	0.0308	0.309 ± 0.015	0.254
3	0.111 ± 0.007	0.1131	0.195 ± 0.008	0.156
4	0.300 ± 0.017	0.287	0.331 ± 0.039	0.336
5	0.890 ± 0.023	0.865	0.110 ± 0.005	0.172
6	———	2.64	0.018[a]	0.045

a) calculated

Table 5 Results of 6-group data for delayed neutron from Am-243

Group	Decay constant λ_i (s^{-1})		Relative yields β_i	
	Present work	ENDF/B-VI	Present work	ENDF/B-VI
1	0.0131 ±0.0002	0.0135	0.024 ±0.013	0.023
2	0.0311 ±0.0009	0.0298	0.291 ±0.011	0.294
3	0.107 ±0.007	0.1138	0.221 ±0.008	0.154
4	0.324 ±0.021	0.299	0.384 ±0.016	0.315
5	0.914 ±0.031	0.882	0.051 ±0.002	0.166
6	———	2.81	0.029[a)]	0.048

a) calculated

4. CONCLUSION

Preliminary results of the experimental program on fission neutron data for minor actinides are reported.

The fission neutron yields, ν, of Np-237 and Am-243 were measured using a 144 keV silicon-filtered neutron beam at University of Missouri Research Reactor. The measured values were about 20 % larger than ENDF/B-VI and JENDL-3.2. The result for U-235 by the same experimental method shows 4% larger value than the data files.

The delayed neutron data for Np-237, Am-241, and Am-243 were measured by using a fast pneumatic transfer system at the Texas A&M University TRIGA reactor. The measured delayed neutron yields per 100 fissions in the thermal neutron spectrum were 1.29±0.04, 0.49±0.02, and 0.84±0.04. The ratios of the present values to those of the evaluated data files were 1.19, 1.14, and 1.05 for ENDF/B-VI, and 1.06, 1.09, and 0.88 for JENDL-3.2.

The 6-group constants, β_i, and λ_i, were also deduced from the experiment. The measured decay constant, λ_i, agreed well with the data file. Large discrepancies were, however, found in the group fraction β_i especially for Am-243.

REFERENCES

1) H. H. Saleh, T. A. Parish, W. H. Miller, H. Oigawa, and S. Raman : "Measurements of the number of neutrons emitted per fission in a fast neutron spectrum for U-235, Np-237, and Am-243", *Nucl. Instr. and Meth. in Phys. Res. B*, **103**, 393 (1995).
2) H. H. Saleh, T. A. Parish, S. Raman, and N. Shinohara : "Measurements of Delayed Neutron Decay Constants and Fission Yields from U-235, Np-237, Am-241, and Am-243", to be published in *Nucl. Sci. Eng.*
3) R. W. Waldo, R. A. Karam, and R. A. Meyer : "Delayed Neutron Yields : Time Dependent Measurements and a Predictive Model", *Phys. Rev. C* **23**, 1113 (1981).
4) G. Benedetti, A. Cesana, V. Sangiust, M. Terrani, and G. Sandrelli : "Delayed Neutron Yields from Fission of Uranium-233, Neptunium-237, Plutonium-238, -240, -241, and Americium-241", *Nucl. Sci. Eng.*, **80**, 379 (1982).
5) W. S. Charlton, T. A. Parish, S. Raman, N. Shinohara, and M. Andoh : "Delayed Neutron Emission Measurements from Fast Fission of U-235 and Np-237", to be presented in *Int. Conf. on the Physics of Reactors, PHYSOR96*, September 16-20, 1996, Mito, Ibaraki, Japan.
6) F. Y. Tsang and R. M. Brugger : "A Versatile Neutron Beam Filter Facility with Silicon and Iron Filters", *Nucl. Instr. and Meth.*, **134**, 441 (1976).
7) G. R. Keepin, T. F. Wimett, and R. K. Zeigler : Delayed Neutron from Fissionable Isotopes of Uranium, Plutonium, and Thorium", *J. Nucl. Energy*, **6**, 1 (1957).
8) R. J. Tuttle : 'Delayed Neutron Data for Reactor Physics Analysis", *Nucl. Sci. Eng.*, **56**, 37 (1975).

PROPERTIES OF NEPTUNIUM-PLUTONIUM MIXED NITRIDE SOLID SOLUTIONS

Yasuo Arai, Kunihisa Nakajima and Yasufumi Suzuki
Department of Chemistry and Fuel Research
Japan Atomic Energy Research Institute
Oarai-machi, Ibaraki-ken, 311-13 Japan

Properties of neptunium-plutonium mixed nitride solid solutions were investigated. The solid solutions covering the whole range of composition were prepared by heating the mixtures of NpN and PuN in nitrogen-hydrogen mixed gas stream at 2023 K. Formation of high-purity solid solution with a single phase was confirmed by X-ray diffraction and chemical analyses and composition dependence of the lattice parameters was examined. Vaporization behavior over the solid solutions was investigated by Knudsen-mass spectrometry and temperature dependence of the partial pressures of Np(g) and Pu(g) was examined. Furthermore, the thermal conductivities were determined from the thermal diffusivities measured and specific heat capacities estimated. The thermal conductivities of the solid solutions lay between those of NpN and PuN.

1. Introduction

Feasibility studies for transmuting minor actinides in fast reactors have been conducted in many countries from the viewpoint of a better management of the high level nuclear waste [1,2]. One of the incentives to using nitride fuel for transmutation is the probable formation of solid solution among actinide mononitrides with an extensive composition besides the superior thermal and neutronic properties. At present, however, the information on the mononitride solid solutions has been quite scarce except that of uranium-plutonium mixed nitride which has been developed as an advanced fuel for fast reactors. So it is significant to prepare the mononitride solid solutions containing minor actinides and determine their properties for the application of nitride fuel to transmutation. This report concerns the preparation and a few properties of neptunium-plutonium mixed nitride solid solutions including their lattice parameters, vaporization behavior and thermal conductivities estimated from thermal diffusivities.

2. Sample preparation

Neptunium-plutonium mixed nitride solid solutions (Np,Pu)N were prepared by heating the mixtures of NpN and PuN synthesized by carbothermic reduction from their oxides. Powders of NpO_2, PuO_2 and graphite were obtained from Harwell Laboratory, British Nuclear Fuels Ltd. and Graphitwerk Kropmühl GmbH, respectively, and their characteristics were described in earlier papers [3,4]. The mixing molar ratios of graphite to the dioxides, C/NpO_2 and C/PuO_2, for carbothermic reduction were chosen at 2.2. The reduction was carried out at 1823 K in N_2 gas stream for 43 ks, followed by decarburization at 1723 K in N_2-8%H_2 mixed gas stream for 86 ks. The products, NpN and PuN, were mixed at the molar ratios PuN/(NpN+PuN) of 0, 0.25, 0.50, 0.75 and 1.0 for the measurement of lattice parameter and vapor pressures and at 0.33 and 0.67 for the thermal diffusivity measurement. The mixed powders were pressed into green pellets under a pressure of ~300 MPa and heated again for the formation of solid solution at 2023 K in N_2-8%H_2 mixed gas stream for 90-180 ks. Then the pellets were subjected to X-ray diffraction and chemical analyses for characterizing the products.

The typical results of characterization were summarized in Table 1. According to the X-ray diffraction pattern, the formation of solid solution (Np,Pu)N with a single phase of *fcc* was confirmed for all the composition investigated. Namely, no other phases than NaCl-type mononitride were identified and the separation of the diffraction lines into $K\alpha1$ and $K\alpha2$ at high angles was fairly good. The results of chemical analysis indicated that both the oxygen and carbon contents in the samples, which are considered as principal impurities in nitride fuel prepared by carbothermic reduction, were lower than 0.05 wt.%. On the other hand, the nitrogen contents almost corresponded to the stoichiometric composition. The manner of the characterization mentioned above was described in detail elsewhere [5]. Although the chemical analyses of neptunium and plutonium were not conducted in this study, it was considered that the nominal composition kept unchanged since no significant loss of actinides by vaporization was observed during the sample preparation stage. In this study, the preparation of samples was carried out in the gloveboxes with high-purity argon gas atmosphere.

3. Results and discussion

3.1 Lattice parameter

Five X-ray diffraction lines of (600/442), (531), (440), (511/333) and (422) were used to calculate the lattice parameter of (Np,Pu)N solid solutions. The composition dependence of the lattice parameter was shown in Fig. 1. Lattice parameters of NpN and PuN were 0.48971±0.00003 and 0.49501±0.00002 nm, respectively, which agreed well with the reported values [6,7]. The lattice parameter increased with PuN content in the solid solution as was anticipated. However, the change in the lattice parameter deviated positively from the Vegard's law between NpN and PuN as shown in the figure.

It is well known that the dissolution of carbon and oxygen in actinide mononitride lattice results in the increase of the lattice parameter [8,9]. However, the present carbon and oxygen contents, lower than

500 ppm, were considered to be too low to influence the lattice parameter significantly. It was also considered from the experimental results that the incompleteness of the formation of solid solution or the heterogeneity of the sample could not affect the lattice parameter measured. On the other hand, the self irradiation damage had been almost recovered since the X-ray diffraction analysis was conducted on the next day of the heat treatment at 2023 K. From the speculation mentioned above, we now consider that the deviation of the lattice parameter from the Vegard's law has some relation with the bonding characteristics of (Np,Pu)N solid solutions.

Furthermore, we have observed the similar results for (U,Pu)N solid solutions, where the lattice parameter deviated positively from the Vegard's law especially in PuN rich region as shown in Fig. 2 [7,10]. The present lattice parameter of NpN just corresponded to halfway between those of UN and PuN. As the atomic number of the elements in the compound increases, the total number of electrons increases with the change of composition. In actinide mononitrides including their solid solutions, part of the electrons outside Rn shell are thought to be localized to the atom, and part of them itinerant and participating in bonding. Since the change in the lattice parameter reflects the nature of electron population in the solid solutions, we consider that the present and previous results may be related with occupancy states in the unfilled 5f-6d hybridized band near the Fermi level.

3.2 Vaporization behavior

Vaporization behavior of (Np,Pu)N solid solutions was investigated by use of Knudsen-effusion mass spectrometry with a tungsten cell having an orifice of 1 mm in diameter. Three kind of solid solutions, (Np0.75Pu0.25)N, (Np0.5Pu0.5)N and (Np0.25Pu0.75)N, were subjected to the measurements. The apparatus used was described in detail elsewhere [11] and an ionization potential was chosen at 10 eV throughout this study. The actinide bearing species observed in gaseous phase were Np(g), NpO(g), Pu(g) and PuO(g). Among them the pressures of NpO(g) and PuO(g) were much smaller than those of Np(g) and Pu(g) except in the initial heating stage. The absolute pressure was calculated from the ion intensity by use of a modified integral method.

Temperature dependence of the pressures of Np(g) and Pu(g) over the solid solutions was shown in Fig. 3. The pressures of Np(g) over the solid solutions showed the similar temperature dependence with that over Np(l) as in the case of NpN [12], which strongly suggested the precipitation of liquid neptunium during the measurements. On the other hand, temperature dependence of Pu(g) over the solid solutions was rather complicated. At temperatures higher than 1773 K, the slope of the logarithmic pressures of Pu(g) versus the reciprocal temperature was similar with the pressure over PuN [13] and there found a composition dependence of the solid solutions. At temperatures lower than 1473 K, however, the temperature dependence approached that over Pu(l) and the composition dependence became indefinite. At intermediate temperatures between 1443 and 1773 K, the transition stage was observed as shown in the figure. It was considered that the pressures of Pu(g) observed at high temperatures reflected the vapor pressure of Pu(g) over (Np,Pu)N being influenced by the Pu/(Np+Pu) ratio in solid phase, while the pressures of Pu(g) observed at lower temperatures the pressure over Pu(l) precipitated during the measurement.

It is well known that UN(s) vaporizes incongruently precipitating liquid uranium on account of the lower pressure of U(g), while PuN(s) vaporizes congruently into Pu(g)+0.5N2(g) [14,15]. Recent study on the vaporization behavior of NpN(s) revealed that the precipitation of liquid neptunium occurred during the measurement [12]. Although further study is needed hereafter, the vaporization behavior of (Np,Pu)N solid solutions seems to have both characteristics of those of NpN and PuN. Qualitative and quantitative thermodynamic analyses are under way in this respect.

3.3 Thermal conductivity

Thermal diffusivities of two kind of solid solutions, (Np0.67Pu0.33)N and (Np0.33Pu0.67)N, were measured from 750 to 1630 K by laser flash method. The apparatus used was described in detail elsewhere [16]. The samples for the measurement, discs of ~8mm in diameter and ~1.4mm thickness, were obtained by slicing the sintered solid solution pellets by a diamond wheel cutter. The results of the thermal diffusivity measurements are shown in Fig. 4. It was seen that the thermal diffusivities gradually increased with temperature and decreased with PuN content in the solid solution over the temperature range investigated, although the exact comparison was difficult on account of

the difference of density between the two samples. The origin of the difference in sintered density is not clear for the moment.

Thermal conductivity could be calculated by the product of thermal diffusivity, specific heat capacity and bulk density of the sample. The specific heat capacities of the (Np,Pu)N solid solutions were unknown unfortunately, and they were evaluated by the Kopp's law as a first approximation. The specific heat capacity of PuN was quoted from the report of Spear and Leitnaker [17] and the value for NpN was estimated from an empirical equation by the authors [18]. The thermal conductivities of two kind of the solid solutions obtained are shown in Fig. 5, in which they are corrected for porosity to the theoretical density by Maxwell-Eucken equation and the results for NpN [18] and PuN [19] are included for comparison.

It was seen from the figure that the thermal conductivities of the present solid solutions lay between those of NpN and PuN and showed almost the similar temperature dependence with them. The thermal conductivities also decreased with PuN content in the solid solutions, especially in NpN rich region. However, we must bear in mind that the results mentioned above have several uncertainties derived from the estimation of specific heat capacity and the correction for porosity besides the experimental error itself. The measurement of the specific heat capacity is planned in near future by use of differential scanning calorimeter.

4. Summary

The solid solutions of neptunium-plutonium mixed nitride (Np,Pu)N were prepared and some properties were examined in this study. The results are summarized as follows.

(1) Formation of the (Np,Pu)N solid solutions with a single phase of *fcc* was confirmed over the whole range of composition.

(2) Change in the lattice parameter of the solid solutions deviated positively from the Vegard's law as was reported in the case of (U,Pu)N solid solutions.

(3) Vapor pressures of Np(g) over the solid solutions suggested the precipitation of liquid neptunium during the measurements, while that of Pu(g) showed a rather complicated temperature dependence.

(4) Thermal conductivities of the solid solution, which were determined from thermal diffusivities measured and specific heat capacities estimated, lay between those of NpN and PuN and decreased with PuN over the temperature range investigated.

Acknowledgement

The authors wish to express their thanks to Drs. M. Hoshi and T. Muromura for the interest in this study.

References

[1] T. Mukaiyama, et al., "Partioning and transmutation program OMEGA at JAERI", Proc. GLOBAL'95, p.110 (1995).

[2] C. Prunier, et al., "The CEA spin program: minor actinide fuel and target aspects", *ibid.*, p.506 (1995).

[3] Y. Suzuki, et al., J. Nucl. Sci. Technol., 31 (1994) 677.

[4] Y. Arai, et al., J. Nucl. Mater., 168 (1989) 280.

[5] A. Maeda, et al., "Quality control of uranium-plutonium mixed carbide and nitride fuel", IAEA-TECDOC-466, p.35 (1988).

[6] C.H. de Novion, et al., J. Phys. Chem. Solids, 29 (1968) 1901.

[7] V. J. Tennery, et al., J. Amer. Ceram. Soc., 54 (1971) 247.

[8] T. Muromura, J. Nucl. Sci. Technol., 19 (1982) 852.

[9] G. C. Jain, et al., J. Nucl. Mater., 202 (1993) 245.

[10] Y. Suzuki, et al., J. Nucl. Sci. Technol., 28 (1991) 689.

[11] H. Takeshita, et al., J. Nucl. Mater., 78 (1978) 281.

[12] K. Nakajima, et al., "Vaporization behavior of neptunium mononitride", 14th IUPAC Conference on Chemical Thermodynamics (ICCT-96), Osaka, Japan (1996).
[13] Y. Suzuki, et al., J. Nucl. Mater., 188 (1992) 239.
[14] C. A. Alexander, et al., *ibid.*, 31 (1969) 13.
[15] C. A. Alexander, et al., "Fabrication and high-temperature thermodynamic and transport properties of PuN", in Plutonium 1975 and other actinides, North-Holland, Amsterdam, p.277 (1976).
[16] S. Fukushima, et al., J. Nucl. Mater., 102 (1981) 30.
[17] K. E. Spear, et al., US Report ORNL-TM-2106 (1968).
[18] Y. Arai, et al., J. Nucl. Mater., 211 (1994) 248.
[19] Y. Arai, et al., *ibid.*, 195 (1992) 37.

Table 1 Typical characteristics of the samples after the heat treatment in N_2-8%H_2 mixed gas stream

Composition	NpN	75NpN-25PuN	67NpN-33PuN	50NpN-50PuN	33NpN-67PuN	25NpN-75PuN	PuN
Heat-treatment period (ks)	43	43	86	43	86	43	43
Phases	fcc	fcc	fcc	fcc	fcc	fcc	fcc
N content (wt.%)	5.65	n.d.	5.64	n.d.	5.60	n.d.	5.57
O content (wt.%)	0.03	n.d.	0.04	n.d.	0.04	n.d.	0.04
C content (wt.%)	0.05	n.d.	0.02	n.d.	0.03	n.d.	0.03

n.d. = Not determined

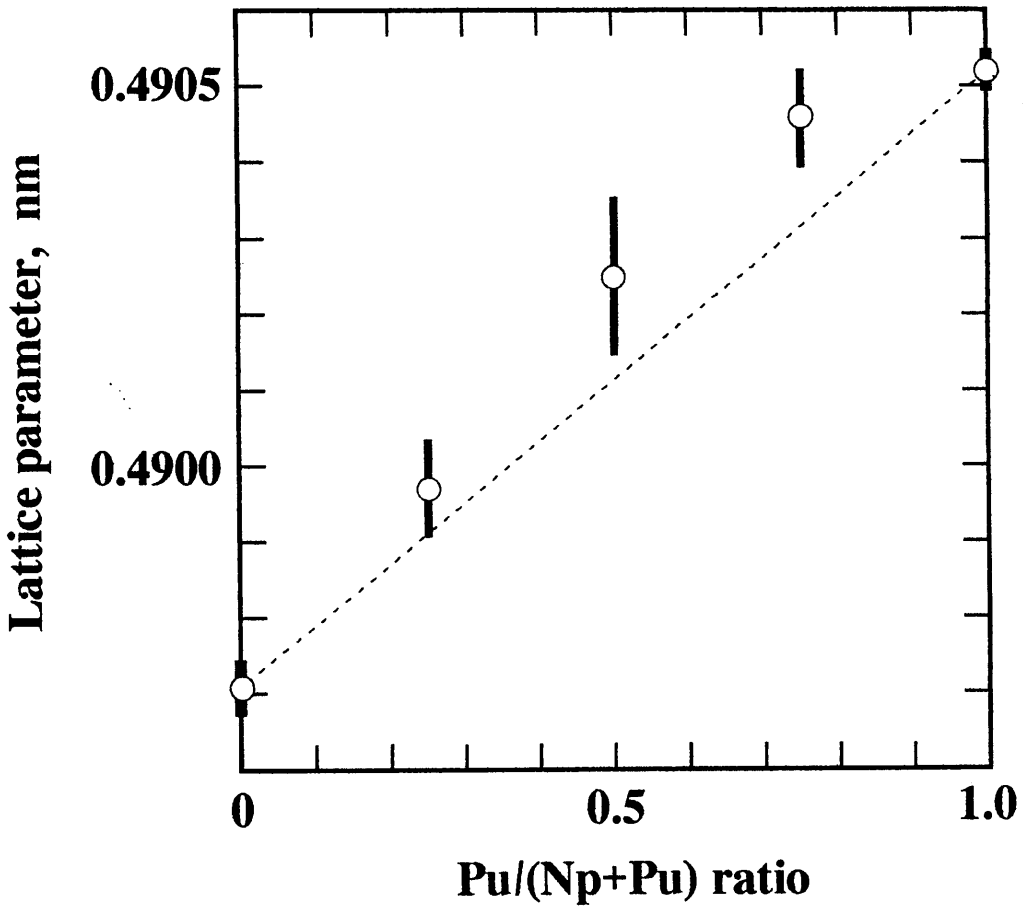

Fig. 1 Lattice parameter of (Np,Pu)N solid solutions

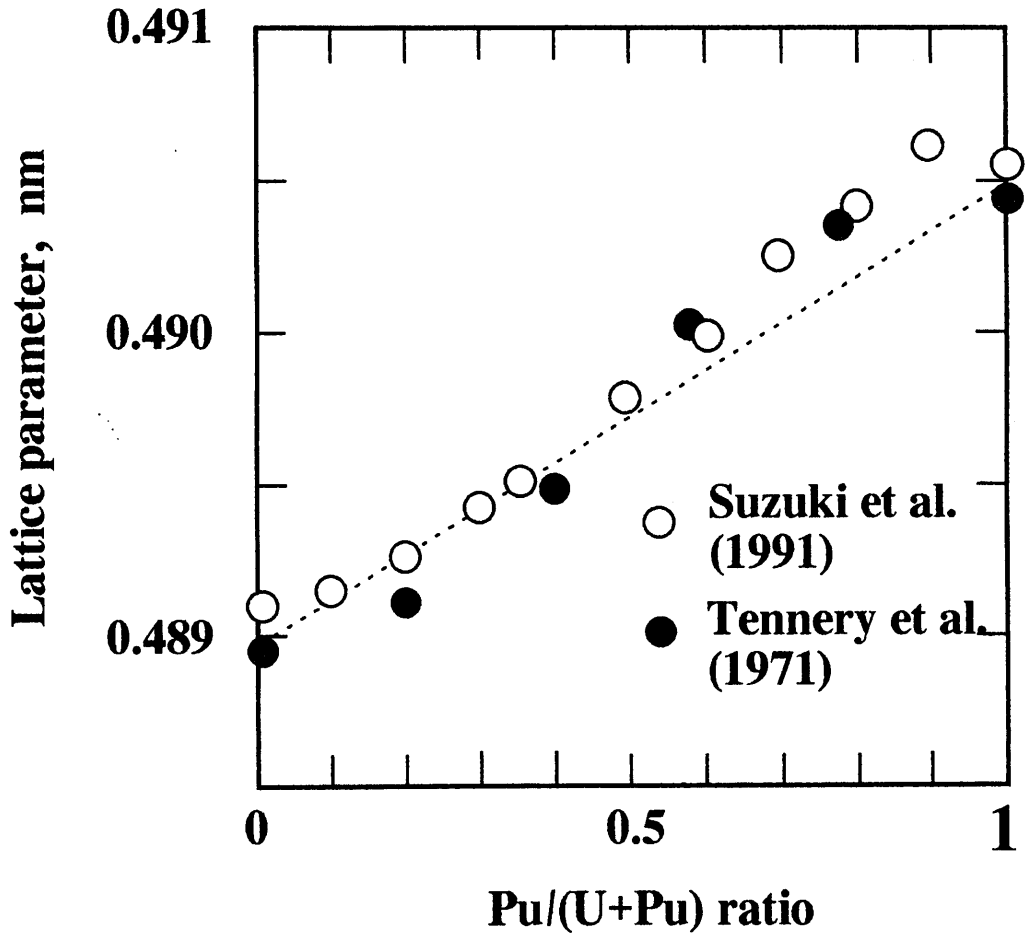

Fig. 2 Lattice parameter of (U,Pu)N solid solutions

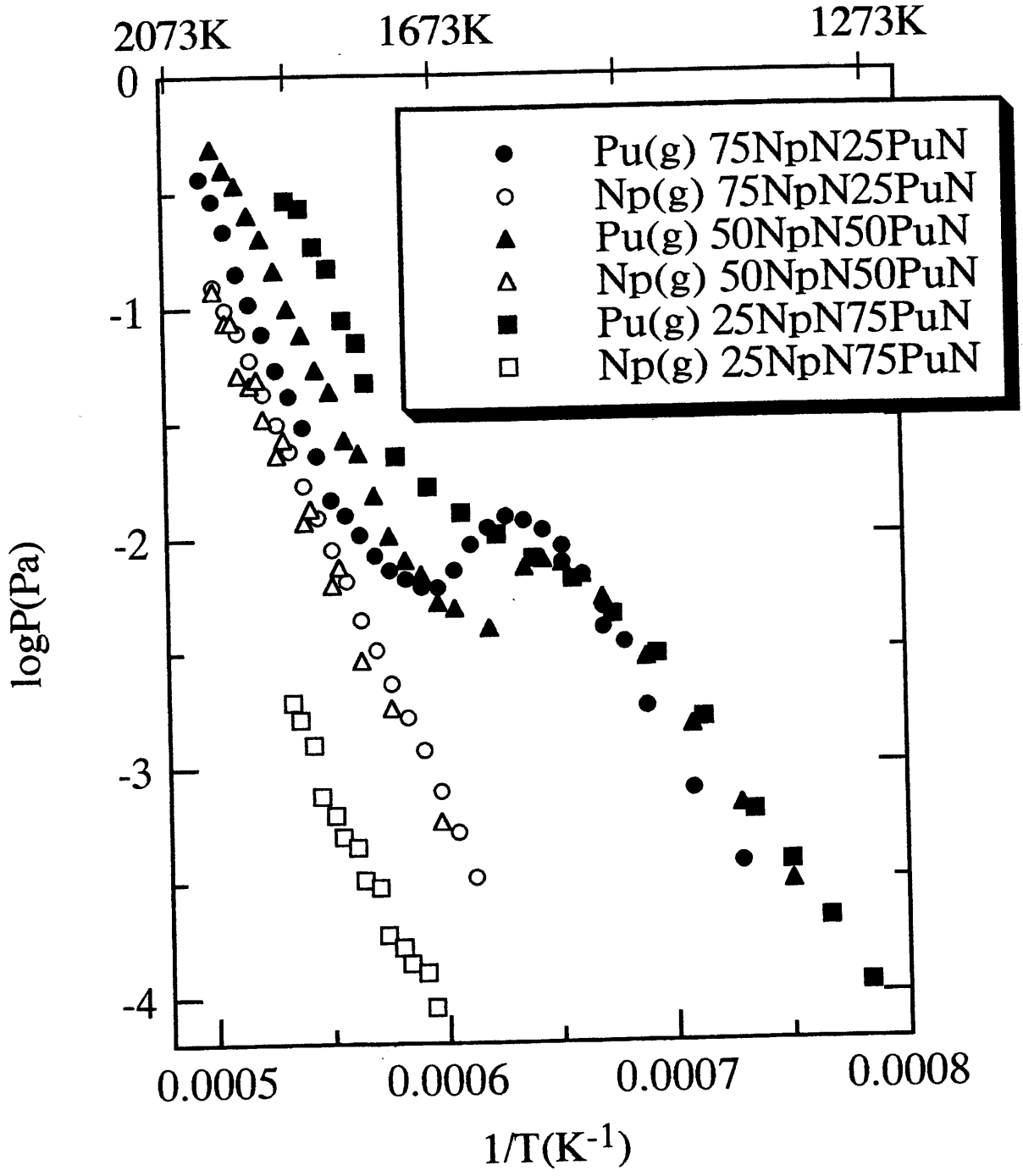

Fig. 3 Vaporization behavior of (Np,Pu)N

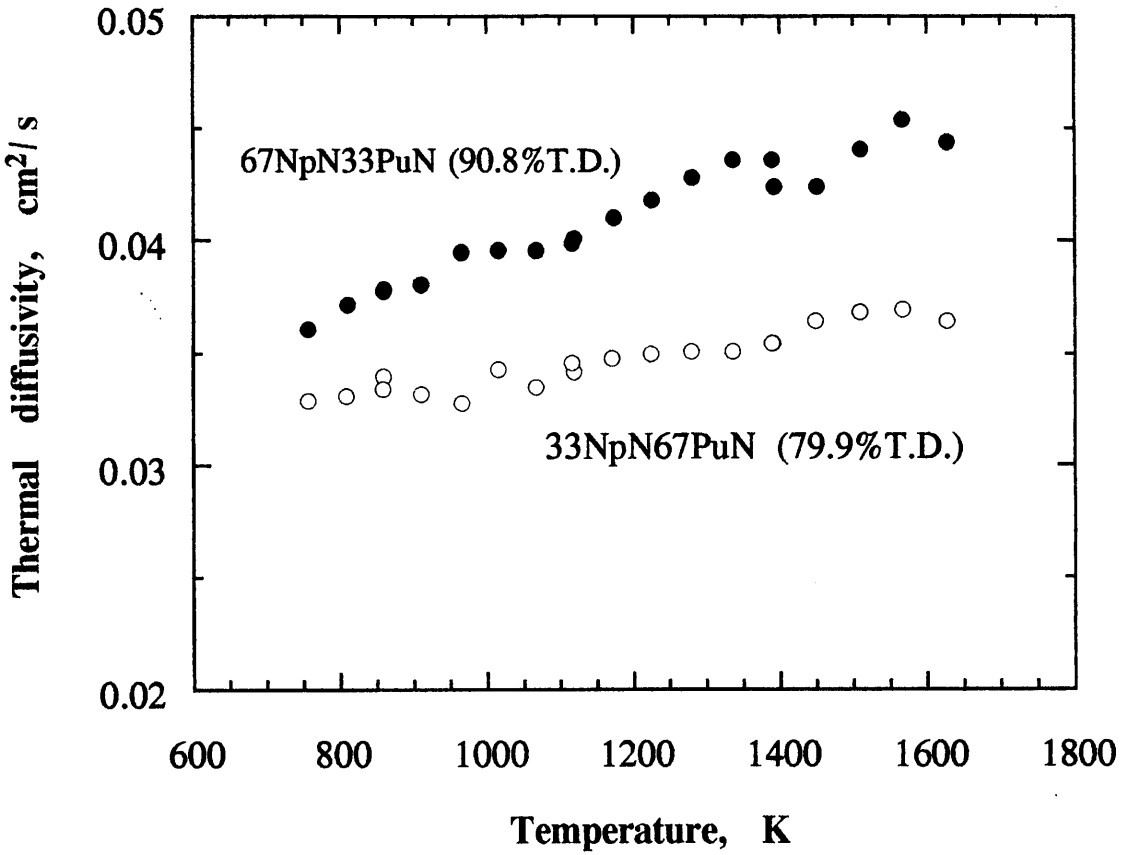

Fig. 4 Thermal diffusivity of (Np,Pu)N solid solutions

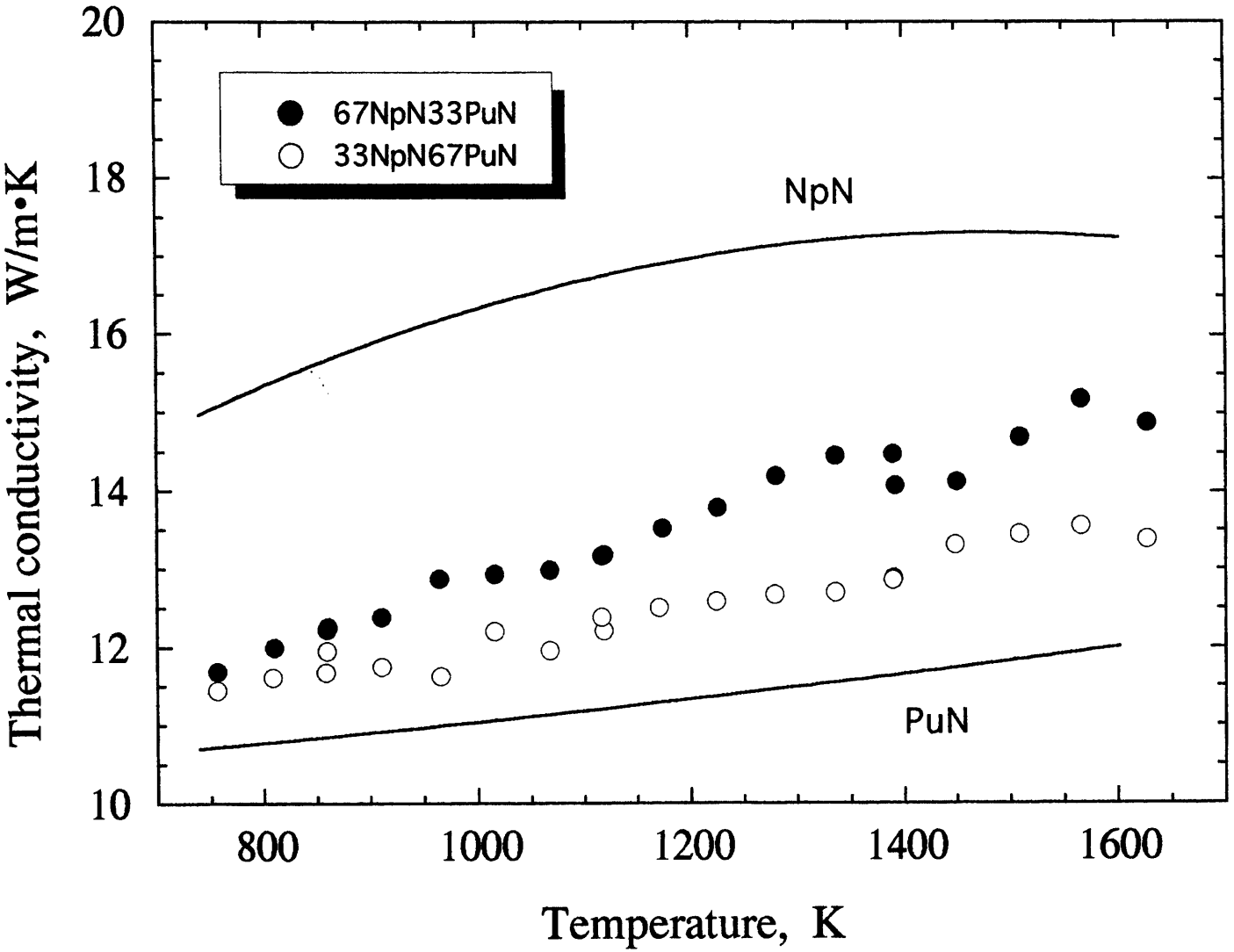

Fig.5 Thermal conductivity of (Np,Pu)N solid solutions corrected to 100%T.D. compared with those of NpN [18] and PuN [19]

NITRIDE-FORMING BEHAVIOR IN LIQUID CADMIUM-URANIUM-LANTHANIDES ALLOYS

Mitsuo Akabori, Akinori Itoh and Toru Ogawa
Department of Chemistry and Fuels Research, Japan Atomic Energy Research Institute
Tokai-mura, Naka-gun, Ibaraki-ken 319-11, Japan

Abstract

The nitride formation reaction of liquid 2wt% U-1wt% Gd-1wt% Ce-Cd alloys has been studied over the temperature range of 773~873 K using graphite and molybdenum crucibles. The Cd-U alloys were contacted with nitrogen gas or Li_3N. Uranium in the liquid Cd alloy was preferentially nitrided to form U_2N_3, which were produced at nitrogen gas-liquid alloy interface. A little gadolinium precipitated as nitrides, GdN or (U,Gd)N phase. The rest of gadolinium and almost all of cerium remained in the Cd phase as MCd_{11} (M: Gd and Ce) intermetallic compounds. Resistance of Ce to nitridation is due to the lower activity coefficient in Cd-rich solution at the temperatures.

1. Introduction

The nitride-forming reaction in liquid alloys containing actinide and lanthanide elements is of interest for both technological and fundamental science. Actinide nitride has been extensively studied as a candidate fuel for actinide burning system. In the proposed pyrochemical processing [1], nitride fuels are recovered as metals or alloys by electrorefining in a LiCl-KCl eutectic salt. The recovered metallic fuels are then converted to the nitrides in liquid Cd-An (An:actinides) alloys. In this process, actinides can be separated from lanthanides as a result of activity coefficient differences between actinides and lanthanides. The further removal of lanthanides from actinides may be achieved if necessary [2]. The use of Cd-An alloys is superior in some points such as high vapor pressure of Cd to other liquid-metal processes, for example, the liquid tin process [3,4]. In the liquid tin process, it is difficult to remove Sn by distillation after nitriding because of its high boiling point. Li_3N may be also used in the liquid Cd process as a nitriding agent, instead of nitrogen gas, because the nitrogen evolved during electrolysing the nitrides in the salt is trapped by lithium to form Li_3N.

The purpose of this study is to understand the basic behavior of nitriding in liquid Cd containing uranium and lanthanides and to determine if lanthanides could be separated by nitride precipitation techniques in Cd-U alloys.

2. Experimental

Nitriding of liquid Cd-U-Gd-Ce alloys was performed in closed quartz ampoules using nitrogen gas or Li_3N. Reaction temperatures used were 773 and/or 873 K. Graphite and/or molybdenum crucibles were used to contain the liquid Cd alloys and they were degassed in a high vacuum at 1023 K before alloying. Molybdenum is considered to be the best material as a container for liquid Cd alloys because the solubility of Mo in liquid Cd is very small at the present temperatures (about 10^{-7}~10^{-6} wt%)[5,6].

Approximately 7 g Cd-2wt%U-1wt%Gd-1wt%Ce alloys were prepared in an inert atmosphere. Uranium, gadolinium, cerium and cadmium metals of 99.9% purities were weighed and placed in quartz tubes together with graphite or molybdenum crucibles in an argon-atmosphered glove box. The samples in the quartz ampoules were sealed in high-purity helium gas and then melted for 20~50 h at 873 K to obtain the homogenized Cd-U-Gd-Ce alloys.

Nitridings were performed in nitrogen gas of 99.995wt% purity. About 250 Torr nitrogen was contained in the quartz ampoule of 20~50cc in volume at room temperature. The nitrogen pressure increased up to about 600~700 Torr at the reaction temperatures of 773 and 873 K, where nitriding times were 100~170 h. For the Mo crucibles, the liquid Cd alloys were often stirred during nitriding using Mo rods which were placed in the Mo crucible. To terminate the nitriding, the quartz ampoules were water-cooled. The amounts of nitrogen absorbed in the liquid alloys were measured by fracturing the quartz ampoules in water after nitriding and correcting the rest of nitrogen gas.

In the case of nitriding with Li_3N, the Cd-U alloy containing Gd and Ce was sealed with Li_3N under vacuum in a quartz ampoule using a graphite crucible and then heated to 773 K. The amount of L_3N added was ~25mg, which was determined from a condition that an increase of inner pressure in the quartz ampoule due to decomposition of Li_3N to N_2 is not in excess of 760 Torr at 773 K.

In addition, a simple technique was employed to measure the time dependences of the amount and pressure of nitrogen reacted with the Cd-U alloy. The Cd-U alloy containing Ce and Gd was held in a long glassy carbon crucible in order to prevent loss of Cd due to vaporization during nitriding. The crucible was then placed in a quartz tubing, which is connected with a pressure gauge for measuring the pressure in the system. The dead volume of the system was measured with pure helium. Nitriding of the alloy with nitrogen was performed at 873 K without stirring.

After nitriding, the samples were cut to half together with the crucibles and products in the Cd alloys were examined. Electron-probe micro-analysis (EPMA) was used to identify phases in the Cd alloys, in particular, the stoichiometry of nitride precipitates of uranium or lanthanides. The acceleration voltage and beam size were 20 KV and ~1 μm in diameter, respectively. The X-ray intensities were converted into compositions using the pure

elements, UN and U_2N_3 standards. The detection limits of the EPMA analysis are about 0.1, 0.1, 0.2, 0.2, 0.5 and 1.0 wt% for Cd, U, Gd, Ce, N and C, respectively.

3. Results

3.1 Reaction with nitrogen gas

3.1.1 Products for the graphite crucibles

Fig.1 shows the results when the Cd-2wt%U-1wt%Gd-1wt%Ce alloys were nitrided for 100 and 170 h at 873 and 773 K, respectively, in the graphite crucibles. The compositions of precipitates found in the alloy solidified from 873 K are summarized in table 1, where the concentration of nitrogen in stoichiometric U_2N_3 is about 8.1 wt%. The EPMA analysis of the Cd alloys solidified from 773 and 873 K clearly indicated that uranium precipitates in the Cd alloys were mainly U_2N_3 and U(C,N) phases. The U_2N_3 phase was found only at the surface of the Cd alloy, that is, the interface between the liquid alloy and nitrogen gas, as shown in figs.1(a) and (d). This suggests that the U_2N_3 phase was formed by a direct reaction between the dissolved uranium in the Cd melt and nitrogen gas in atmosphere. The formation reaction of the U_2N_3 can be described by the equation,

$$2\underline{U}(\text{dissolved}) + 3/2\ N_2(g) = U_2N_3(s).$$

The reaction appears to be rapid at 873 K, producing porous reaction layers, accompanied by considerable amounts of spalled fragments. From the EPMA analysis of the U_2N_3 precipitates, they contained a little gadolinium and cadmium of 0.4 and 0.5 wt%, respectively. However it was not obvious whether the chemical form of Gd is nitride or metallic. As a result of the high density of U_2N_3 compared with Cd, the U_2N_3 precipitates formed at the alloy surface were expected to sink to the bottom of the graphite crucible. However the U_2N_3 did not sink and increased its thickness at the alloy surface through nitriding. This is mainly due to formation of the layered nitride at the liquid alloy surface as a result of static nitriding reaction without stirring, as clearly shown in fig.1(d), where formation and growth of very thin adherent U_2N_3 layer at the alloy surface solidified from 773 K can be observed. The U_2N_3 layer formed on the overall surface of the liquid alloy would depress further nitridation of uranium dissolved in the Cd alloy. In a deed, the amount of nitrogen absorbed in the liquid alloy nitrided for 170 h at 773 K was below about 1 ccSTP, which correspond to about 10% in conversion rate of U dissolved in the Cd alloy to U_2N_3.

By contrast, the U(C,N) phase concentrated at the near bottom of the crucible, as shown in fig.1(c). Precipitates of uranium carbide, probably, UC, were also observed around the bottom of the Cd alloy homogenized in a helium atmosphere at 873 K before nitriding. This means that the UC precipitates were produced by a reaction between uranium and free carbon in the liquid Cd. Therefore, formation of the U(C,N) precipitates in the nitrided alloy was due to nitridation of the UC precipitates formed during alloying with atomic nitrogen dissolved in the Cd melt. On the other hand, the concentration of U in the Cd phase nitrided at 873 K was below about 0.1wt% which corresponds to the detection limit of the EPMA analysis. However, a small fragment of pure uranium was found at the near bottom of the Cd alloy nitrided at 773 K, suggesting that 2 wt%U may be in excess of the solubility of U in the Cd alloy at 773 K. From the U-Cd binary phase diagram [5], the solubilities of U in Cd are 2.35 and 2.14 wt% at 773 and 873 K, respectively.

The lanthanides, in particular, cerium, were quite different in their precipitation behavior from uranium. Cerium nitride, probably CeN, or Ce-contained U-N phases cannot be found in the Cd alloys nitrided at 773 and 873 K. Almost all the lanthanide elements precipitated in the Cd alloy as a M(M:Gd,Ce)-Cd intermetallic compound. From the EPMA analysis, the M-Cd intermetallic compound was estimated to be $(Gd,Ce)Cd_{11}$ phase, where the concentrations of Gd and Ce were a little scattered among the precipitates, as shown in table 1. The intermetallic compound MCd_{11} formed on water-cooling after nitriding and remained in suspension in the Cd melt. The result that unlike U, the lanthanides, in particular, cerium, did not form the nitrides can be explained by the very low activity coefficients of lanthanides in cadmium, compared with that of uranium. The activity coefficients of U, Gd and Ce in Cd are 75, 6.3E-7 and 1.3E-8 at 773 K, respectively [6] and indicate that the Cd-Ce, Gd alloys are very stable and the much larger concentrations are necessary to equal the chemical activity of U.

3.1.2 Products for the Mo crucibles

The appearance of nitride precipitates for the Mo crucible was significantly different from that for the graphite crucible. Table 2 indicates the compositions of precipitates found in the alloy nitrided for 100 h at 873 K. Fig.2 shows typical sections of the near bottom and near surface regions of the Cd alloys nitrided for 100 h at 873 and 773K, respectively. From the EPMA analysis, both the precipitates appear to consist of U_2N_3 and U-N phases containing gadolinium. The formation of the nitride layer on the alloy surface found at 773 K is also very similar to those for the graphite crucible without stirring. The nitride precipitates found on the near bottom region are likely to have a very thin layer structure, suggesting that the precipitates were formed at the alloy surface. Sinking of the nitride precipitates to the bottom can be explained by fragmentation of the nitride layer formed at the surface due to mechanical stirring during nitriding.

As shown in table 2, the EPMA analysis of the thin layered U-N precipitates found at 873 K, which contained a little gadolinium, showed that the precipitates have low nitrogen contents, 6.4~7.2 wt%, compared with that of U_2N_3 phase (8.1wt%), and 0.3~2.4 wt% Gd was present in the precipitates. This result suggests the product to be the mixture phase of uranium and gadolinium nitrides. The formation of U_2N_3 occurs initially and a decrease in concentration of U in the liquid Cd promotes formation of gadolinium nitride, GdN or (U,Gd)N. The amounts of nitrogen absorbed in the liquid alloys during nitriding are summarized in table 3. For the nitriding at 873 K, the conversion of U to U_2N_3 attained to about 92%. At this stage where the concentration of U in Cd is very low, the chemical activity of U would be greatly reduced to approximately that of Gd and Gd is likely to form the nitride, probably GdN or (U,Gd)N, because the activity coefficient of Gd in Cd is higher than that of Ce. The formation of (U,Gd)N at the alloy surface means coprecipitation of U and Gd. Moreover, decomposition of U_2N_3 to UN in the liquid Cd could occur, because the solubility of nitrogen in liquid Cd is expected to be very low. The nitride layer formed on the alloy surface at 773 K, as shown in fig.2(b) also contained 0.9 wt% Gd, suggesting that both U_2N_3 and GdN or (U,Gd)N could be formed simultaneously.

On the other hand, all of Ce precipitated in MCd_{11} intermetallic phases together with Gd in the Cd alloys solidified from both 773 and 873 K. As mentioned before, the strong resistance of Ce to nitride forming, compared with U and Gd, can be explained by its lower activity coefficient in Cd, that is, its greater stability of Cd-Ce alloys. The composition of the MCd_{11} seems to be scattered among the precipitates, as shown in table 2. This tendency was very similar to that for the graphite crucible. Some of the MCd_{11} precipitates found in the alloy nitrided at 773 K contained a little uranium and the conversion of U to U_2N_3 was low, compared with that at 873 K. This indicates that uranium in the Cd alloy would be not completely nitrided at 773 K.

3.1.3 Time dependence of nitriding reaction

Fig.3 shows the time dependences of nitrogen pressure in the quartz ampoule and conversion of uranium in the Cd-U alloy to U_2N_3 during nitriding at 873 K. The conversion was calculated from the amount of nitrogen absorbed in the Cd alloy. The equilibrium amount of U_2N_3 formed was about 45%. Therefore, the nitriding of uranium dissolved in the Cd alloy was not completed. The time dependence of conversion demonstrates that the reaction rate increases rapidly at early stage, attains the maximum at ~5 hours and then decreases gradually. This tendency means that U_2N_3 layer formed at the alloy surface prevented further progress of nitriding reaction. From the EPMA analysis, the formation of U_2N_3 layer at the alloy surface was also observed. As mentioned before, it is likely that mechanical stirring is an effective technique for enhancing or completing the conversion of uranium to nitride.

3.2 Reaction with Li_3N

Fig.4 shows typical cross sections of surface regions for the Li_3N contained Cd alloy annealed at 773 K. From the EPMA analysis, it was found that the reaction of the liquid Cd-U alloy with Li_3N yields the uranium sesquinitride, U_2N_3. The formation of U_2N_3 occurred at both the surface of the liquid Cd alloy and the interface between Cd-Li phase and the liquid Cd alloys. The U_2N_3 precipitates contained a little Gd. U(C,N) phase also precipitated at the near bottom of the alloy. Lanthanides, Ce and Gd, concentrated in the MCd_{11} intermetallic phase. The nitriding behavior of Cd-U-lanthanides alloy with Li_3N appears to be very similar to those with nitrogen gas. On the other hand, the Cd-Li precipitates floated to the alloy surface, suggesting that the reaction between Cd and Li_3N yields a low density Cd-Li intermetallic compound. The composition of the Cd-Li alloy lies in the range of $CdLi_2$~$CdLi_{3.5}$; the phase diagram of Cd-Li system suggests the product to be $CdLi_3$ [5].

About 7 cc nitrogen remained in the quartz ampoule after nitriding. The amount of nitrogen evolved by complete decomposition of Li_3N is estimated to be ~8 cc. This suggests that almost all of Li_3N was decomposed by the reaction with Cd to evolve nitrogen gas and ~1 cc of the evolved nitrogen contributed the nitriding of uranium in the Cd alloy. The conversion of uranium to U_2N_3 was no more than ~ 10%. This conversion rate is significantly lower than those for the nitriding with stirring.

The results of the present experiment described above indicate that the nitride precipitation technique using liquid Cd alloy could be a useful technique in separating lanthanides, in particular, light elements such as La ~ Nd from actinides. The Li_3N can be also used as a nitriding agent in this process, instead of nitrogen.

Acknowledgments

The authors are grateful to Drs. Hoshi and Muromura at the Japan Atomic Energy Research Institute for support of this study. We want to express thanks to F.Kobayashi for providing some experimental materials.

References

[1] M.Hand, F.Kobayashi and H.Katsuta, JAERI-RDIPF Seminar on Lead Cooled Fast Reactor, Mito, Japan, Oct.28-29, 1993.
[2] T.Ogawa, M.Akabori, F.Kobayashi and R.G.Haire, paper presented at the 9th International Symposium on Thermodynamics of Nuclear Materials (STNM-9), Osaka, Japan, August 26-30, 1996.
[3] N.A.D.Parlee and R.N.Anderson, Nitride-Forming Reactions in Liquid Uranium Alloys, USAEC report DOE/SF/00326-T1(1973).
[4] T.Schicks, R.N.Anderson and N.A.D.Parlee, High Tem. Sci., 6(1974)351.
[5] T.B.Massalski ed., Binary Phase Diagram (American Society for Metals, Metals Park, Ohio, 1986).
[6] T.Koyama et al., Pyrometallurgy Data Book, CRIEPI report T93033, (1994).

Table 1
The composition of products in the Cd alloy at 873 K for the graphite crucible

Phases	Concentrations (wt%)					
	Cd	U	Gd	Ce	N	C
Cd matrix	99.9	<0.1	<0.2	<0.2	<0.5	
U_2N_3	0.5	91.0	0.4	<0.2	8.2	
$(Gd,Ce)Cd_{11}$	88.1~88.3	<0.1	7.7~5.5	4.2~6.2	<0.5	
U(C,N)	<0.1	95.8	<0.2	<0.2	2.3	1.9

Table 2
The composition of products in the Cd alloy at 873 K for the Mo crucible

Phases	Concentrations (wt%)					
	Cd	U	Gd	Ce	N	C
Cd matrix	100	<0.1	<0.2	<0.2	<0.5	
U_2N_3	<0.1	91.9	<0.2	<0.2	8.1	
$(Gd,Ce)Cd_{11}$	89.12~88.4	<0.1	2.6~7.5	8.2~4.2	<0.5	
U-N-Gd	1~0.9	89.4~92.4	2.4~0.3	<0.2	7.2~6.4	

Table 3
The amounts of nitrogen absorbed into the Cd alloys in the Mo crucibles

Temp. (K)	Time (h)	Initial volume (cc at STP/ g U)	Absorbed volume (cc at STP/g U)	Conversion to U_2N_3 (%)
773	100	100.2	55.3	78.3
873	100	89.8	64.6	91.5

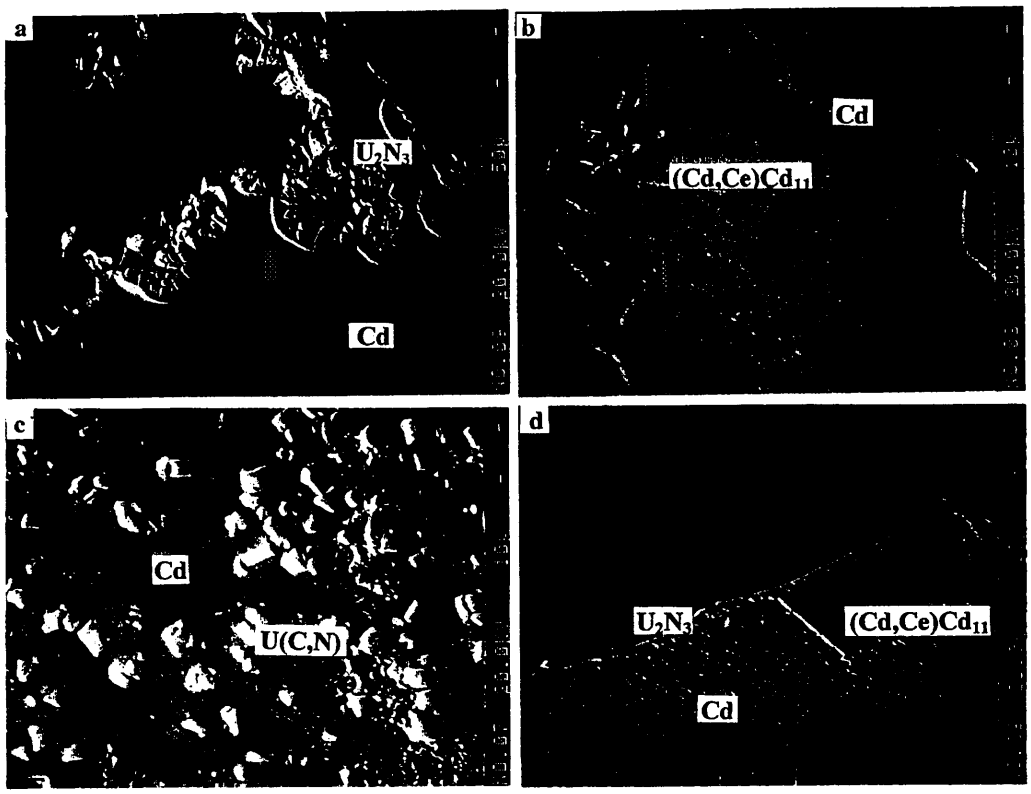

Figure 1 Backscattered electron micrographs of the Cd alloys in graphite crucibles : Micrographs a), b) and c) were taken of the near surface, center and near bottom regions of the alloy solidified from 873 K, respectively. Micrograph d) was taken of the near surface region of the alloy solidified from 773 K.

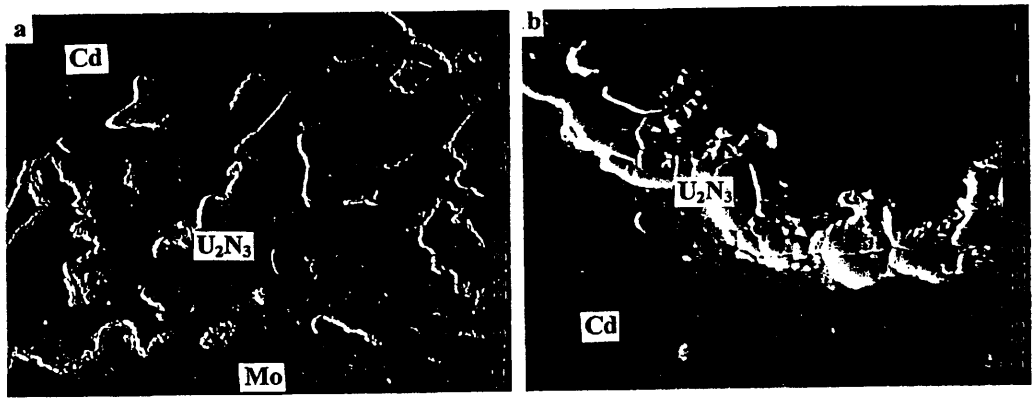

Figure 2 Backscattered electron micrographs of the Cd alloys in Mo crucibles: Micrographs a) and b) were taken of the near bottom and the near surface regions of the alloys solidified from 873 and 773 K, respectively. Both the precipitates are U_2N_3 containing GdN or (U,Gd)N.

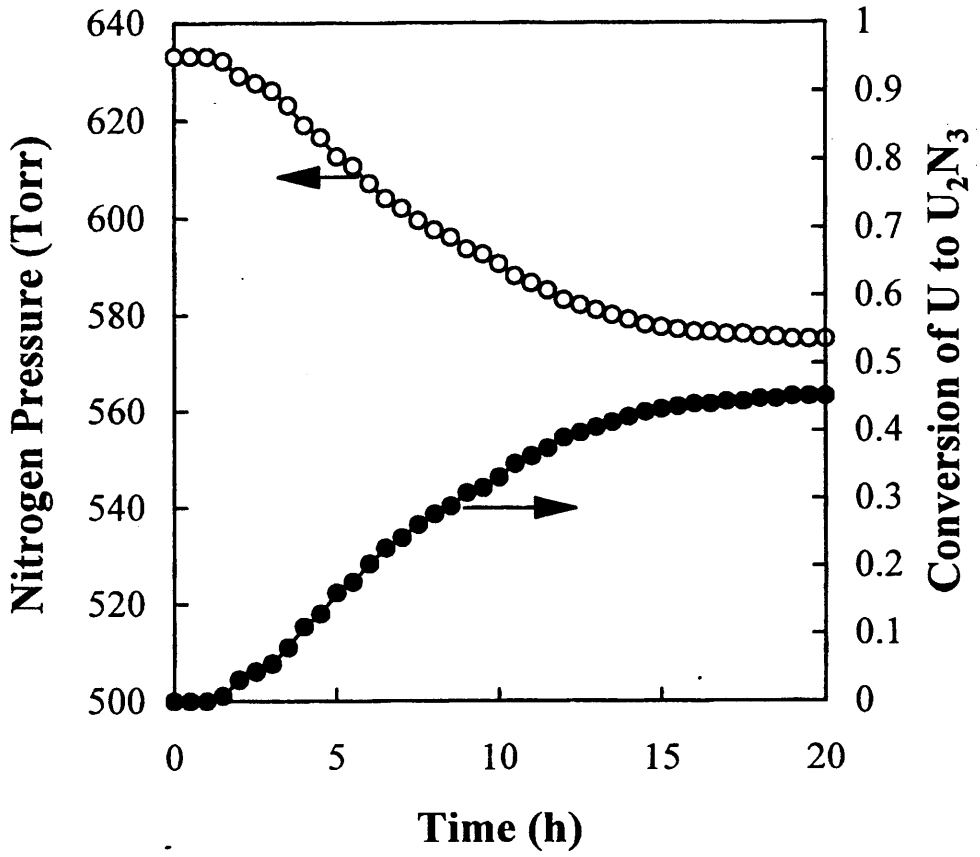

Figure 3 Time dependences of nitrogen pressure and conversion of uranium to U_2N_3 for the Cd-U alloy nitrided at 873 K.

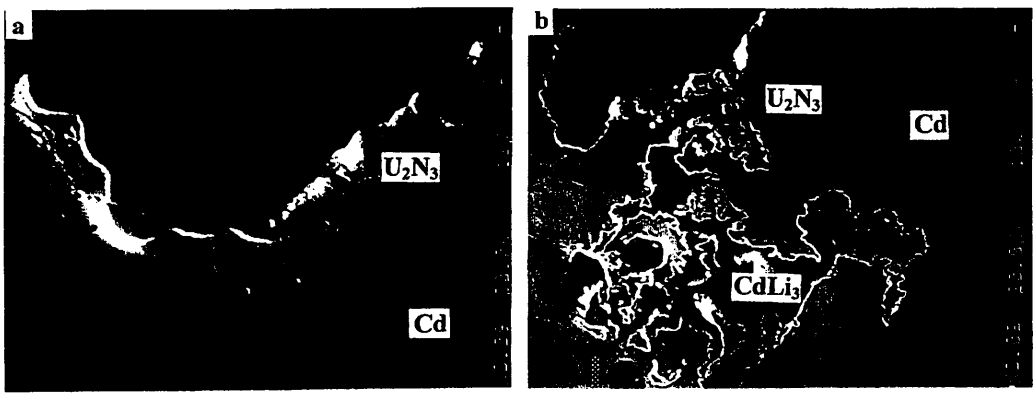

Figure 4 Backscattered electron micrographs of the Cd alloy nitrided with Li_3N: Micrographs a) and b) were taken of the near surface regions of the alloy solidified from 773 K. Gd-contained U_2N_3 precipitates were found at the alloy surface and the interface between the Cd-Li intermetallic compound ($CdLi_3$) and the Cd alloy